AD-A273 486

CONTINUOUS-COOLING-TRANSFORMATION BEHAVIOR,
MICROSTRUCTURE, AND PROPERTIES OF
0.02C-3.5Ni-3.6Mo HIGH-STRENGTH STEELS
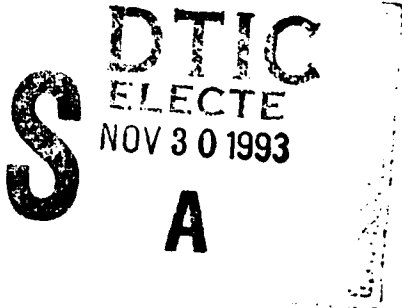
by:

Masoud Molaei

Master of Science Thesis

August, 1992

Continuous-Cooling-Transformation Behavior, Microstructure,

and Properties of 0.02C-3.5Ni-3.6Mo High-Strength Steels

DTIC QUALITY INSPECTED 8

Accesion For	
NTIS CRA&I	☑
DTIC TAB	☐
Unannounced	☐
Justification	
By	
Distribution /	
Availability Codes	
Dist	Avail and/or Special
A-1	

by

Masoud Molaei

T-4223

A thesis submitted to the Faculty and the Board of
Trustees of the Colorado School of Mines in partial
fulfillment of the requirements for the degree of Master of
Science (Metallurgical and Materials Engineering).

Golden, Colorado
Date 8/18/92

Signed: _Masoud Molaei_
Masoud Molaei

Approved: _Dr. Steven W. Thompson_
Dr. Steven W. Thompson
Thesis Advisor

Golden, Colorado
Date 8/18/92

Glen Edwards for JJM.
Dr. John J. Moore
Department Head
Department of Metallurgical
and Materials Engineering

ii

ABSTRACT

The continuous-cooling-transformation (CCT) behavior, microstructures, and properties of 0.02% C, 3.6% Mo, and 3.5% Ni steels with manganese contents ranging from 1 to 1.76% were investigated. The effects of cooling rate and prior austenite grain size were examined as part of the CCT work for the steel with 1.5% Mn. The CCT diagram for this steel is "flat-topped," with almost no variation in the transformation start and finish temperatures as a function of cooling rate.

A fully martensitic microstructure forms in response to cooling rates faster than about 37°C/s for a prior austenite grain size of about 7 μm. At cooling rates faster than 25°C/s, martensite forms for the 1.5% Mn steel with a prior austenite grain size of about 34 μm. At cooling rates slower than 25°C/s and 7°C/s for the prior austenite grain sizes of about 7 μm and 34 μm, respectively, the microstructure consists of acicular ferrite with micron-sized islands of martensite and austenite. At intermediate cooling rates, a mixture forms, made up of large packets of martensite and large packets of acicular ferrite. In this intermediate range of cooling rates, the volume fraction of martensite increases as the cooling rate increases.

The martensitic microstructures are characterized by a high dislocation density, some coarse twins, no detectable retained austenite, comparatively high hardness, a poor response to metallographic etching, and a good response to electrochemical thinning. Features of acicular ferrite are an equally high dislocation density, no twins, a significant volume fraction of retained austenite, comparatively low hardness, a good response to metallographic etching, and a poor response to electrochemical thinning. In addition, some small islands of austenite, between laths of acicular ferrite, transform to islands of high-carbon martensite, which frequently contain fine twins. Unlike previous investigations of low-carbon steels, granular ferrite was not observed, even at cooling rates as slow as 0.05°C/s.

For a cooling rate of about 1°C/s, yield strengths above 700 MPa (100 ksi) were obtained in the non-tempered condition. As manganese content increased, strength increased. Tempering resulted in lower strength and improved toughness. A single reaustenitizing treatment resulted in higher strength, although poorer toughness, than a double reaustenitizing treatment.

TABLE OF CONTENTS

LIST OF FIGURES

LIST OF FIGURES
(CONTINUED)

LIST OF FIGURES
(CONTINUED)

LIST OF FIGURES
(CONTINUED)

T-4223

LIST OF FIGURES
(CONTINUED)

LIST OF FIGURES
(CONTINUED)

LIST OF FIGURES
(CONTINUED)

LIST OF FIGURES
(CONTINUED)

T-4223

LIST OF TABLES

T-4223

ACKNOWLEDGEMENTS

1.0 INTRODUCTION

1.1 High-Strength, Low-Alloy Steels: A Brief Summary

Low-carbon or mild steels have traditionally been used in the construction industry. For many years, ASTM A7 (now ASTM A283, Grade D) was the specification for the most commonly used structural steel for both bridges and buildings. Minimum yield strength for this steel is 230 MPa (33 ksi). Although it has the lowest unit price of any structural steel, it also has one of the highest price-to-yield-strength ratios (1).

In the early 1900's, the design of high-strength, hot-rolled steels was based on tensile strength, and there was little attention given to weldability, formability and resistance to brittle fracture (2). Riveting was the most common form of joining structural components, and the high tensile strength required for constructional purposes was achieved through employment of carbon (up to 0.3%) as an alloying element. Mangenese was another major alloying element used to achieve higher strength.

During World War II, welding (rather than riveting) was introduced as a method of joining, and major structural failures in the steels then available required an

improvement in weldability and fracture resistance through reduction of carbon content (1,3). At the same time, the importance of both fracture toughness and low impact transition temperature were recognized. Similarly, the advantages of high manganese-to-carbon ratios for impact toughness were appreciated, and the significance of grain size was also established (2).

By the early 1950's, refinement of grain size by grain-refining additions, and the beneficial effects of ferrite-grain refinement on both yield stress and the ductile-to-brittle transition temperature had been demonstrated (2,3). During this period, the first steps toward achieving higher strength through grain refinement were taken by the introduction of aluminum to steels, which then combined with the nitrogen already present. Further increases in yield stress were then obtained by precipitation hardening. Vanadium, niobium and titanium were used, although the impact toughness was still not good, because the as-rolled grain size was coarse. Controlled rolling was then developed to improve the poor impact-transition properties of niobium steels, and this method turned out to be very successful. The result was that higher yield strengths of 450-525 MPa (65 to 75 ksi) along with low impact-transition temperatures, as low as -80°C, were obtained (1-3).

The development of high-strength, low-alloy (HSLA) steels was encouraged by the increasing demand for strong, tough, weldable steels for natural gas transmission lines, ships and off-shore drilling platforms (4). More recently, these steels have been used to increase the miles-per-gallon (MPG) efficiency of automobiles (5), to reduce the cost/weight ratio, to meet the notch-toughness requirements in constructional applications such as bridges, buildings and transmission towers (6-8) and for several other applications. The American Iron and Steel Institute (9) states that high-strength, low-alloy steels are "generally produced with emphasis on mechanical properties requirements rather than to *chemical composition limits*".

Beginning in about 1950, low-carbon bainitic steels were developed on a commercial scale simultaneously with ferrite-pearlite HSLA steels. Carbon contents in these steels ranged from 0.1 to 0.15%, and many combinations of alloying elements were used to produce bainitic structures during air cooling in a wide range of section sizes. Yield strengths in the range of 450-900 MPa (65 to 130 ksi) were achieved, depending on the carbon content and austenite transformation temperature (2). Bainite form at temperatures intermediate to those at which polygonal ferrite and martensite form. It has been shown (2) that

bainitic structures can be produced with a wide range of strengths (Figure 1.1).

Pickering (2,10,11) has summarized the aims of the development of low-carbon bainitic steels:

One goal is to produce a bainitic structure by air cooling, therefore minimizing the economic disadvantage of quenching and tempering. Through air cooling, yield strengths of 450-900 MPa (65-130 ksi) and tensile strengths of 600-1200 MPa (85-175 ksi), which are higher than those typically obtained for ferritic-pearlitic steels are also achievable. In addition, it was discovered that using a low carbon content and carbon equivalent would increase weldability and formability.

The next goals that arose were to provide a minimum variation of properties over a wide range of section sizes and to obtain good toughness with high strength levels. In low-carbon steels, the impact resistance of upper bainite is inferior to that of lower bainite, so most of the developments have been based either on lower bainite or low-carbon acicular ferrite. The formation of these acicular transformation products is beneficial in obtaining high strength levels.

Those who worked with low-carbon steels also recognized that a lower carbon content resulted in improved toughness
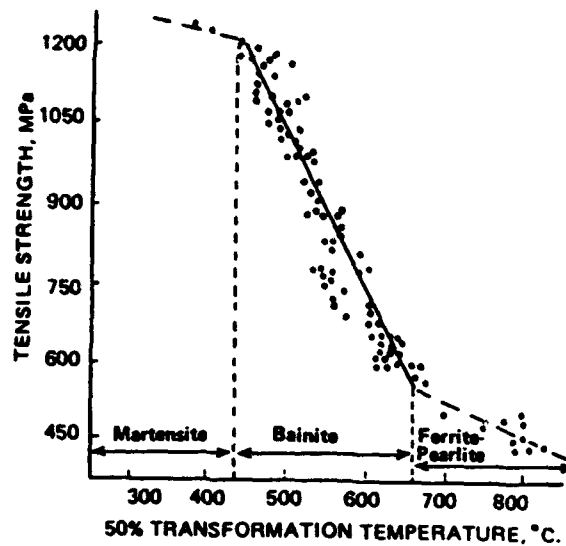
Figure 1.1   Effect of 50% transformation temperature on
             tensile strength of bainitic steels (2).

(1,2), compared with higher-carbon steels. An extreme

example of a very low-carbon steel was the development of

the 0.02% carbon, 3% nickel, 3% molybdenum, niobium-

containing, aluminum-treated steels (12,13). These steels

possessed a "bainite-like" microstructure with yield

strengths of more than 700 MPa (100 ksi) and transition

temperatures below -75°C. However, these steels are

uneconomical for general structural engineering (2). During

this time, other alloying combinations (Mn-Mo-Nb, Ni-Cr, Mo-

B and Ni-Cu-B) were also investigated, but they showed lower

strength levels (14-16).

As mentioned above, structural steels required for

critical applications such as shipbuilding, arctic pipeline,
off-shore oil drilling platform and construction equipment
require not only good weldability, but also high strength
and notch-toughness in addition to a low impact transition
temperature. High-strength steels were developed with these
applications (primarily Navy shipbuilding) in mind. Such
steels have yield strengths of 550 to 700 MPa (80 to 100
ksi), and are known as HY-80 and HY-100. These steels were
quenched and tempered to provide good, low-temperature
toughness with minimum strength levels of 80 ksi and 100
ksi, respectively (17).

To some extent, these alloys have been replaced by more
economical (18,19) precipitation-hardened HSLA-80 and HSLA-
100 steels that have been studied thoroughly by several
investigators (17,19,20,21). The transformation behavior
and mechanical properties of these HSLA steels will be
compared with those of this study.

In recent years, somewhat similar alloys to those of
McEvily et al. (12,13) have been studied by DeArdo and his
co-workers (22), who refer to them as "ultra-low carbon
bainitic" (ULCB) steels. They have investigated the
pos ible candidacy of the ULCB steels to replace the
traditionally heat-treated HTS and HY steels. The HTS
steels are C-Mn steels which, like the HY steels, rely on

carbon for strength, except that the latter also contain
alloying elements required for adequate hardenability. Both
the HTS and HY steels exhibit base-plate properties which
are adequate for their intended purposes. However, the HY
steels suffer from poor weldability (i.e., susceptibility to
heat-affected-zone cracking under all conditions) which is
caused by both high carbon content and high carbon-
equivalent values (22). Figure 1.2 shows the critical
importance of low carbon contents in improving the
weldability and weldment toughness in steels.

DeArdo et al. showed that ULCB steels are very
attractive for heavy-section applications and do not need to
be heat treated to obtain good mechanical properties. The
ULCB steels obtain their high strength and high resistance
to both ductile and brittle fracture through the application
of specially designed alloys and advanced thermomechanical
processing. DeArdo's group also suggested that these steels
show a very good combination of strength and toughness in
the as-hot-rolled condition, e.g., a 745 MPa (121 ksi) yield
strength with a ductile-brittle transition temperature below
-70°C.

Although there has been some research done to explore
the isothermal transformation behavior of this unique class
of ferrous alloy (12,13), the continuous cooling
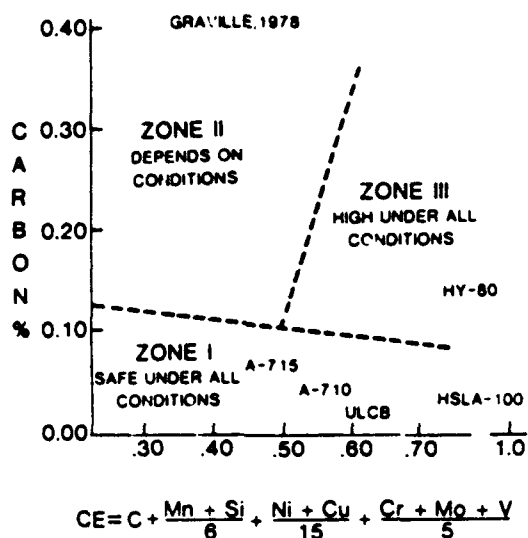
Figure 1.2 Effect of carbon level and carbon equivalent (CE) on the susceptibility to heat-affected-zone (HAZ) cracking (22).

transformation kinetics and the microstructural characterization of these steels are yet to be understood. Also uncertain is how the transformation behavior of these steels compares with low-carbon, copper-bearing alloys. The aim of this project is to address these needs, and the results of this study will be compared with the HSLA copper-bearing class of steels.

1.2 Purpose of The Project

Great demand for high-strength, tough steels with good weldability encourages metallurgists to develop new alloys.

The common ground for many of the newest HSLA steels is low carbon content. This is because carbon and/or carbides in high-temperature transformation structures, such as pearlite, are detrimental to weldability, formability, impact toughness and ductility (10). The formation of carbides can be avoided by reducing the carbon content of the steel.

As mentioned in the previous section, there is a wide range of compositions to consider for the new steels, with a wide range of mechanical properties. Although a great deal of attention has been paid to the intermediate transformation products (bainite) (10-16,23-34), more work needs to be done to obtain a better understanding of the transformation behavior of these products. In particular, the effect of chemical composition and cooling rate on austenite decomposition needs to be addressed.

The aim of this project is to explore the continuous-cooling-transformation behavior and microstructure of a unique class of ultra-low-carbon bainitic steels. McEvily and his co-workers (12,13) studied the isothermal transformation and hardenability of similar steels. Their isothermal transformation studies (Figure 1.3) showed that a high-temperature transformation product would form above a deep bay in the transformation diagram. Below the

a. Diffusion Dominated
Shear Dominated
Temperature
Time

b. Ni 2.8%, Mo 2.8%, Cb 0.05%, C 0.04%
$f_T = 0.05$ $f_T = 0.5$ $f_T = 0.95$
$f_T = 0.50$ (3% Ni - 2.8% Mo - 0.05% Cb - 0.002% C)
Transformation Temperature, C
Transformation Temperature, F
Time, hours
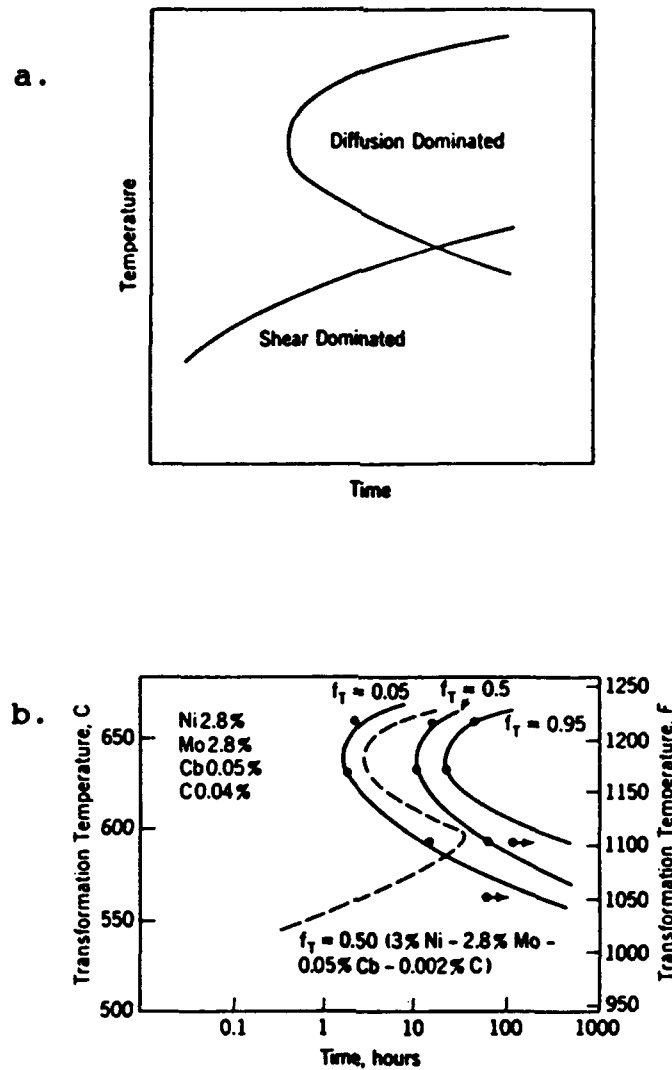
Figure 1.3   a. Schematic isothermal diagram indicating
diffusion-dominated and shear-dominated
austenitic transformation ranges.
b. Isothermal transformation diagram for high-
nickel, high-molybdenum alloy where f_T refers to
the fraction transformed at the indicated time
(12).

bay, a shear-dominated transformation product would form. Based on their isothermal studies, they concluded that high strength (more than 700 MPa) and good toughness (about 240 J at room temperature) could readily be obtained upon air cooling. They suggested that these excellent properties are due to the strength of austenite and the shear transformation products.

Because of the high cost of alloying (2), no attention was paid to these steels until a few years ago, when DeArdo et al. (22) studied the structure and properties of similar steels. They placed the emphasis of their research on austenite conditioning as a way to improve the mechanical properties of these steels. Their results showed that the as-hot-rolled combination of strength and toughness was quite good, that is, a 745 MPa yield strength with a ductile-brittle transition temperature below -70°C. They also suggested that tempering will improve toughness but does not affect the strength of these steels.

Although there has been some work done to explore the transformation behavior of this unique class of steels, there is very little information available about their microstructural characterization. Even more noticeable is the absence of information about the continuous-cooling transformation of these steels.

It is very important to consider the fact that the paths followed by the austenite in the metastable field (austenite+ferrite) are largely different in the case of isothermal transformation from that of continuous-cooling transformation. Although the fundamental mechanisms of transformation are not dissimilar, the produced microstructures may be very different (35).

Recent and ongoing work at the Colorado School of Mines (20,36-38) has revealed interesting austenite phase-transformation behavior in low-carbon (0.04-0.06%) copper-containing steels. These steels contain approximately 1.5% Mn, 0.7% Cr, 0.4% Mo, and 1 to 3.5% Ni (20,37,38). Figure 1.4 shows a typical continuous cooling transformation diagram for these steels generated by Colvin (36). As shown in the diagram, acicular ferrite and granular ferrite form over a wide range of intermediate cooling rates, while polygonal ferrite and Widmanstätten ferrite form during slow cooling, and martensite forms as a result of fast cooling rates.

As mentioned before, it is desirable to achieve similar properties upon cooling over the widest possible range of rates for the production of heavy section sizes (39). In order to obtain this goal, polygonal ferrite transformation ought to be delayed, and the bainite shelf on a CCT diagram
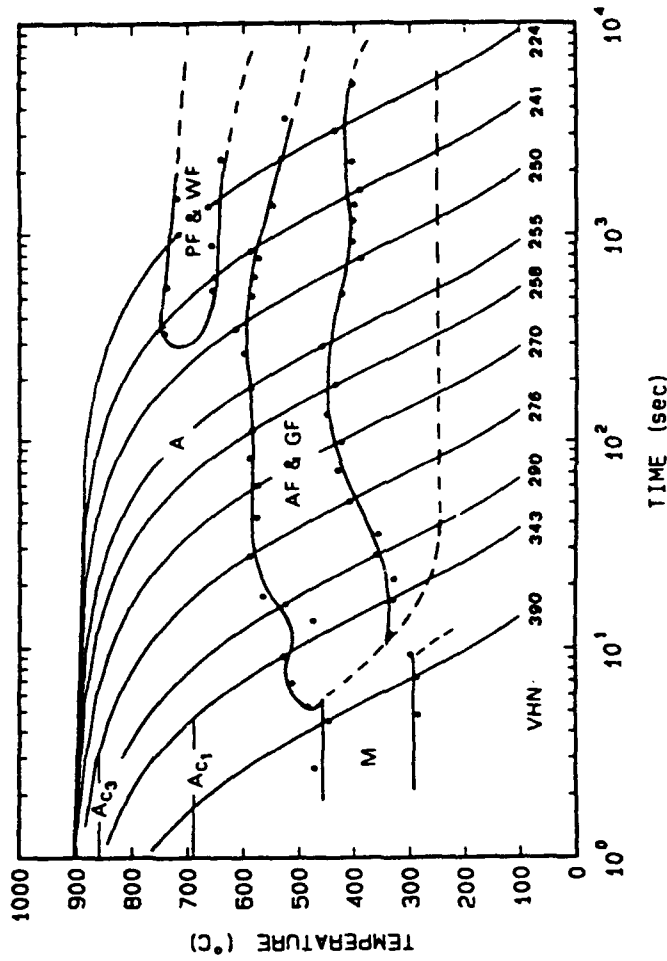
Figure 1.4   Continuous-cooling-transformation diagram for a low-carbon, copper-containing HSLA steel (37).

should be as horizontal (flat topped) as possible (36,39).
The steels under investigation are assumed to be capable of
these requirements (12,13,22).

1.3 Effect of Alloying Elements in HSLA Steels

1.3.1 Introduction

Plain-carbon steels are satisfactory in applications
requiring moderate strength and toughness, and where mild
environments are encountered. The relatively low
hardenability of these steels limits the strength which can
be obtained, except in fairly thin sections. However, most
of the limitations of plain-carbon steels may be overcome by
the use of alloying elements (40). This is true in the case
of HSLA steels as well. Figure 1.5 shows the hardening
effect of various alloying elements present in solid
solution within iron (41). Some of the most important
purposes of adding alloying elements to HSLA steels are (2):
- To increase hardenability;
- To improve strength at ordinary temperatures;
- To improve mechanical properties at either high or low
    temperatures;
- To improve toughness;
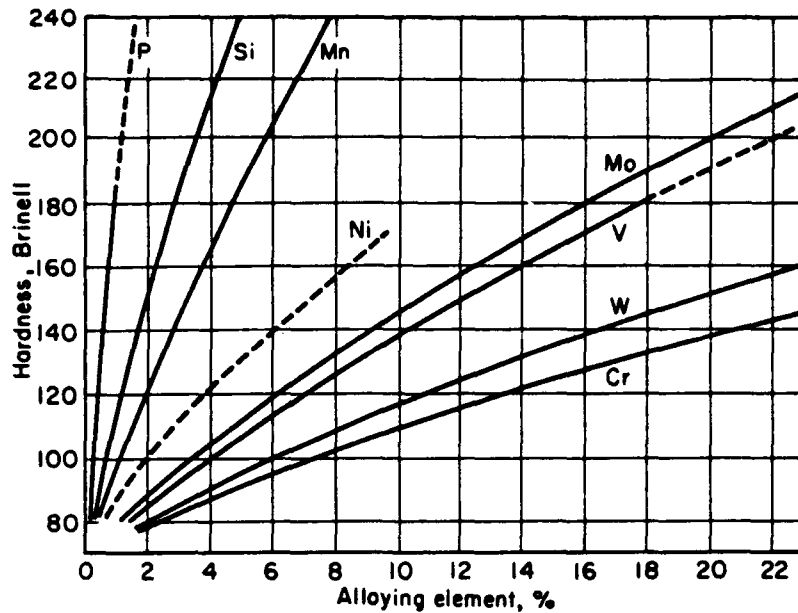
Figure 1.5   Solid solution hardening effects of the various
             elements as dissolved in pure iron (41).

- To improve wear resistance, and;

- To improve corrosion resistance.

Alloying elements in general act to depress the
austenite-to-bainite transformation temperature, primarily
through their effects on the diffusion of carbon which is
necessarily associated with high-temperature transformations
(e.g., pearlite) (14). The effect of some of the most
popular alloying elements used in HSLA steels will be
discussed briefly in this section.

1.3.2   Carbon

Carbon is the least expensive alloying element. It is present in iron as an interstitial solute atom. Carbon has a maximum solubility of 4.3% in austenite at 1148°C; by contrast, its solubility in ferrite at room temperature is essentially zero. Therefore, quenching a solid solution of carbon in face-centered-cubic (fcc) iron to a temperature below the eutectoid temperature results in the formation of body-centered-cubic (bcc) iron and the precipitation of carbon in the form of iron-carbide particles, or the formation of the non-equilibrium martensite phase which is supersaturated with carbon (11,41). Independent of microstructure type, increasing carbon content in steel produces a higher strength product.

Although increasing the carbon content of steel has positive effects on strength and hardness, a high carbon level has detrimental effects on impact strength and transition temperature. These negative effects explain the industry-wide tendency to reduce the carbon content and the carbon equivalent of HSLA steels to the lowest levels possible (2,12,39). Figure 1.6 shows the effect of carbon content on impact-transition temperature curves of ferrite-pearlite steels.
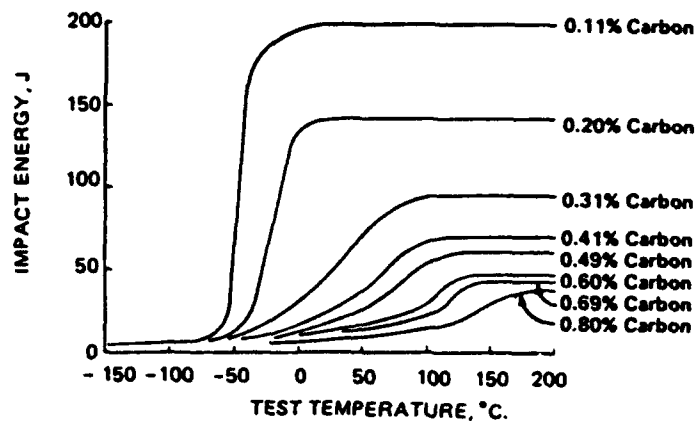
Figure 1.6   The effect of carbon content and hence the
             pearlite content on impact-transition
             temperature curves of ferrite-pearlite
             steels (2).

1.3.3   Chromium

Chromium, a bcc metal, has at most 20% solubility in

austenite with 0.5% carbon and unlimited solubility in

ferrite (41).   Chromium shrinks the austenite phase field in

accord with its role as a ferrite stabilizer (Figure 1.7).

In addition to being a moderate carbide former, chromium

strengthens the ferrite matrix and controls grain size (19).

It also increases resistance to corrosion (41).

1.3.4   Copper

Copper was originally added to steels to provide

resistance to atmospheric corrosion (42).   Later it was
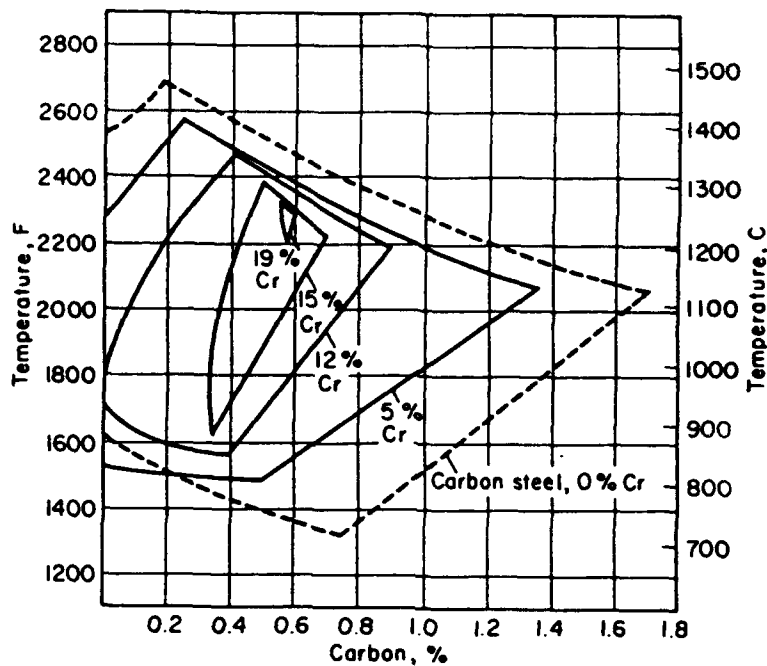
Figure 1.7   Effect of chromium content on the single-phase
             austenite region for Fe-Cr-C alloys (41).

found that this element could be used as a moderate solid-

solution strengthener and also as a precipitation

strengthener. It has fcc an structure and is an austenite

stabilizer.   Since its solubility in ferrite is much less

than in austenite, precipitation may occur during the

austenite to ferrite transformation, or in the ferrite after

it forms (43).

1.3.5 Manganese

Manganese has unlimited solubility in austenite, while its solubility in ferrite reduces to 3% at room temperature (40). Manganese is a very common alloying element in steel because it is inexpensive, and because it improves the hardenability of steel by inhibiting the transformation of austenite to polygonal ferrite (12-16). Manganese also improves the strength of steel by its solid-solution strengthening effect.

1.3.6 Molybdenum

This bcc metal is a ferrite stabilizer and a strong carbide former. Its maximum solubility in ferrite is 37.5%, which lowers with decreasing temperatures (40,41). Molybdenum strongly increases hardenability of steel by delaying austenite decomposition at high temperatures (650 to 500°C), Figure 1.8. In addition, it provides significant solid-solution strengthening (12-15,45). It reduces the susceptibility of steel to temper embrittlement and increases secondary hardening, while retarding softening during tempering of steel (44,46). These effects are shown in Figures 1.9 and 1.10. Molybdenum decreases the activity
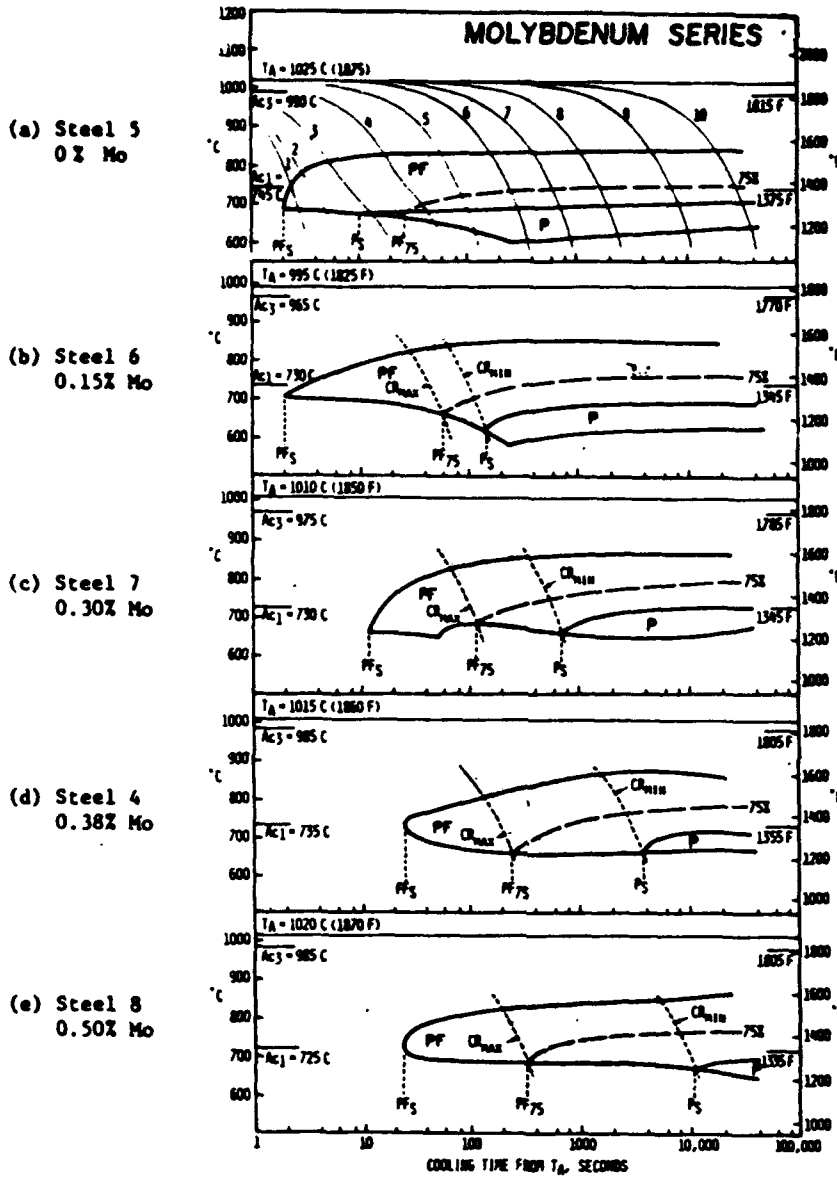
Figure 1.8 Upper portions of CCT diagrams for steels
alloyed with Mo. Nominal phase composition is
0.05 pct. C, 0.9 pct. Mn, 1.2 pct. Si and 0.5
pct. Cr (all wt. pct.).
PF is polygonal ferrite and P is pearlite (52).
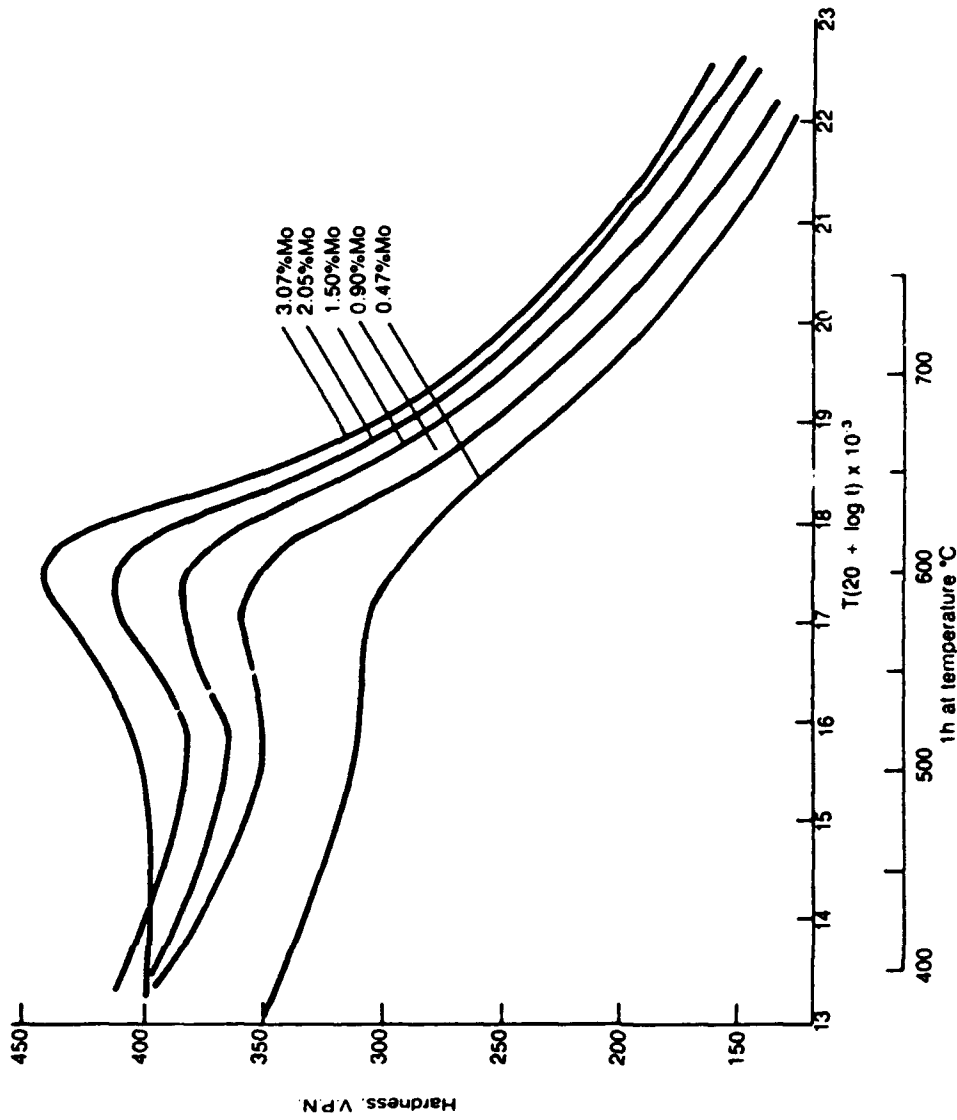
Figure 1.9   Retardation of softening and secondary hardening during tempering of steels with various molybdenum levels (44).
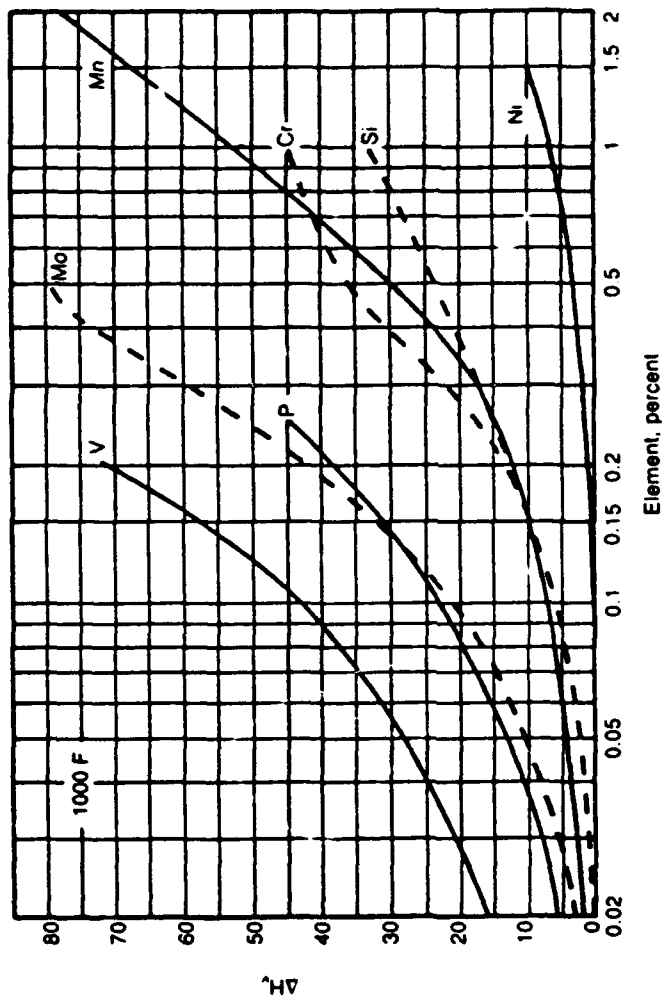
Figure 1.10   Effect of alloying elements on the retardation of softening during tempering at 540°C (1000°F) relative to Fe-C alloys (44).

coefficient of carbon in austenite (47) and in ferrite (48),
therefore retarding the formation and growth of ferrite
(49,50).

1.3.7 Nickel

Nickel is an austenite stabilizer with unlimited
solubility in austenite and 10% solubility in ferrite at
room temperature, irrespective of carbon content (40). It
has an fcc structure and, like manganese, depresses
austenbite transformation temperatures upon cooling. It
also increases the hardenabiliry of steel primarily by
delaying the proeutectoid ferrite transformation (13,44).
Nickel improves the impact properties of steel by its
presence in solid solution in ferrite (12,35,41). It also
increases steel strength by grain refinement in addition to
solid- solution hardening (51).

1.3.8 Niobium

Three important roles of Nb(C,N) precipitation in HSLA
steels containing Mn, Mo and Nb are: inhibiting austenite
recrystallization during rolling, precipitation
strengthening and contributing to improved hardenability

(15).

Niobium is mainly used for grain refinement purposes and
also precipitation strengthening (42). Precipitation of
Nb(C,N) can retard or inhibit recrystallization and
subsequent grain growth of austenite, which in turn will
lead to grain refinement of ferrite.

Like copper, the solubility of niobium in ferrite is
much less than in austenite. Therefore, particles may
precipitate during transformation of austenite to ferrite or
within the ferrite after it forms (42). If used in
combination with manganese, niobium's solubility in
austenite will increase, which in turn further lowers
austenite transformation temperature and also limits the
premature precipitation of niobium in austenite. The
presence of nickel in conjunction with manganese may also
tend to limit the premature precipitation of niobium (53).

1.3.9 Nitrogen

Nitrogen is an interstitial alloying element, and like
carbon, this element is an austenite stabilizer and improves
both the yield and tensile strength of steel. At the same
time, nitrogen promotes brittle fracture and increases the
impact transition temperature. Because of the high

electronegativity of nitrogen, nitrides usually form before carbides and are very stable.

1.3.10 Silicon

Even though silicon is a ferrite stabilizer element, it also stabilizes retained austenite by retardation of cementite formation (23-26,40,41). Silicon contributes to solid-solution hardening and increases both yield and tensile strength. It also improves the resistance of steel to oxidation.

1.4 *Strengthening Mechanisms in HSLA Steels*

1.4.1 Grain Refinement

For a given composition of steel, it has been shown that the most important factor controlling strength and associated ductility is grain size (54,55). Pickering (3) calls this "the unique feature of grain-size strengthening" which is "the only strengthening mechanism that also increases the toughness." According to the Hall-Petch equation (56,57), the yield strength of a ferritic steel increases with decreasing grain size (58):

$$\sigma_y = \sigma_i + k_y d^{-\frac{1}{2}} \qquad\qquad (1.1)$$

where σ_y = yield stress

σ_i = stress needed to move dislocations in the

grains (friction stress), an experimental

constant

k_y = an experimental constant

d = grain diameter

A typical plot is given for a 0.1%C mild steel in
Figure 1.11, where the linear relationship of the impact
transition temperature with $d^{-\frac{1}{2}}$ has been described and the
effect of refining the grain size on both the yield strength
and the impact transition temperature is shown.   Armstrong
(59) has an excellent analysis on the influence of
grain size on several mechanical properties of
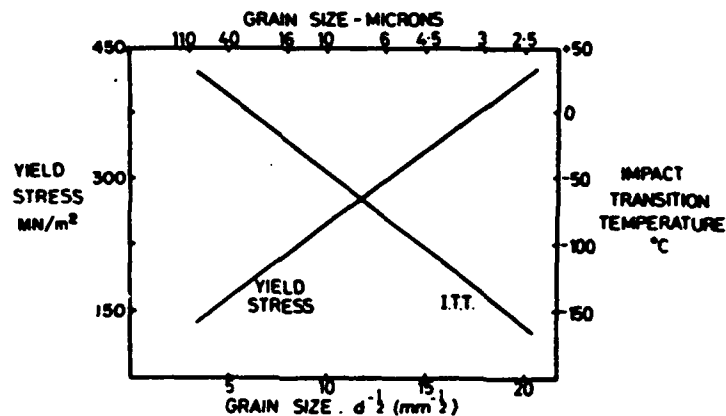
Figure 1.11   Effect of grain size of ferrite on yield stress
and impact transition temperature of a steel
containing 0.1%C, 0.5%Mn, 0.2%Si and 0.006%N (3).

polycrystalline materials, based on the Hall-Petch
relations. He concludes that hardness, fatigue strength and
yield strength, as well as ductile-brittle transition
temperature, usually increase by decreasing the grain size.
The effect of grain size on creep properties of materials
are dependent on the temperature and the applied stress.

A simple explanation of how grain size can affect
mechanical properties of materials is that grain boundaries
act as barriers to dislocation motion. However, Irvine
(60), in reference to upper and lower bainite, states that:
"In the bainitic structure, the yield strength is related to
the bainitic ferrite grain size, whereas the impact strength
is more dependent on the prior austenite grain size."
Irvine goes on to explain that the low-angle boundaries of
the bainitic ferrite plates are not as effective barriers to
propagation of cracks as the high angle boundaries and the
carbide aggregates. In lower bainite, the situation is
different, because of the presence of carbide within the
ferrite grains, which impedes fracture. Here, the prior
austenite grain size becomes less important and the
microstructural features of fine ferritic grain size plus
the carbides precipitated within the ferrite control the
fracture characteristics (60). Different methods of grain
refining have been used, such as controlled rolling, thermal

cycling and microalloying with aluminum, niobium, titanium, vanadium, etc.

By the late 1960s and early 1970s, it was widely recognized that attractive combinations of yield strength and toughness could be developed at modest cost using properly processed steels with unique compositions (61-63). Such methods as controlled rolling at a low finish-rolling temperature were found to produce a fine austenite grain size, and consequently a fine ferrite grain size, while retaining some potential for precipitation strengthening (2).

Tanaka et al. (64) defined controlled rolling in three stages. Their definition is based on the fact that there should be a definite difference in the physical properties of steel between deformation in the austenite region and that in the austenite-ferrite region.

Stage one includes simultaneous deformation and recrystallization. This stage takes place at high temperatures, above 1000°C, where dynamic recrystallization occurs concurrent with deformation. During this stage, there is a critical amount of deformation below which recrystallization will not be completed. A deformation level below 8% causes partial recrystallization as well as strain-induced grain boundary migration, which will result

in the formation of a mixed austenite grain structure.
Completing this stage with a total reduction of about 60%
gives a final grain size not smaller than 20μm.

The second stage consists of low-temperature (950°C to
Ar$_3$) deformation of austenite, during which austenite grains
become progressively more flattened with increasing amounts
of deformation, resulting in an increasing surface-to-volume
(S$_v$) ratio for the austenite grain structure. Increasing S$_v$
results in increased ferrite nucleation rates, giving rise
to a finer ferrite grain size in air-cooled specimens. An
increase in the amount of deformation will increase the
number of deformation bands, hence finer and more uniform
ferrite grains will form. At this stage, variations in
deformation temperature and the amount of deformation have a
minor effect on yield stress and almost no effect on tensile
strength.

Deformation in the austenite-ferrite region, the third
stage, takes place at temperatures below Ar$_3$. Deformation
at this stage has a much larger influence on the mechanical
properties than the deformation present in the second stage.
IN addition with an increase in the amount of deformation,
both yield and tensile strengths increase noticeably and
impact transition temperature decreases rapidly. These
considerable improvements in the mechanical properties after

deformation in stage three are mostly attributed to
substructural strengthening in the ferrite.

The other method of grain refinement uses thermal
cycling between room temperature and some temperature above
the Ac1. This technique has been widely used to refine the
grain size of steel, therefore improving its mechanical
properties. Conventionally, this method involves multiple
austenitization steps above the Ac_3 followed by quenching or
air cooling (65), whereas a non-conventional technique
involves partial reaustenitization between Ac_1 and Ac_3 (66).
In addition, rapid heat treatment has also been suggested by
some investigators (66,67). Figure 1.12 shows a schematic
representation of these thermal cycles.

On the average, each ferrite grain transforms to an
austenite grain upon complete austenitization, and upon
cooling each austenite grain will transform into about three
polygonal ferrite grains (68). However, Karlsson (65) has
reported a reduction of six times in ferrite grain size
after one-step austenitizing. He suggests that this
reduction is almost independent of carbon content, being
only slightly smaller in low-carbon material. His data also
indicate that the refinement diminishes on further cycling.
Similar results will be reported later in this thesis.

The effects of microalloying with aluminum, niobium,
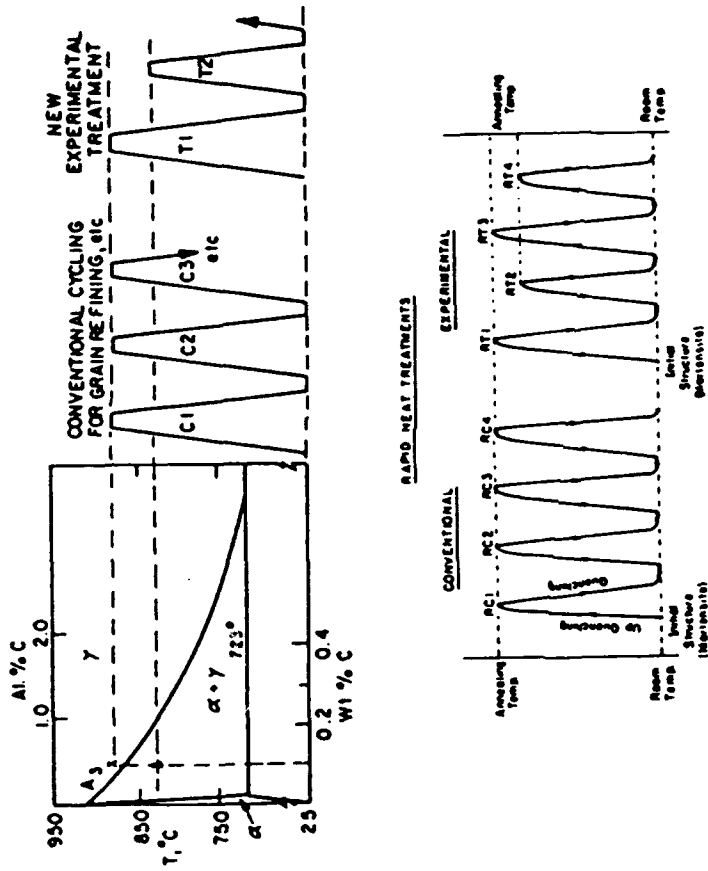
Figure 1.12   (a) Schematic representation of experimental thermal cycles in
comparison with conventional heat treating cycles, referred to part
of the Fe/C equilibrium phase diagram.   (b) Schematic representation
of conventional and experimental rapid heat treating cycles (66).

vanadium and titanium have been studied by many

investigators (15,16,42,51-53,69-74). Aluminum was the

first element to be used in combination with nitrogen as a

grain refiner (2), with the effect that fine aluminum

nitride particles control austenite grain growth (44).

But niobium is the alloying element which has attracted

the most attention (2), and is considered to have the most

beneficial effect on the strength-toughness combination of

steels (63). In addition to grain refinement, niobium

carbonitride particles also inhibit austenite

recrystallization during rolling. Niobium in solution

enhances hardenability, and it can promote precipitation

strengthening (73). However, a substantial amount of

niobium must remain in the austenite solid solution after

hot rolling in order to maintain its effectiveness in the

areas of hardenability and precipitation strengthening (60).

As precipitation of Nb(C,N) in the austenite removes niobium

from the solution, there will be effectively less niobium in

solution to further precipitate in ferrite. In particular,

Coldren et al. (15) observed a loss in acicular ferrite

hardenability when the amount of niobium dissolved in

austenite decreased below ~0.03%.

Furthermore, the effect of precipitates on austenite

recrystallization and grain growth of austenite or ferrite

is strongly particle size-dependent. Small precipitates
($\leq$ 200μm) are most effective in preventing recrystallization
(61).

Vanadium is another strong carbide former that is used
primarily as a microalloying element for precipitation
hardening. Vanadium carbide has one of the highest
solubility levels among other carbides and nitrides in steel
(75) and tends to form interphase precipitates of vanadium
carbonitride partcles in polygonal ferrite (76).

Titanium reacts with interstitial atoms to form a
variety of compounds. Some of these precipitates are
desirable and some have detrimental effects on the
mechanical properties of steel. Reasons for using titanium
as a microalloying element include grain refinement and
precipitation strengthening (74).

Figures 1.13 and 1.14 show the effects of niobium,
vanadium and titanium on grain refinement and precipitation
hardening as well as on continuous cooling transformations,
respectively (62,77).

1.4.2 Solid-Solution Strengthening

Strengthening of pure iron by the introduction of
alloying elements is well known (41,78). The effect of
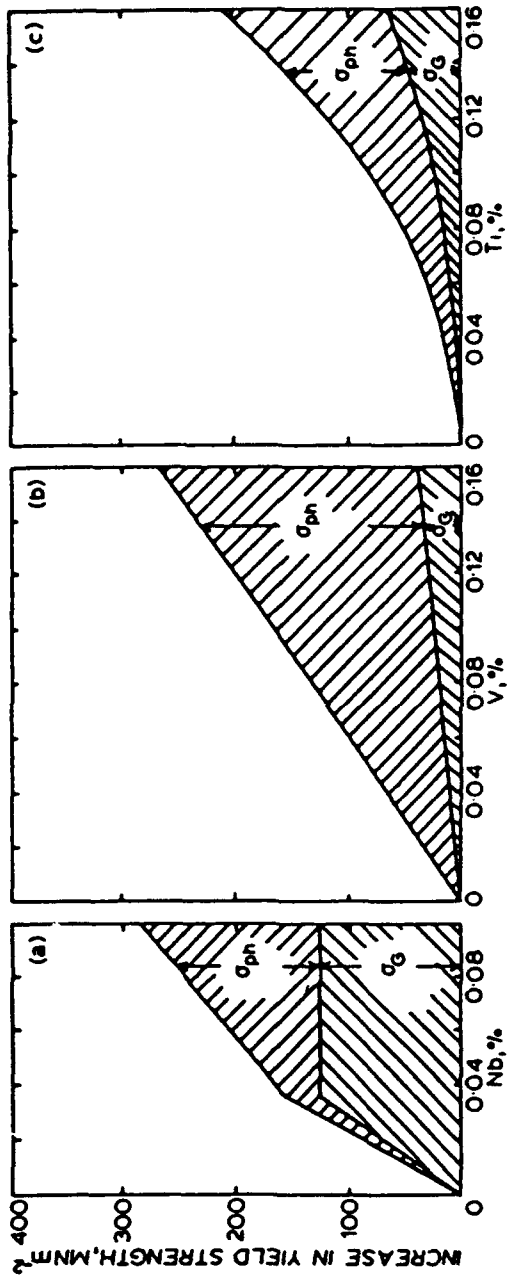
Figure 1.13   Correlation between microalloy content and increase in yield strength. Increase in strength is due to grain refinement (σ_G) and precipitation strengthening (σ_{PH}) (77).
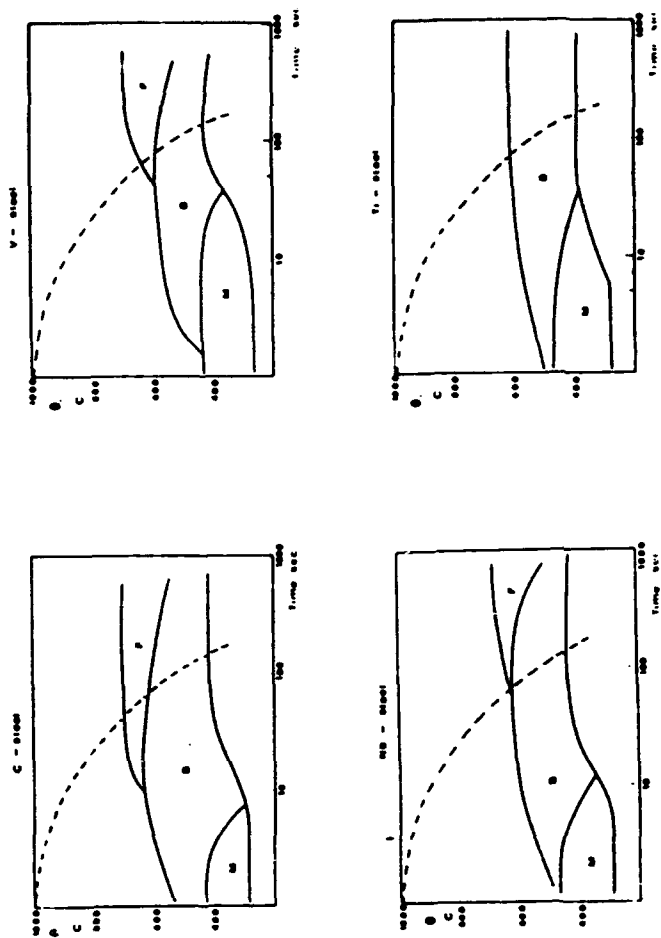
Figure 1.14   Effect of V, Nb, and Ti on CCT curves of a steel containing
2.5% Mn (62).

alloying elements on the mechanical properties of iron is
the consequence of the influence exerted by the solution of
those elements in the iron lattice. The result is a solid
solution, which occurs in two types: substitutional and
interstitial. In the case of a substitutional solid
solution, the solute atoms take positions that are normally
occupied by solvent atoms. By contrast, interstitial solid
solution happens when solute atoms do not displace solvent
atoms but enter the holes, or interstices, between the
solvent atoms (79).

Generally, substitutional atoms cause symmetrical
distortion of the solvent lattice, therefore the
strengthening effect is relatively moderate. Asymmetrical
distortion caused by interstitial solutes has a more
pronounced effect on solid-solution hardening (3). However,
there are a number of factors that contribute to solid-
solution strengthening. According to Dieter (80), the most
important ones are relative size factor, relative modulus
factor, electrical interaction, chemical interaction (Suzuki
interaction) and configurational interaction (Fisher
effect). Relative size factor or the size misfit between
solute and matrix atoms gives an approximate idea of the
amount of strengthening that can be obtained, although some
elements such as nickel and manganese provide more

strengthening than would be expected by their misfit (4).

Detailed explanation of each of these factors is outside the

scope of this brief review.

Although the overall effect of substitutional solid-

solution hardening is considered to be small (81), Speich

and Swann (82) showed that the solid-solution hardening

effect of nickel (at 20%Ni) is responsible for 75% of the

overall strength of a martensitic alloy with 0.0034 wt% of

carbon. Figure 1.15 shows the effect of various

substitutional solute atoms on the yield strength of high-

purity polycrystalline ferrite at room temperature (78).

Further discussion of solute atoms was presented in previous

sections.

1.4.3 Precipitation Hardening

Precipitation hardening is defined (44) as

"hardening caused by the precipitation of a constituent from

a supersaturated solid solution." This strengthening

phenomenon occurs when a solid solution at elevated

temperature is cooled to a lower temperature, and

precipitates form because of the decrease in solubility

(80). More conventionally, a solid solution is quenched to

"freeze in" the solute atoms, and a subsequent aging or
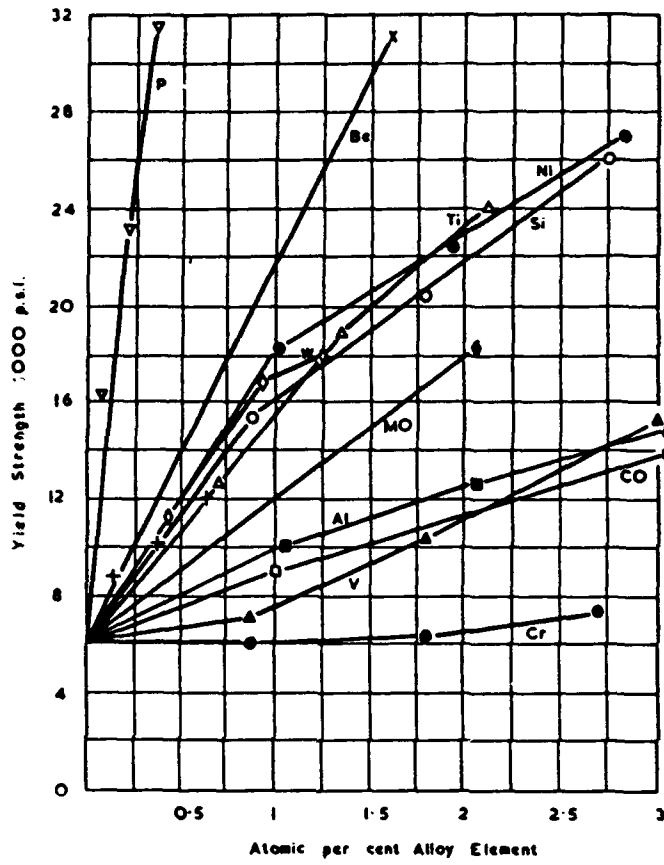
Figure 1.15   Yield strength versus atomic percent for
various alloying elements (78).

tempering treatment results in precipitation. Any particles
that form at high temperatures in austenite do not cause
strengthening because they are typically too coarse and
widely spaced (4). Additionally, these particles lose
coherency with the matrix when the austenite-ferrite
transformation interface sweeps through the structure (15).
However, these precipitates are effective in controlling
grain growth. The particles that form at low temperatures
in austenite, during transformation at the austenite-ferrite
interface, or in ferrite during cooling are effective
strengtheners (4).

The ratio of carbide-forming element to carbon is also
important for precipitation hardening. Elements such as
vanadium, niobium, titanium, molybdenum, tungsten and
chromium are used to strengthen HSLA steels. A
number of investigators have studied the effect of these
alloying elements on mechanical properties of HSLA steels
(15,19,39,42,53,69). Some of these effects have already
been discussed.

Copper has been used in HSLA steels to take advantage
of its precipitation in absence of carbon (19,37,42,53,83).
Copper taken into solid solution in the austenite can be
precipitated as fine ε-copper particles in ferrite. To
increase the degree of supersaturation of copper and to

avoid its premature precipitation in austenite, faster
cooling rates (84) and lower transformation temperatures
(53) have been recommended.

1.4.4   Transformation Strengthening

Substantial substructural strengthening produced by
transformation is largely due to the temperature at which
the transformation occurs (3,12).   In general, lower
transformation temperatures, result in a greater
strengthening effect.   Most strengthening mechanisms can be
intensified by lower transformation temperatures (3).   In
particular, it is possible to produce finer grain sizes in
the transformation product, increase the dislocation density
and the precipitate density, and make the precipitate size
finer if transformation temperature is lowered.

Because of a substantial decrease in the diffusion rate
of alloying elements at lower transformation temperatures,
there is a tendency to retain solute in solution, and
subsequently solid solution strengthening will increase.
Complex results (3) arise with the interaction of all of
these effects.   Although all of the aforementioned factors
contribute to strength, each has its own unique impact on
toughness and ductility (3).

An attractive combination of strength and impact
properties can be obtained in low-carbon steels with
acicular-ferrite structures (15,16,85). Acicular ferrite is
defined by Smith et al. (16) as:

"a highly substructured, non-equiaxed ferrite that forms on
continuous cooling by a mixed diffusion and shear mode of
transformation that begins at a temperature slightly higher
than the upper bainite temperature transformation range. It
is distinguished from bainite for two reasons: (1) the
limited amount of carbon available results in there being
only a small amount of carbide present, and (2) the term
bainite has been applied to such a wide variety of
structures that it is somewhat indefinite."

One advantage of the acicular ferrite transformation is its
function as a catalyst for aiding both the grain refinement
and the precipitation hardening components of the
strengthening mechanism, relative to those components
obtainable from ferrite-pearlite steels. Because of its
relatively low transformation temperature, acicular ferrite
is characteristically fine-grained and contains a
substructure with a high dislocation density (12,16). The
low transformation temperature also leads to a slower rate
of precipitation, which is easier to control. This
controlled precipitation will result in more homogeneous
properties throughout the plate thickness (16).

High yield strengths, in addition to excellent fracture
toughness and weldability, are obtainable at unusually low
carbon levels. This is due to the great potential of the

acicular ferrite matrix to extract large strengthening components from grain refinement, generating a highly dislocated substructure and aiding precipitation strengthening (15,16).

Proper alloying additions facilitate the formation of bainitic structures upon continuous cooling by suppressing the polygonal ferrite transformation. Alloying increases strength by lowering the transformation temperature, which in turn refines the bainitic structure and increases the dislocation density (39) and the solid solution hardening effect. In particular, the elements molybdenum, manganese (16) and niobium (53) help generate the acicular ferrite structure.

According to Morcinek et al. (85), an analysis of the strengthening mechanisms operating in low-alloy steels suggests that the two mechanisms which contribute the most are dislocation and precipitation strengthening. Although they suggest that the strengthening component related to grain refinement can be included with the dislocation contribution, others (2,86) believe that grain boundaries are the most effective barriers in resisting fracture. In the case of martensitic structures, internal twins also play an important role in strengthening (81). Bainitic lath size and dissolved carbon (which probably strengthens by

interacting with the dislocations) are other features which, in addition to the previously stated mechanisms, control the strength of bainitic steel (2,72). For example, Gemmill (87) states that hardening may occur by an interaction between solid-solution elements and dislocations, and he refers specifically to the influence of both manganese and nitrogen on the high-temperature properties of carbon-manganese steels.

Discussing transformation strengthening in steels without considering the martensitic transformation is incomplete. The diffusionless shear-type transformation of austenite to martensite is one of the most common strengthening mechanisms used in steels (80). The high strength and often brittle nature (88) of martensite in steels is an indication of strong barriers to dislocation motion in this structure (80). Although substructural strengthening in martensitic transformation is responsible for a great degree of the strength of martensite, this high strength can not solely be attributed to the fine structure of this austenite transformation product (88).

Hardness of martensite is very sensitive to the carbon content of steel for the values below 0.2%, and increases with an increase in carbon content (80). In the absence of carbon (0.0034%), Speich and Swann (82) showed that three

quarters of the strength of martesite in an Fe-Ni alloy with 20%Ni is due to the solid-solution strengthening effect of nickel.

1.5   Microstructure of Low-Carbon Steels

Decomposition of austenite at subcritical temperatures (11) produces a variety of microstructures that are somewhat well known to ferrous metallurgy students. As a result of this decomposition, pearlite, polygonal ferrite and Widmanstätten ferrite form at higher temperatures, while upper bainite, granular bainite (also called granular structure), granular ferrite, lower bainite and acicular ferrite form at intermediate temperatures or cooling rates. By decreasing the temperature even more or by increasing the rate of cooling, martensite forms.

There has been tremendous debate since the discovery of the intermediate structure over the mechanism of its formation and consequently the terminology, and there is no sign of compromise (27) between the three major theories developed by different groups of investigators. These three theories are summarized by Ironstone as follows:

1. The generalized microstructural definition considers bainite to be the product of a non-lamellar (as opposed to

pearlite), and more generally, a non-cooperative mode of transformation. It is believed that the two product phases form by diffusional nucleation and growth and differ continuously in composition from the matrix and each other.

2. The overall reaction kinetics definition views the bainite reaction as having its own C-curve on a TTT-diagram. No bainite can form above the highest temperature of this curve, which may be termed the kinetic-B_s temperature. At isothermal reaction temperatures near the kinetic-B_s, transformation of austenite to bainite is increasingly incomplete.

3. The surface relief definition usually considers bainite to be precipitate plates formed by shear at rates paced in some manner by diffusion. In some versions of this definition, however, the diffusion process may occur either before or after formation of a single product phase.

Upper bainite nucleates mainly at the austenite grain boundaries (11). The ferrite crystals are lath or plate-like in shape and second-phase carbide particles form between ferrite laths (28-30). According to the diffusion-controlled growth models, while ferrite laths grow, carbon is rejected into the austenite and makes the austenite rich in carbon. This enriched austenite usually transforms to carbide, although sometimes it remains between the adjacent

ferrite laths as pools of retained austenite or it
transforms to high-carbon martensite (11). Bainite without
carbide has been referred to as granular bainite (35).

In opposition to this model, Oblak and Hehemann (31)
proposed that formation of both upper and lower bainite
occurs by repeated nucleation of substructural units and
rapid growth to a limited size. These subunits are thought
to form by a cooperative transfer of lattice atoms, although
not necessarily at the rate characteristic of martensitic
reaction. The rate of formation is controlled by this
multiple nucleation process. This suggestion has been
supported by Bhadesia and Waugh (32).

Purdy and Hillert (33) suggested that subunits of
bainite have similar orientations, whereas new units of
plate martensite have new orientations, an indication that
does not relate to the autocatalysis (martensitic) growth
of bainite. On the other hand, they admitted that the
elastic strains are important in both formation and growth
of ferritic subunits.

Aaronson and Kinsman showed that the lengthening
mechanism of proeutectoid ferrite and upper bainitic
crystals is controlled by the formation and lateral movement
of ledges. They also concluded that the subunits in the
bainite sheaves lengthen by the formation and the diffusion-

controlled lateral movement of ledges. Both the "cessation of the thickening of sheaves" and the "rapid increase in the rate of sympathetic nucleation at lower temperatures" have been explained in terms of the "solute drag effect" (89). The special effect of alloying elements upon growth kinetics has been interpreted (90,91) in terms of a "drag effect" produced by the segregation of certain alloying elements to austenite-ferrite boundaries. Alloying elements that reduce the activity of carbon in austenite are particularly involved in such segregation. The tendency for segregation increases as the temperature decreases, especially because of the high concentration of carbon in the austenite at austenite-ferrite boundaries. When the drag effect is larger than the driving force for growth, an upper nose will develop in the TTT diagram (see Figure 1.3). On the other hand, as the drag effect approaches saturation and the driving force begins to overcome this effect, a bay will begin to develop in the TTT diagram. In this regard, the role of molybdenum in the formation of bay is very interesting. Based on thermodynamic arguments, it is expected that molybdenum displace the TTT diagram to shorter times compare with an iron-carbon alloy of the same carbon content, thereby decreasing rather than markedly increasing the hardenability of steel. It is the kinetic solute-drag

effect which provides the marked increase of hardenability
in molybdenum-containing steels (90).

Regarding different forms of bainite, as the
transformation temperature is lowered, bainite laths tend to
become finer (10,11), but the carbide's orientation
relationship with the ferrite does not change (30). The
orientation relationship observed for the ferrite and
cementite in upper bainite shows that they both are related
through the parent austenite (30). As is true of upper
bainite, prior austenite grain boundaries are the first
sites for the nucleation of lower bainite, although
nucleation tends to happen within the grains as well (11).
The ferrite is acicular and the carbide particles form
within ferrite laths at an angle of about 55-65° to the long
direction of the ferrite lath (30). The reason for the
formation of carbide within the ferrite plates is that lower
bainite is significantly supersaturated with carbon,
therefore the formation of such a ferrite occurs in
association with the precipitation of carbide particles
(11). The orientation relationship between ferrite and
carbide in lower bainite reinforces the opinion that carbide
precipitates from ferrite (30). Therefore, even if the
morphology of upper and lower bainite appears to be similar,
these orientation relationships are very effective evidence

to distinguish between the two different microstructures
(30).

Up-quenching experiments (34) have shown that there are
major internal structural differences between upper and
lower bainite, and that these differences appear as a result
of alteration in the kinetics of formation and growth of
these products. Even though there are some similarities
between the bainitic (especially lower bainite) and
martensitic structures, such as similar orientation
relationships and surface relief effect, a true martensitic
structure is diffusionless (92).

There is considerable confusion regarding the
terminology for the microstructures formed at intermediate
temperatures upon cooling (35,37), or by interrupted
transformation of austenite to bainite and ferrite (93) in
low-carbon alloyed steels. The equiaxed morphology of
granular ferrite is similar to that of polygonal ferrite,
however it is distinguished from polygonal ferrite by higher
dislocation density content and finer structure (37).
Granular ferrite formation is a diffusion-controlled
transformation, and there has been evidence indicating that
no shear is involved in the formation of this microstructure
(37). Consequently, it should be differentiated from
granular bainite or granular structure, since these
structures are considered to be formed by a shear-type

transformation. Hehemann (89) believes that impingement is the reason for nonacicular nature of granular bainite. According to Bhadeshia and Christian (94), acicular ferrite is essentially identical to bainite, and the reason that its detailed morphology differs from conventional bainite is that the former nucleates intragranularly at inclusions within large austenite grains, while the latter nucleates initially at austenite grain boundaries (11,94). However, other investigators (95) believe that acicular ferrite is not identical to bainite. Although nucleation of acicular ferrite involves diffusion of carbon (and other interstitial atoms), there is no reconstructive diffusion during growth (96).

The observation of "steps" or "carbon-enriched residual austenite" can not be taken to imply that acicular ferrite is indeed Widmanstätten ferrite (as it is sometimes considered to be), because the mechanism for interface motion (step mechanism) does not relate to the mechanism of transformation. The enrichment of austenite, on the other hand, can happen during or after the transformation (94).

In an attempt to unify the definitions of the microstructures produced upon continuous cooling in very low-carbon steels, the bainite committee of the Iron and Steel Institute of Japan (ISIJ) has conducted some

investigations. The results appear in "Atlas for Bainitic
Microstructures, Vol. 1", which lists some microstructures
and the corresponding definitions (97).

Martensite in steels is formed by a diffusionless
transformation of austenite (44) in an athermal or near-
athermal fashion (33). This transformation involves a
complete military (displacive) motion of atoms where (in
principle) none of the atoms changes place with its
neighbors (88). The martensitic transformation occurs by a
shear mechanism, which is more likely to happen at lower
temperatures. Surface tilting is an important feature of
this transformation, which implies that there has been
cooperative transfer of atoms across the advancing interface
(44,98).

By lowering the transformation temperature or
increasing the carbon content (or in general increasing the
strength of austenite by alloying addition), the morphology
of martensite changes from lath to plate morphology (44).
The inhomogeneous shear in plate martensite is compensated
by internal twinning, and therefore the dislocation density
in plate martensite is not very high (44,81). In lath
martensite, however, less internal twinning is observed and
this is an implication of the compensation of the
inhomogeneous shear by slip, which is in agreement with high

dislocation density of lath martensite (44,81).

Very low-carbon steels exhibit massive transformations at both high and low transformation temperatures. While the high-temperature product has been identified as massive ferrite, martensitic transformation is the product of lower transformation temperatures (99-106). Goodenow and Hehemann (107) reported similar observations of martensitic reactions in very low-carbon steels containing 9% Ni. They proposed "low-carbon martensite" as an alternative name for "massive martensite". Massive martensite refers to the blocks (108) of martensitic regions which consists of fine laths of martensite. Because of the similar shear directions (100) and low-angle boundaries of martensitic laths, only packet boundaries respond to etching. For this reason, the microstructure appears to consist of blocks of non-etched regions. Similar observations are presented in Chapter 3. Although it was once customary to use surface rumpling as an indication of martensitic reaction, Gordon Parr (101) suggested that this criterion was not a fair indication of the transformation mechanism.

To reduce the confusion about terminology, Krauss and Marder (109) proposed the term "lath martensite" for the martensitic structure produced in low carbon steels. This structure had been referred to as massive or low-carbon

martensite, or as high-temperature martensite. Acicular or low-temperature martensite was proposed to be called "plate martensite". Plate martensite forms at lower temperatures than lath martensite, and that is because of a high carbon content or other alloying elements in the steel. These two terms - lath martensite and plate martensite - have been accepted by many investigators.

2.0   EXPERIMENTAL PROCEDURES

2.1   As-Received Plates

2.1.1   Geometry and Chemistry

David Taylor Research Center (DTRC) supplied five plates with three different chemistries for this project. Plates were melted as experimental heats at the USS Technical Center, hot-rolled and air cooled. The general designation for these plates is 8902-8025. The specific designation for each chemistry and the dimensions of each plate *are shown in* Table 2.1:

Table 2.1 The specific designations and the dimensions of the as-received plates.

Designation	Dimensions (mm)	Dimensions (in)
A3	254x165x19	10x6½x¾
A4	267x203x19	10½x8x¾
B3	267x197x19	10½x7¾x¾
B4	260x197x19	10¼x7¾x¾
C4	254x197x19	10x7¾x¾

Ladle and product chemistries were provided by the USS Technical Center. Additional chemical analyses of the steel

products were performed at the Colorado School of Mines

(CSM) and at the USS Technical Center, using emission

spectroscopy and Leco interstitial analyses. The emission

spectroscopy and interstitial analyses were conducted at

various points on each plate, ranging from the edge to the

center of the plate. The resulting compositions are

reported in the Chapter Three. Because the compositions of

the plates A3 and A4 and those of the plates B3 and B4 are

identical, they were recorded by using the names A for A3

and A4, B for B3 and B4, and C for C4. It should be

mentioned that plate C in the as-received condition was bent

and contained a number of cracks.

2.1.2   General Structure

A long sample (half the width of each plate) was

examined to reveal the possibility of any variation in

general microstructure and grain size as a function of

position (Figure 2.1). Standard metallographic techniques

were employed in preparing the specimens. After cutting and

grinding the samples to a 600 grit finish, they were

polished with 6 μm diamond paste. After the remainder of

the diamond paste was cleaned from the surface of the

specimens, they were polished on microcloth with 1 μm and
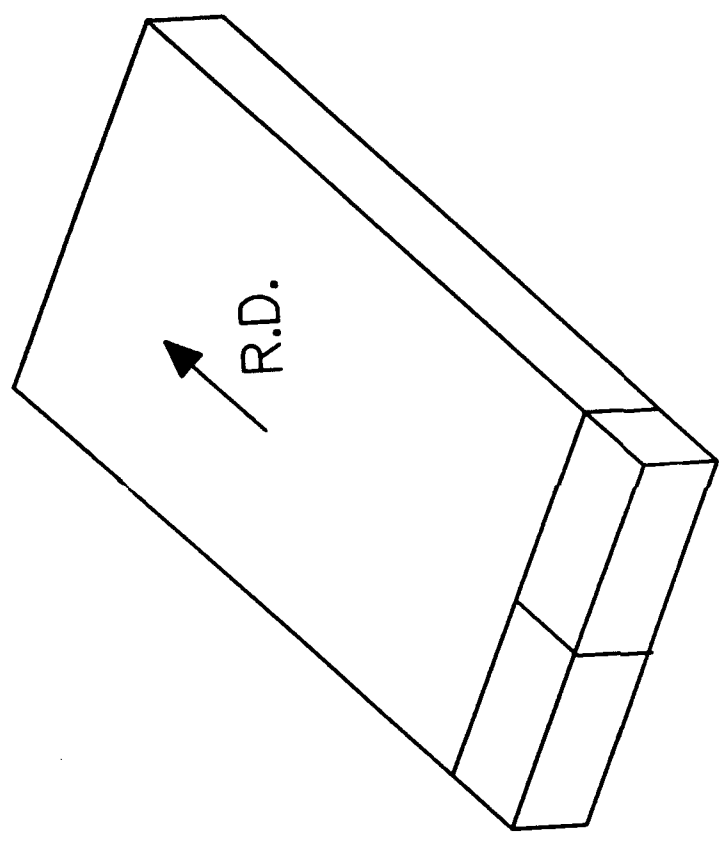
Figure 2.1   Blanks cut to examine the variation in the microstructure and grain size.

0.05 μm alumina powder. A solution of 2% nital was used to etch the above samples.

2.1.3   Inclusions

To determine the morphology, comparative number density, distribution and chemical composition of inclusions in the as-received plates, samples from all three steels were cut as shown in Figure 2.2. The above samples were then mounted in bakelite, polished using standard procedures, and examined with a Neophot 21 metallograph. In addition, energy dispersive spectroscopy (EDS) in the scanning electron microscope (SEM) was used to determine the chemistry of the inclusions observed in these steels.

2.1.4   Hardness Testing

Hardness testing was conducted on specimens from the as-received steels. One piece, the same as that shown in Figure 2.2, was cut from each plate and surface ground to a 600 grit finish. A Leco Hardness Tester (model R-600) was used to obtain the hardness measurements (110). The average of measurements on eight areas of each sample were taken, and reported as the Rockwell C Hardness Number (HRC).

R.D.

Metallography surface
(Transverse Plane)
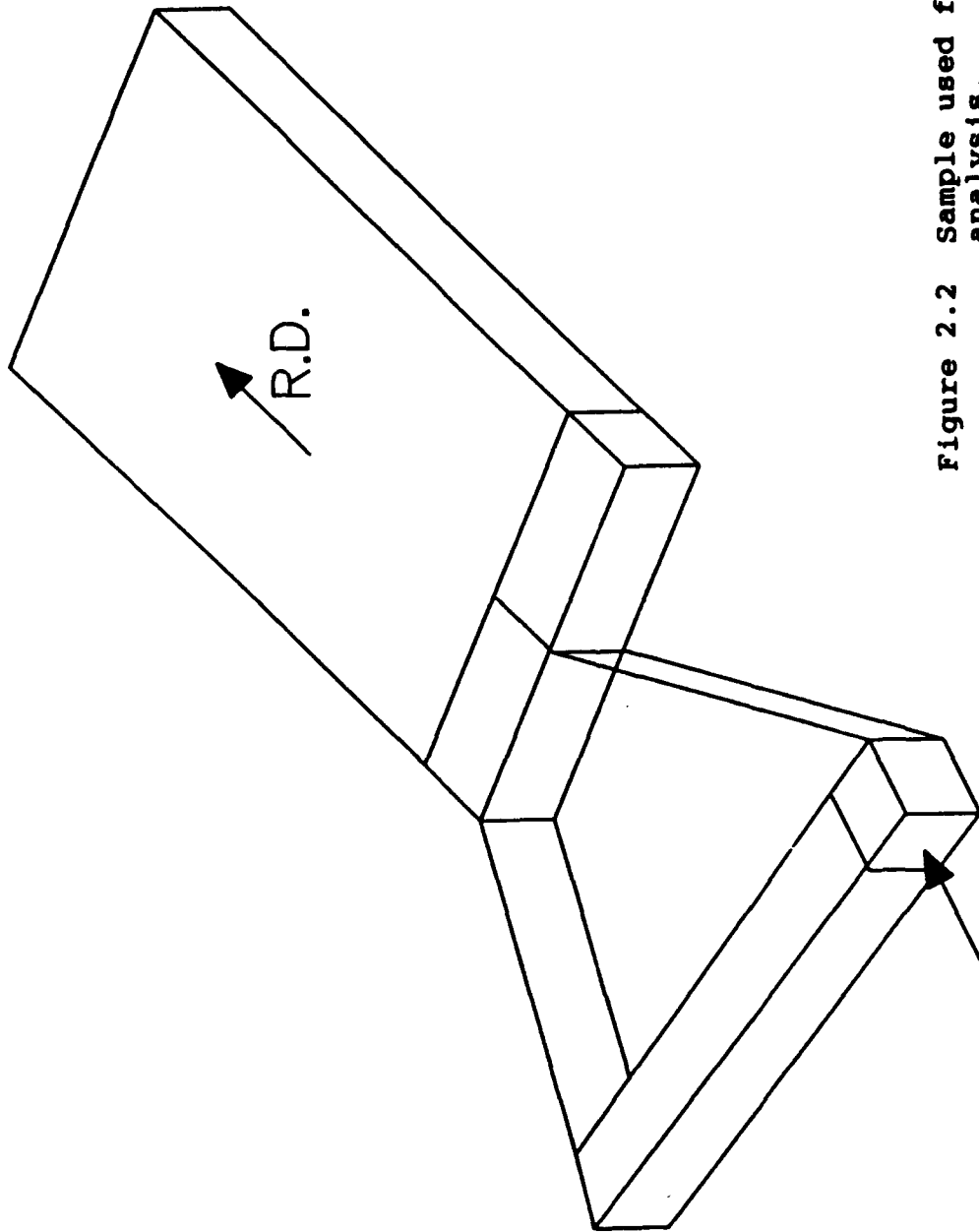
Figure 2.2 Sample used for inclusion analysis.

2.2 Ac_1 and Ac_3 Determination

In an attempt to study microstructural evolution in these steels, pieces from the as-received plates (as documented in the previous section) were used as the basis for further study. The temperatures at which austenite starts to form and finishes forming during heating, Ac_1 and Ac_3, respectively, were determined. A thermomechanical test system, Gleeble 1500, was used for this study. This system will be described in detail in section 2.4.1.

As shown in Figure 2.3, cylindrical samples were machined from each steel to a size of 105 mm (4 inches) in length and 6 mm (0.25 inch) in diameter. These samples were then heated up to 1200°C at the rate of 3°C per second (111) and cooled to room temperature at a rate of 50°C/s. The dilatometric data and the corresponding critical temperatures for all the three steels, as well as the calculated data, are given in the Chapter 3. Microstructures, prior austenite grain sizes and hardness values of specimens cooled at various rates were examined in detail.
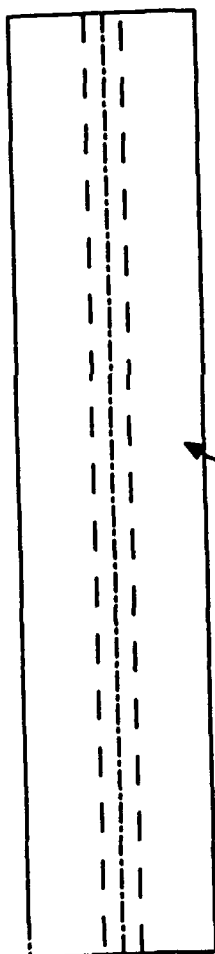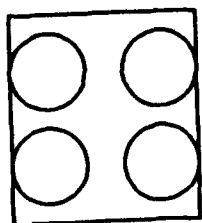
Transverse Plane

Figure 2.3   Samples used for Ac_1 and Ac_3 determinations.   Note that the center-line segregation was avoided.

2.3   Prior Austenite Grain Size

2.3.1   Introduction

Grain size is one of the most important factors in determining the strength and toughness of steel products. One of the goals of this research program is to compare as closely as possible the transformation behavior of a low-carbon modified A710 steel (20) with the present alloys. Colvin (20) used 905°C as the austenitizing temperature for his study, and determined that an austenite grain size of about 10 to 15 μm was generated after 5 minutes holding at this temperature. He also found that longer holding times do not have a noticeable effect on the grain size.

2.3.2   Heat treatment

Small coupons (19x19x3 mm) were cut from each steel using a band saw (Figure 2.4). Various heat treatments were conducted in salt baths or muffle furnaces, and because the results of the muffle furnace method were reproducible, this method was chosen for the rest of study.

At the first stage of these heat treatments, six samples from each steel were used. Samples were soaked in
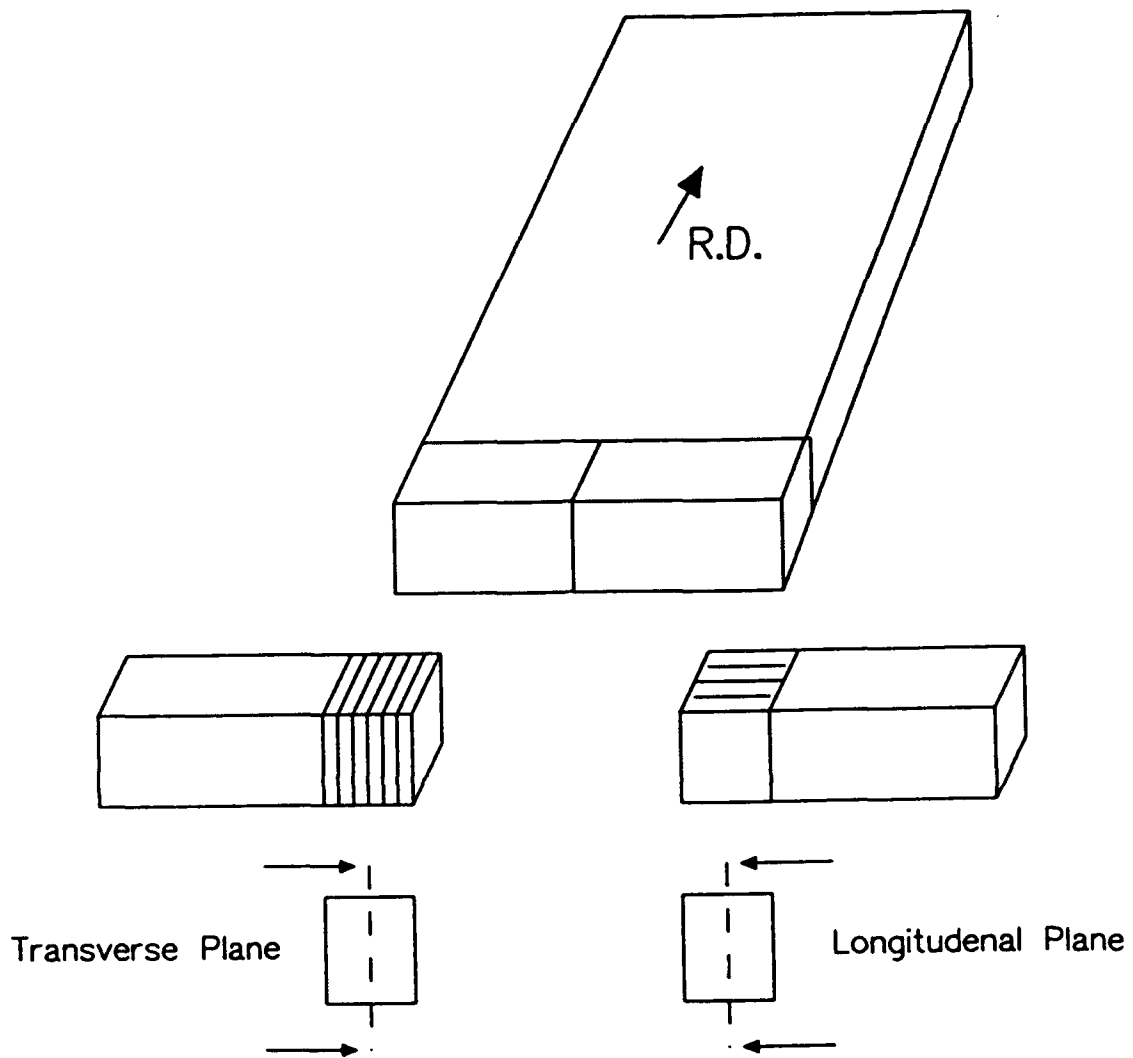
Figure 2.4   Wafers used for grain size studies.

the salt pot at 905-910°C for $\frac{1}{2}$, 2, 5, 15, 30 and 60 minutes
and then water-quenched. These samples were designated A1-
A6, B1-B6 and C1-C6.

The results of these treatments showed that a holding time
of 905°C does not have a noticeable effect on the grain
size. A five minute holding time was chosen. Since the
goal of a 10-15 μm grain size was not achieved, new heat
treatment schedules were designed. These treatments
included reaustenitizing at 905°C, followed by water
quenching and/or air cooling. Another important factor was
the composition of the steels. For the sake of comparison
with other research programs at CSM, steel B (which contains
1.5% Mn) was chosen for the rest of study. These heat
treatments are shown in Figure 2.5 and the results are
presented in Chapter 3.

Specimen preparation for optical microscopy was done as
described before. Chemical etching was very difficult.
Eventually several etching and staining solutions were used.
The best way found to reveal the prior austenite grain
boundaries for these steels was a combination of the
following etchants and back polishing technique.

1. 50 ml of Nital 2%, two drops of each H_2SO_4 and H_2O_2.

2. Saturated picric acid and wetting agent.

The first etchant was developed experimentally and works the
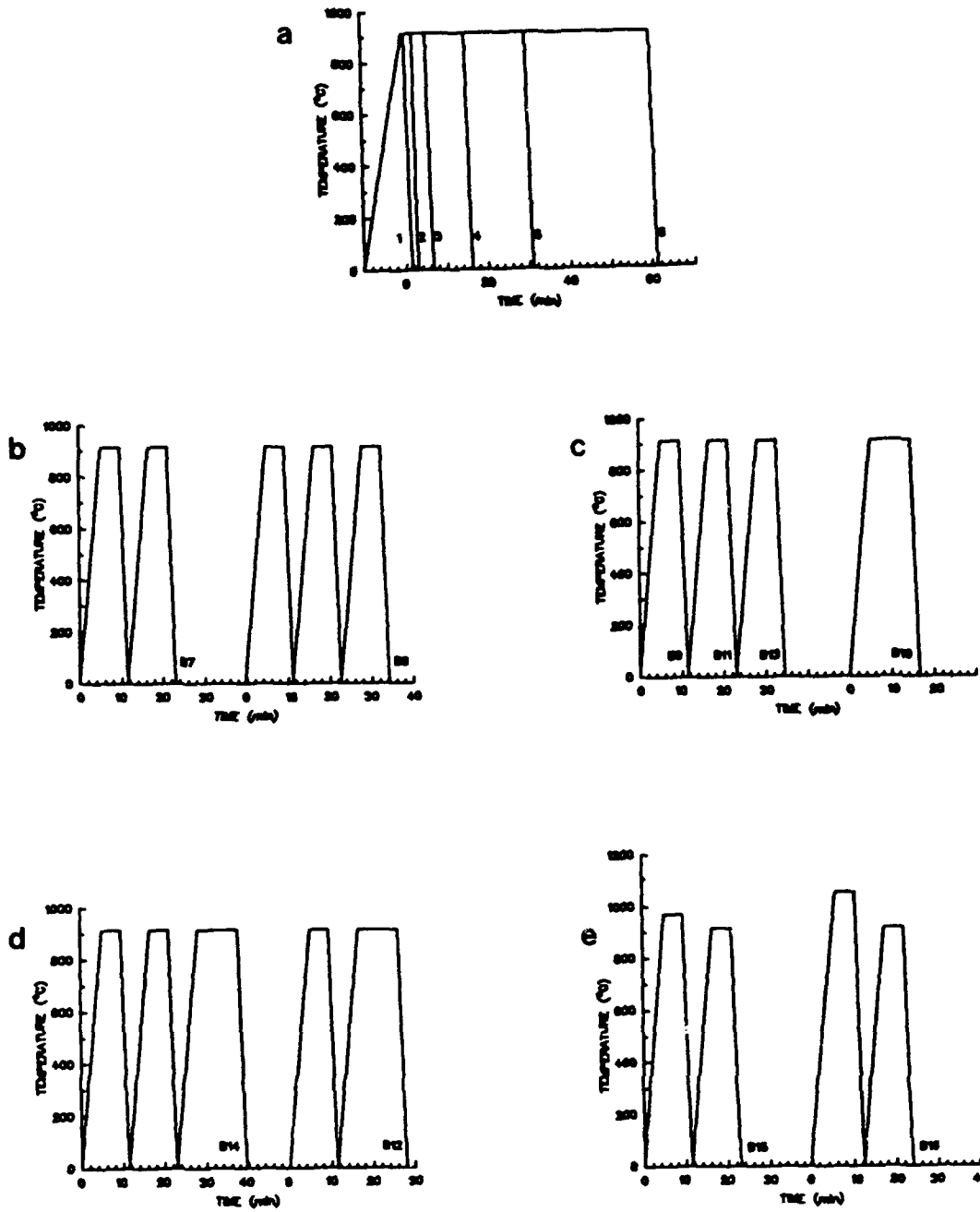
Figure 2.5   Different heat treatment schedules for grain
             size study.
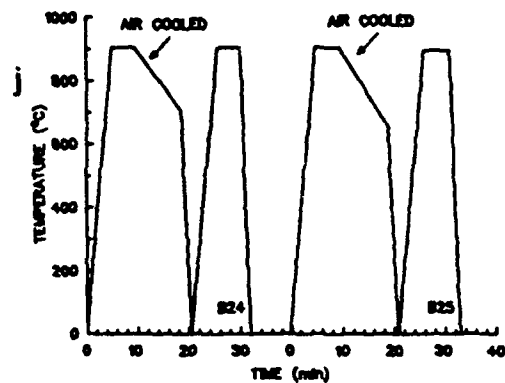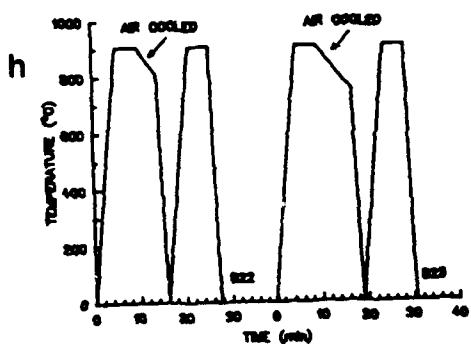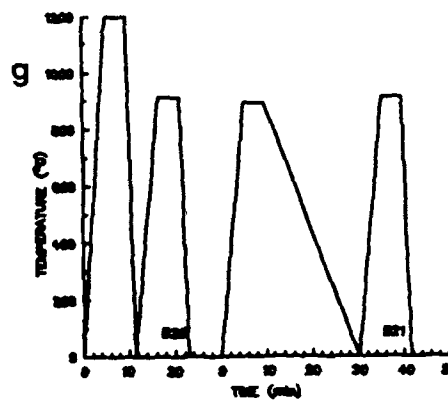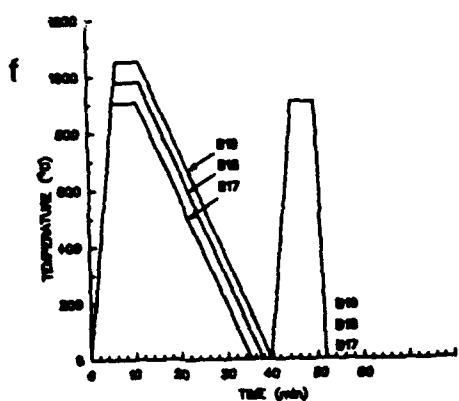
Figure 2.5   (continued)

best in conjunction with back polishing. Tempering at 450°C

for 24 hours is sometimes helpful to reveal the prior

austenite grain size. The second etchant has the best

effect on small-grain-size samples. The average grain size

was determined by standard linear intercept method

techniques (112-115).

2.4   Transformation Kinetics

2.4.1   Gleeble 1500

The Gleeble 1500 is a computer controlled

thermomechanical test system which has been designed for

both thermal and mechanical testing simultaneously (116).

The thermal capability of the Gleeble 1500 was used

exclusively for the current study.

Since electric resistance heating produces a more

uniform temperature zone than induction heating (Figure

2.6), the Gleeble 1500 has been designed to take advantage

of electric resistance heating, although it is possible to

use induction heating as well. In the case of induction

heating, the magnetic field generated by a high frequency

current passing through a coil produces heat inside the

material at the core of the coil. By contrast, electric

resistance heating consists of passing an electric current
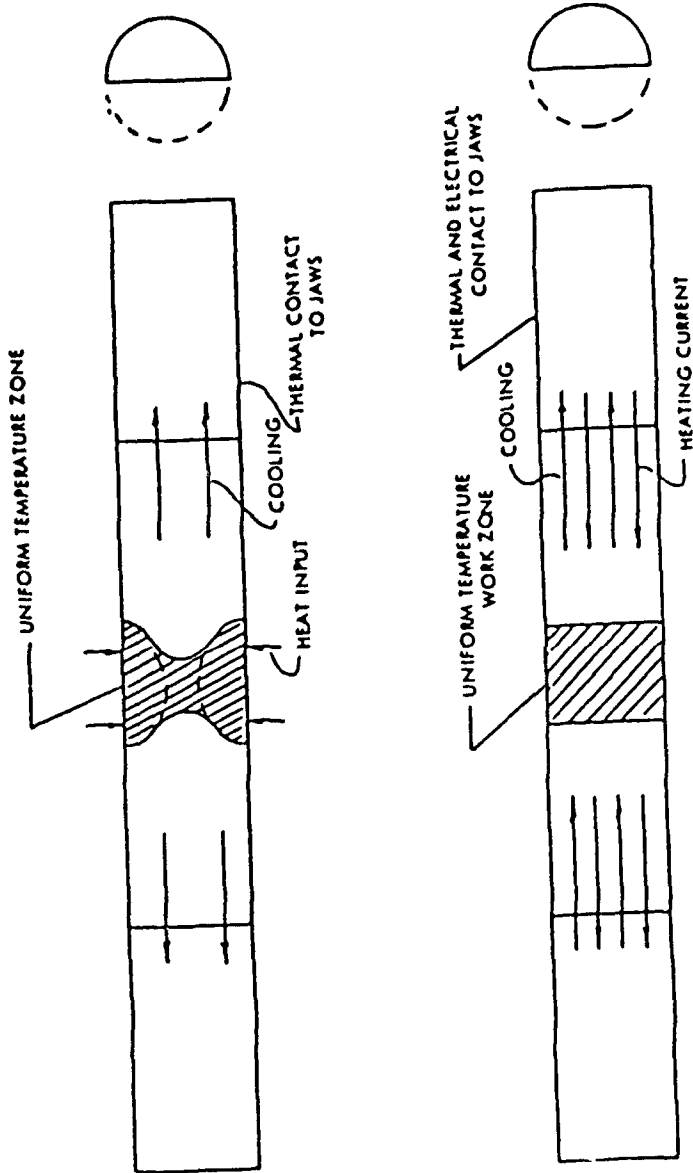
Figure 2.6 Schematic diagrams showing the uniformity of temperature zone in: induction heated/conduction cooled (top), and electric resistance heated/conduction cooled (bottom) specimens (116).

through a metallic specimen, where the resistance of the material to the flow of current generates heat.

Distribution of this current in the test sample is controlled by the cross section of the specimen and the water-cooled copper jaws which are used to mount the specimen. Although water-cooled jaws cause the heat to flow through the length of the specimen, Figure 2.7 (116) shows that radial conduction cooling is practically zero and causes no temperature gradient through the cross section of the sample. This means a uniform temperature along the cross section of the work zone, which is illustrated in Figure 2.8, (116). Considering electric resistance heating and conduction cooling, the flat thermal profile can be maintained even if the heating rate exceeds 20,000°C/sec (116).

Because the measurements of temperature and dilation are taken across an isothermal plane, alumel and chromel wires must be welded to the center of the specimen's midspan very carefully. When electric current flows through these thermocouple wires, the instant temperature of the midspan will be transferred to the computer. For working temperatures up to 1200°C, alumel and chromel make an ideal thermocouple for most of materials.

A C-strain (circumferential strain) fixture
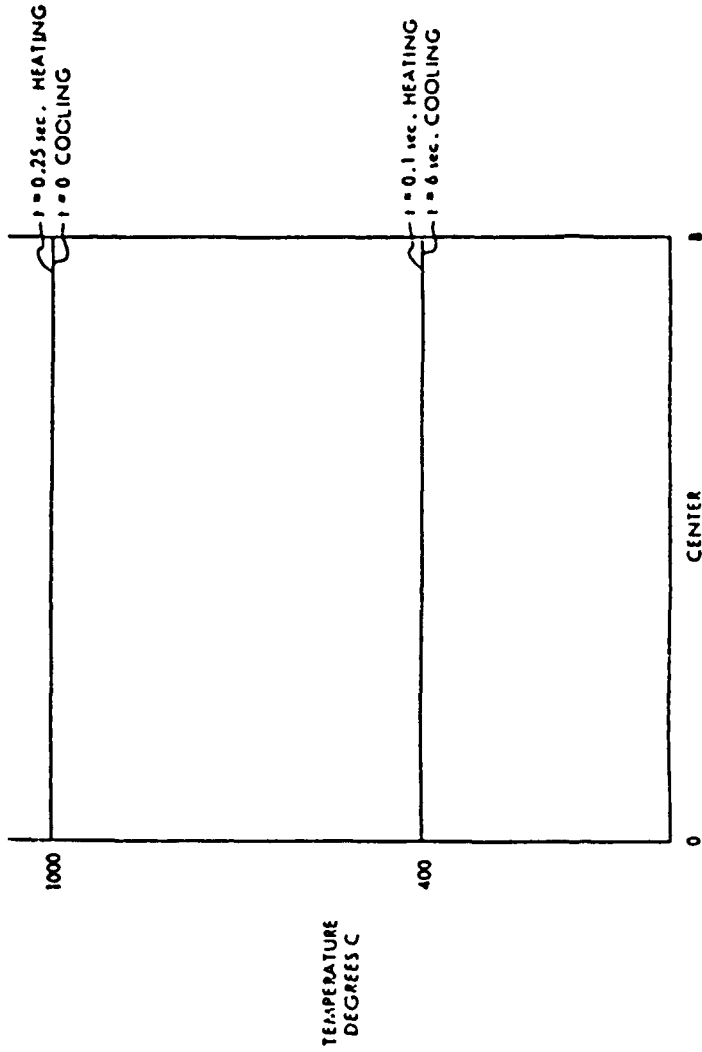
Figure 2.7 Radial temperature gradient for an austenitic stainless steel subjected to electric resistance heating and axial conduction cooling. Heating rate: 4000°C/s, cooling rate: 100°C/s (116).
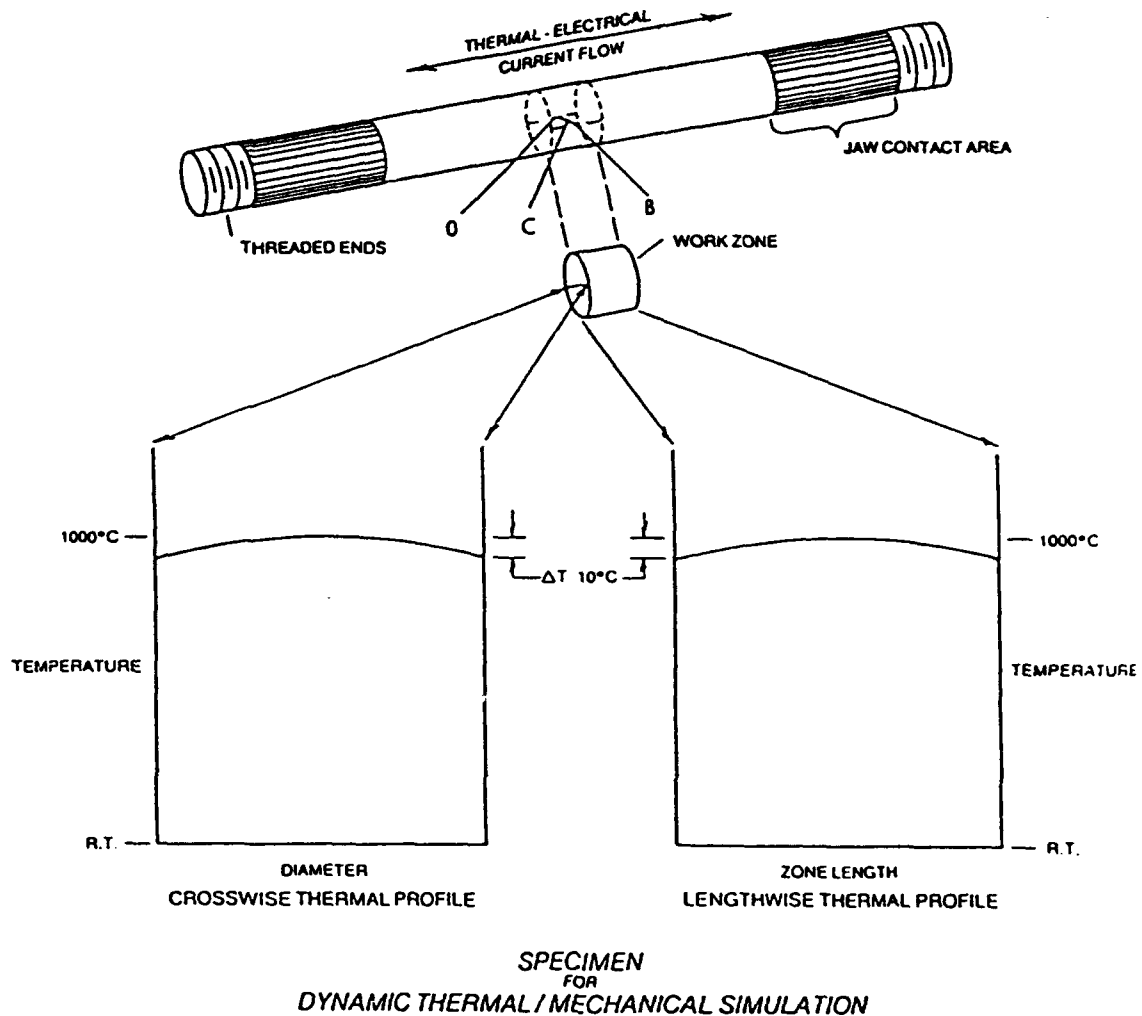
Figure 2.8   Schematic diagram showing the electric
             resistance heating of a sample used in the
             Gleeble.   Uniform heating is produced across the
             work zone length and diameter (116).

(dilatometer) measures the strain in the isothermal plane.
The resolution of the transducer used for these measurements
is essentially infinite (116). The method of mounting of
the C-strain fixture is very important. To get the best
results, the dilatometer should be mounted as tightly as
possible, to guarantee measurement of very small
displacements.

The atmosphere of the test can be changed, depending on
the desire of the researcher. Argon and helium gas are the
most common types of atmosphere used for CCT tests.
A data acquisition system and ASYST data manipulation
software have been installed to the system available at the
Colorado School of Mines.

2.4.2   Sample Geometry

The geometries of the samples used in this study were
determined based on previous and current work done at the
Colorado School of Mines (20,38). The most important
factors to consider when choosing a certain geometry are
axial cooling capacity of the samples, without using any
further aid such as gas cooling and so on, as well as
maintaining an isothermal plane during heating and cooling.

Figure 2.9 shows the four different geometries that
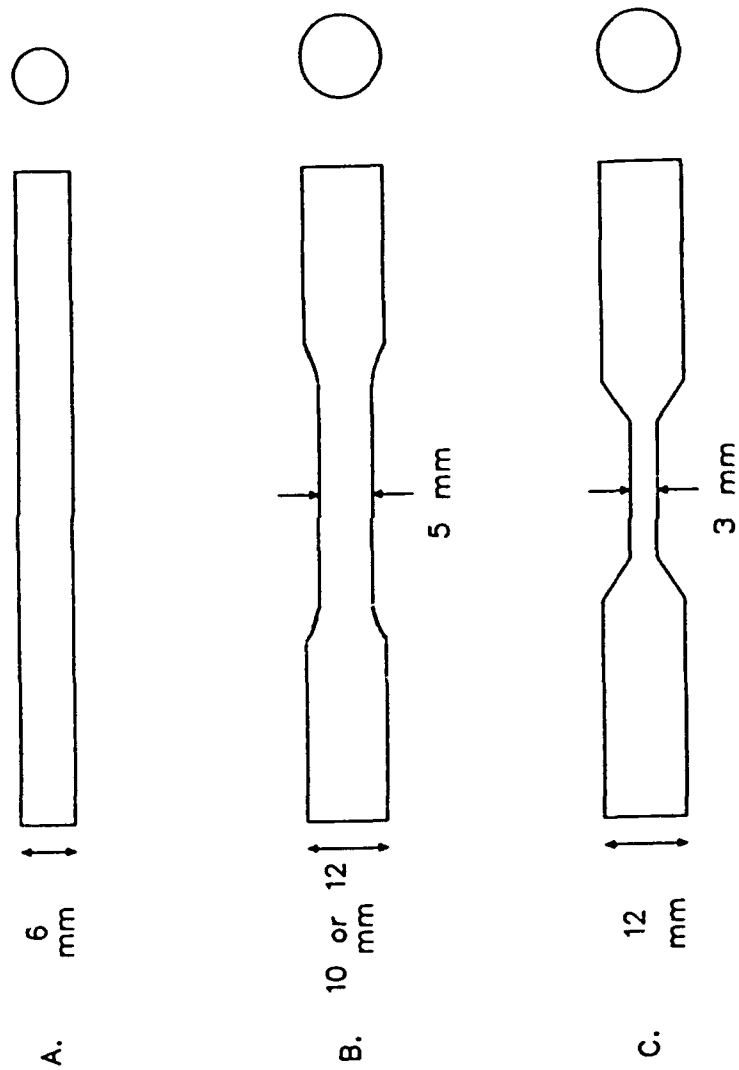
Figure 2.9   Geometry of Gleeble samples.   (a) Cooling rates ≤ 10°C/s.
(b) (10 mm) 10°C/s ≤ C.R. ≤ 25°C/s, (12 mm) 25°C/s ≤ C.R. ≤ 75°C/s.
(c) C.R. ≥ 75°C/s.

were used in this study. Type A was used for slow cooling rates (below 10°C/sec), while type B (10 mm) was observed to be more suitable for intermediate cooling rates between 10°C/sec to 25°C/sec. For cooling rates between 25°C/sec up to 75°C/sec type B (12 mm) was used, and type C was used for fast cooling rates above 75°C/sec. In this way, good agreement between the actual temperature and the program temperature was obtained (38).

To avoid the center-line segregation bands, machining of the above samples was designed to be off-centered. Figure 2.9 shows more details about the dimensions and design of these specimens.

2.4.3   Dilatometry as a Function of Heating and Cooling Rate

It is well known that the transformation temperature in both heating and cooling is affected by the rate of input or output of heat (40,116,117). It has been suggested (117) that heating rates of 2 to 3°C/sec do not change the transformation temperatures. Considering the above facts, 3°C/sec was chosen as the heating rate throughout the experiments. Since the exponential cooling is more close to reality than linear cooling, an exponential cooling program

(20), similar to those calculated with the Newtonian formula
(118), was used for this research. The program considers
the austenitizing temperature, upper and lower boundary
temperatures and time between these temperatures to simulate
the desired exponential cooling rates. Because most of the
austenite transformations in hypoeutectoid steels occur
between 800°C and 500°C (111,118), the time interval between
these temperatures (Δt_{8-5}) is a base for calculation of the
cooling rate. These temperatures were chosen as upper and
lower boundaries for cooling programs.

2.4.4   Dilatometry

Determining transformation temperature has
traditionally been done through measurements of the magnetic
properties of a material, or by measuring volume change
taking place during the transformation (111). The latter
method is preferred by many investigators (111), and was
used in the present work.

In the process, radial contraction of the midspan for
each specimen as a function of the actual temperature was
measured. Dilatometric measurements were conducted using a
dilatometer that has been designed by Duffers Inc. for the
Gleeble 1500. It is also important to note that proper

insulation or water cooling should be used to protect the transducer at working temperatures higher than 900°C.

2.4.5   Testing Procedure

Thermocouple wires and a C-strain fixture are the two most important accessories in these tests. To guarantee proper attachment of the above accessories, all the test specimens were polished with a 600 grit silicon carbide paper and then cleaned with ethanol. To maintain good electric contact, copper grips were checked and cleaned. After putting a ceramic insulator on thermocouple wires prior to each test, they were attached to the proper switch. The dilatometer then was placed on the center of the midspan opposite the thermocouple. The test chamber was evacuated after a chamber cover was put in place. This process was continued by purging argon gas into the chamber. After filling the chamber with the argon gas and maintaining a positive pressure, evacuation took place one more time, followed by a second argon gas purging. When the chamber pressure reached a level slightly above the atmosphere pressure, a safety valve was opened to maintain constant pressure inside the chamber. The above procedures prevent samples from being oxidized or decarburized.

Samples were heated at a rate of 3°C/sec to an austenitizing temperature of 905°C for steels B and C, and 920°C for steel A. Each sample was held at the proper temperature for 5 minutes prior to cooling. Basically, two CCT diagrams were generated for steel B based on prior austenite grain size.

A single cycle (1X) of austenitizing corresponded with a prior austenite grain size of about 30 μm; 2X meant a double-cycle austenitizing treatment and corresponded with about a 7 μm prior austenite grain size. Cooling rates varied between 150°C/sec and 0.05°C/sec.

The dilatometric data for each test of steel B were plotted versus actual cooling temperature. Therefore, for each cooling rate, there are at least two sets of data based on two starting grain sizes. Five cooling rates were chosen to examine the relative position of CCT diagrams for steels A and C with respect to steel B.

Transformation start and finish temperatures were determined by drawing tangents to C-strain versus temperature curves. An excellent guide to this practice is given by Eldis (111). The times and temperatures which correspond to 25%, 50% and 75% transformation of austenite were also measured graphically using the dilatometric graphs (Figure 2.10).
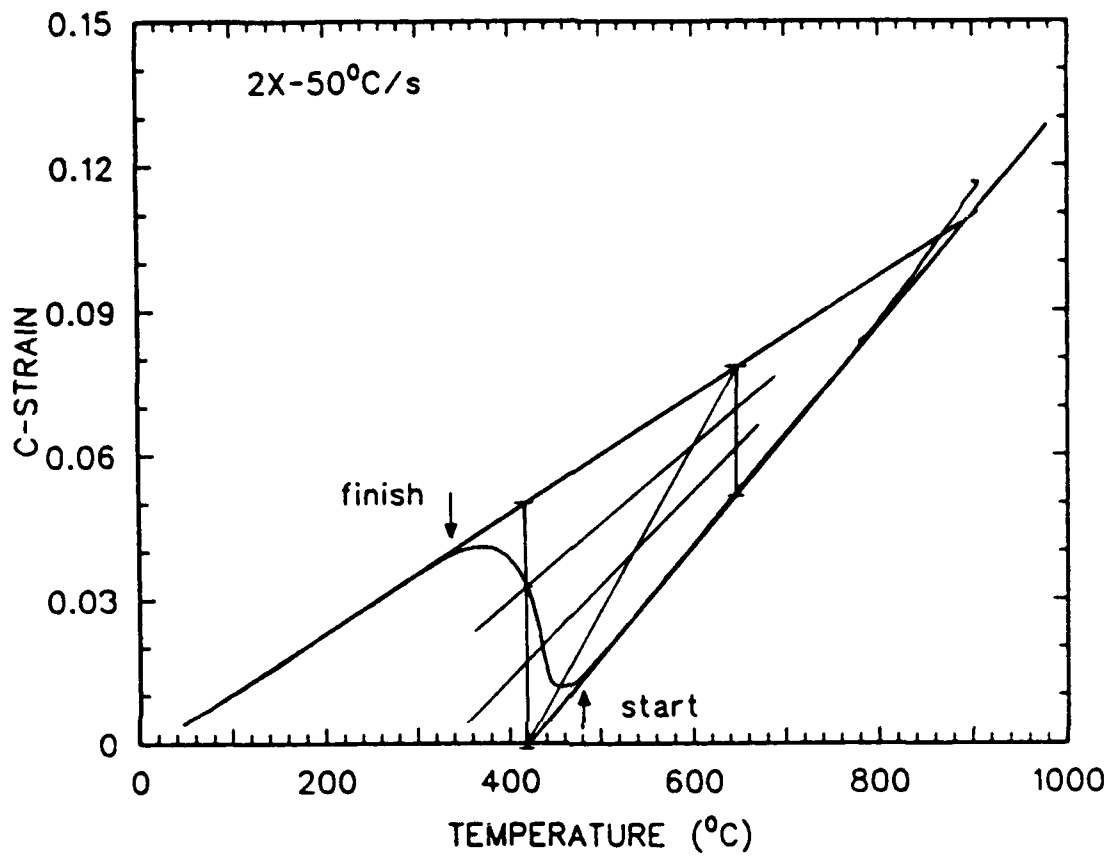
Figure 2.10   Graphical measurements of the 25, 50 and 75 percent transformation temperatures.

According to Eldis's studies (111), the uncertainties in the transformation start and finish temperatures recorded for any cooling curve are as much as $\pm$ 5°C and $\pm$ 35°C, respectively. The high uncertainty number for the finish temperature has been observed when there is a marked curvature in the C-strain versus temperature data.

Following each test, a diamond saw was used to cut each sample from the middle of the dilatometry sample (as close to the isothermal plane as possible.) After mounting and polishing, the small samples were examined microstructurally, and microhardness was determined.

2.5 Microhardness Measurements

Diamond pyramid hardness (DPH) measurements were conducted according to ASTM specification E92-82 (119) on a Leco microhardness tester (model M-400A). A 500-gram load was used throughout the tests. The average of at least ten measurements is given as the overall hardness of each specimen. These values (Vickers hardness numbers (VHN)) were plotted versus log (Δt_{8-5}) to produce a hardness profile.

2.6   Microstructural Characterization using SEM and TEM

In addition to optical microscopy, scanning electron microscopy (SEM) was performed with a JEOL JXA 840 electron probe micro-analyzer. Samples were coated with gold to 300 μm thickness to reduce the charging effect.

Transmission electron microscopy (TEM) was performed using a PHILIPS EM400. Three specimens for examination by TEM were sliced from the middle of each Gleeble sample to a thickness of 0.20 to 0.40 mm using a Buehler Isomet saw, as shown in Figure 2.11.
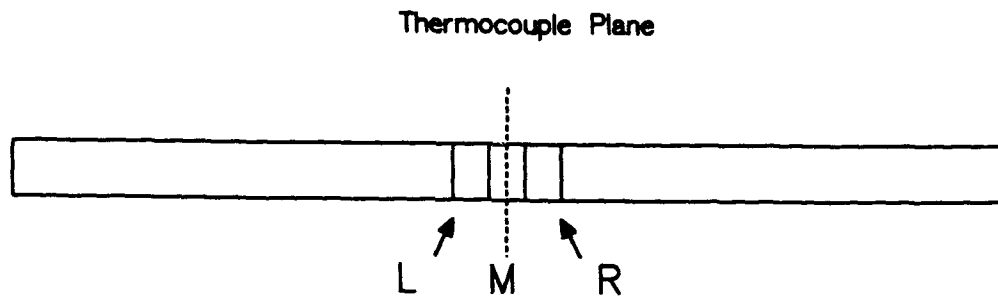
Figure 2.11   Positions of the wafers cut for TEM studies
               relative to the position of the thermocouple
               (L: left, M: middle, R: right).

Some wafers from the as-received steel B were also cut to be examined by TEM. The above specimens were then mechanically thinned on 600 grit silicon carbide paper to about 0.2 mm. Three-mm discs were punched except for the samples with 3-mm reduced section. These discs were thinned

mechanically by the same technique as before to approximately 0.06 mm. Care was taken during the mechanical cutting and thinning processes in order not to induce heat or deformation into the specimens.

A Fischione twin-jet electropolisher was used for further thinning of the foils. Two different solutions were used in order to get the best results. The first solution consisted of 95 volume percent acetic acid and 5 volume percent perchloric acid. The discs were thinned to perforation at room temperature with 80 volts and 80 milliamperes. Microscopy was performed at an accelerating voltage of 120 kV. Bright field (BF) and centered dark-field (CDF) imaging techniques were employed in addition to the generation and analysis of selected-area diffraction patterns (SADPs). The quality of foils was fair.

A second solution was used which consisted of 70 volume percent ethanol, 25 volume percent glycerol and 5 volume percent perchloric acid. This solution improved the quality of the foils slightly.

2.7   Tensile Testing

Six blanks from each steel were cut with a band saw and heat treated prior to machining (Figure 2.12). Heat
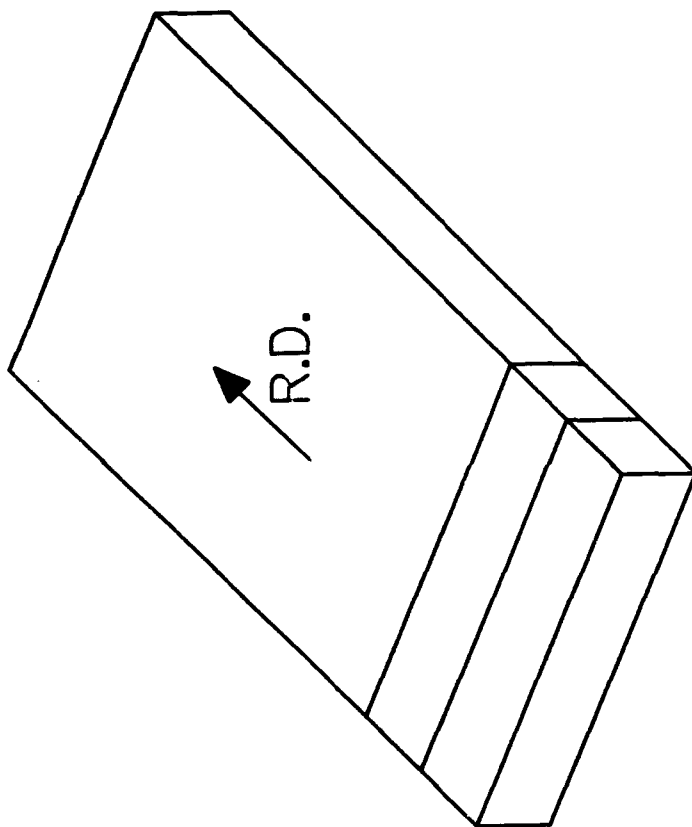
Figure 2.12 Orientation of tensile bars and Charpy bars relative to the rolling direction.

treating was conducted in a muffle furnace at 905°C for steels B and C, and at 920°C for steel A. The austenitizing time was five minutes for each sample. Three samples from each steel were air cooled after five minutes of heat treating, and they are designated as 1X. The remaining three samples from each steel underwent two rounds of austenitizing, of which the first round was followed by water quenching and the second round by air cooling. These samples were designated as 2X. To maintain a 1°C/sec cooling rate, each sample was placed between two plates to simulate a total thickness of one inch.

In addition to the above samples, six extra blanks from steel A were cut and underwent the same heat treatments as well as 35 minutes tempering at 620°C for each sample. These samples were designated AT-1X and AT-2X. Off-centered machining was conducted on all of the specimens to avoid the segregation line. Standard, round-bar tensile specimens were machined to ASTM specification E8-82 (120). Tests were performed on an Instron screw machine located at the Colorado School of Mines. Cross-head velocity was set at 0.02 mm/sec (0.05 in/min). A 25.4 mm (1 inch) extensometer was used to measure displacement. Load-displacement data were plotted directly on a strip-chart recorder. This chart was used to determine the 0.2% offset

yield point and ultimate tensile strength (120,121). In
addition to the strip chart recorder, load-displacement-time
data were collected on a Compaq 386-SX PC which is equipped
with a Labtech Notebook software.

2.8   Charpy Impact Testing

Charpy V-notch specimens were machined according to
ASTM specification E23-82 (122) after being heat treated.
Blanks were cut from each steel as shown in Figure 2.12.
These samples were then heat treated as explained for
tensile specimens and were designated 1X and 2X, depending
on the number of reaustenitizing treatments. Extra
specimens from steel A were tempered for 35 minutes at 620°C
after the aforementioned heat treatings and designated as
AT-1X and AT-2X.

The heat-treated specimens were then machined in
transverse orientation, with the notch perpendicular to the
rolling plane (the T-L orientation). In this way, the crack
will propagate in the rolling direction during testing.

For Charpy V-notch testing, temperatures higher than
room temperature were achieved in a hot oil bath, while
temperatures below 0°C were obtained with a mixture of
ethanol and liquid nitrogen. Ice water was used for tests

at 0°C. Specimens were held at the test temperatures for a
minimum of seven minutes and were broken within three
seconds after being taken from the bath. The absorbed
energy on impact was directly read from the Charpy impact
machine dial. Samples were then preserved for further study
by spraying lubricant on the broken surfaces.
To determine the ductile-to-brittle transition, CVN energy
data were plotted versus test temperatures.

2.9 Fractography

Fractography was performed on six samples from steel B.
Three samples from 1X condition and three samples from 2X
condition were each chosen from the upper shelf (100°C test
temperature), transition region (room temperature) and lower
shelf (liquid nitrogen temperature). A JEOL JXA-840 scanning
electron microscope (SEM) was used. Pictures were taken at
three different magnifications of 500X, 1000X and 2000X from
each sample.

3.0 RESULTS AND DISCUSSION

3.1 As-Received Plates

The chemical compositions, general microstructures, inclusion contents and hardness values of all the as-received steels are presented in this section. Chemistries of the three as-received steels are reported in Table 3.1. For each steel, no variation in chemical compositions was observed (considering the size of the probe) through the width of the plate.

All of the three steels exhibited very large, unrecrystallized prior austenite grains at the plate edges. These grains were limited to regions of about two centimeters from the edges, and these regions were avoided in further studies. Segregation in the form of wide, white (difficult-to-etch regions) bands was present, to some extent, at the centerline of all steels. The effect was most pronounced in steel C, which has the highest manganese content. This phenomenon was probably due to manganese and/or molybdenum and nickel segregation. Off-centered cuttings were designed, when it was necessary, to avoid the segregation bands.

Light microscopy and SEM were used to determine the

Table 3.1 Chemical Compositions of Steels.

STEEL/ANALYSIS	C	Mn	Mo	Ni	Nb	Cr	Si	S	P	Al	Ti	N	O
A/USS-L	.022	1.00	3.51	3.40	.061	.230	.200	.003	.001	.015	.010	.010	.006
*A/USS-P	.025	1.00	3.67	3.57	.054	.230	.200	.003	.005	.013	.010	.010	NA
A/CSM-P	.012	1.08	3.47	3.34	.062	.273	.277	.003	.007	.003	.009	NA	NA
B/USS-L	.023	1.47	3.46	3.35	.061	.230	.220	.003	.002	.011	.006	.010	.006
*B/USS-P	.024	1.45	3.62	3.55	.055	.230	.180	.003	.005	.009	.009	.010	NA
B/CSM-L	.010	1.55	3.34	3.18	.063	.270	.329	.003	.008	.003	.007	NA	NA
C/USS-L	.023	2.00	3.44	3.34	.060	.230	.200	.004	.001	.010	.006	.009	.006
*C/USS-P	.020	1.76	3.58	3.47	.054	.230	.210	.003	.005	.009	.008	.012	NA
C/CSM-P	.012	1.97	3.16	2.98	.065	.277	.286	.004	.009	.004	.006	NA	NA

USS: U.S. Steel Technical Center
CSM: Colorado School of Mines
L: Ladle Analysis
P: Product Analysis
*: This analysis is considered to be the most accurate analysis.

morphology, distribution, relative number density and
chemistry of numerous inclusions in all three steels.
In general, all three steels contained three types of
inclusions: rectangular or square inclusions (which will be
referred to as type I), round or oval inclusions (type II)
and irregularly shaped, angular inclusions (type III).
All three steels exhibited large numbers of types I and II
inclusions. The relative numbers of type III inclusions
increased dramatically in going from steel A to steel B to
steel C.

Energy-dispersive-spectroscopy (EDS) analysis in the
SEM showed that the type I inclusions contained high
titanium levels. These could be titanium nitrides formed
during solidification. Type II inclusions showed high
manganese and sulfur levels, with some aluminum or silicon.
These inclusions are manganese sulfides, with the aluminum
probably present in the form of a small region of Al_2O_3, and
silicon as SiO_2. As shown in Figure 2.2, these observations
were made from transverse sections, and that explains why
these inclusions are not described as stringers (the
elongation of MnS is obscured in this section). The type
III inclusions were apparently clusters of type I and type
II inclusions. Figure 3.1 shows a light micrograph and two
SEM micrographs, which are representative of the observed
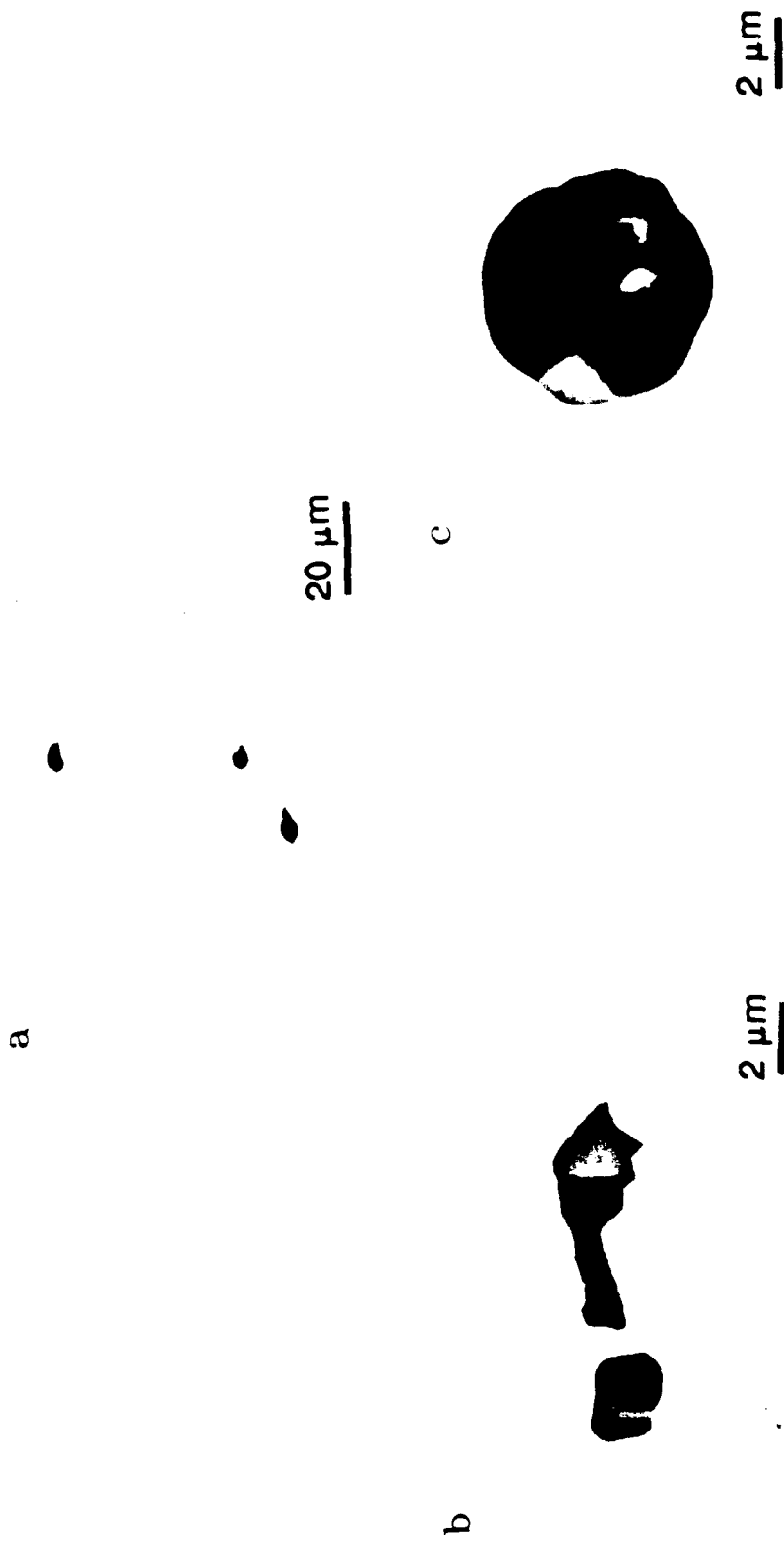
Figure 3.1 (a) Light micrograph showing MnS inclusions. (b) and (c) SEM micrographs showing Ti- and Mn-rich inclusion clusters.

inclusions. The EDS analysis of manganese- and titanium-
rich inclusions re shown in Figure 3.2.

Table 3.2 shows the as-received hardness values of the three

steels. The hardness increases by two HRC for each 0.5 wt.

pct. increase in manganese content. This trend could be

Table 3.2 Hardness of the as-received steels.

STEEL	HRC
A	30
B	32
C	34

explained by the role of mangenese as an austenite

stabilizer. By increasing the amount of mangenese in steel,

the austenite to ferrite transformation temperature as well

as the M_s temperature will decrease, which, in turn,

promotes smaller ferrite crystals, finer packet sizes, more

martensite and higher dislocation density. One or more of

these features are responsible for increasing strength and

hardness.

Figure 3.3 shows the microstructures of the as-received

steels A, B and C. At this magnification, the bainite-like
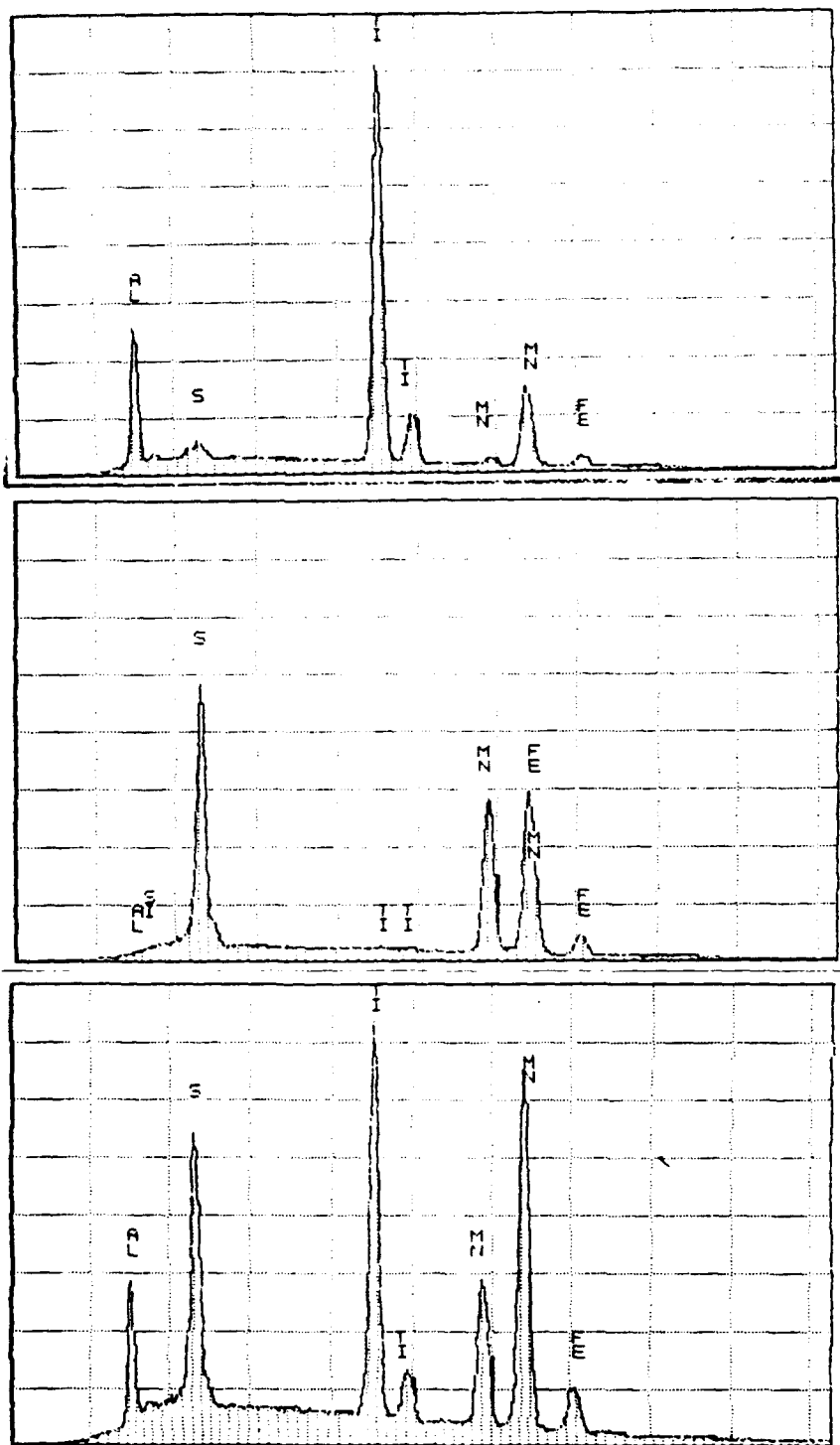
Figure 3.2   Representative of EDS spectra for inclusions in
             steels A, B and C.
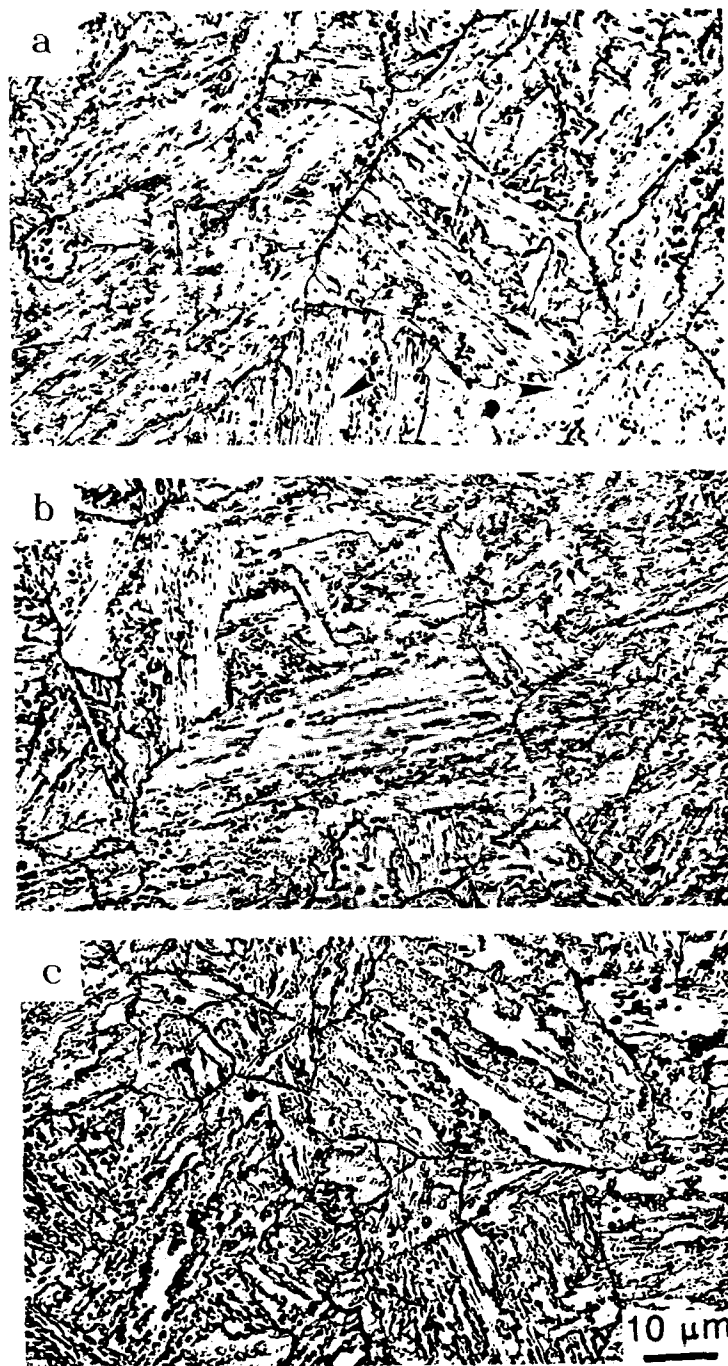
Figure 3.3   The as-received microstructures of (a) steel A,
(b) steel B and (c) steel C.   Light micrographs.

microstructures of all of these steels are clear.

Bainite consists of bainitic ferrite laths with interlath second-phase particles. The dark small particles are probably retained austenite or martensite. Because of the very low carbon content of these steels, these particles could not be considered as interlath carbides, since the volume fraction of these particles is too high to be carbides. This will be shown later in TEM micrographs. The high alloy content of these steels could be responsible for the presence of retained austenite.

3.2 Ac_1 and Ac_3 determinations

Empirical formulas were used to calculate the transformations from ferrite to austenite, upon heating. According to Andrews (123) the Ac_1 is given in (°C) as:

$$Ac_1 = 723 - 10.7 \text{ Mn} - 16.9 \text{ Ni} + 29.1 \text{ Si} + 16.9 \text{ Cr} + 290$$
$$\text{As} + 6.38 \text{ W} \qquad (3.1)$$

and the Ac_3 is given by:

$$Ac_3 = 910 - 203\sqrt{C} - 15.2\text{Ni} + 44.7\text{Si} - 104\text{V} + 31.5 \text{ Mo}$$
$$+ 13.1\text{W} - 30\text{Mn} - 11\text{Cr} - 20\text{Cu} + 700\text{P} + 400\text{Al}$$
$$+ 120 \text{ As} + 400 \text{ Ti} \qquad (3.2)$$

In both of the above formulas, all elements are in wt. pct.
These equations have been determined for certain ranges of
weight percent for each alloying element (123). Although
most elements were within the given ranges by Andrews, there
were two exceptions. The lowest carbon content used for the
above formulas was 0.08% and the highest molybdenum content
was 2.6%. Calculated values based on these equations as
well as experimental (measured) values are presented in
Table 3.3. The experimental values are based on
dilatometric inflections in the C-strain versus temperature
curves obtained for specimens heated up to 1200°C at the
rate of 3°C per second.

Table 3.3   Calculated and measured austenite formation
            temperatures for steels A, B and C.

Steel	Calculated		Measured	
	Ac_3 (°C)	Ac_1 (°C)	Ac_3 (°C)	Ac_1 (°C)
A	926	664	901	794
B	909	660	886	766
C	890	655	882	755

Figure 3.4 shows a plot of C-strain (circumferential strain)
versus temperature as obtained in the Gleeble for steel B.
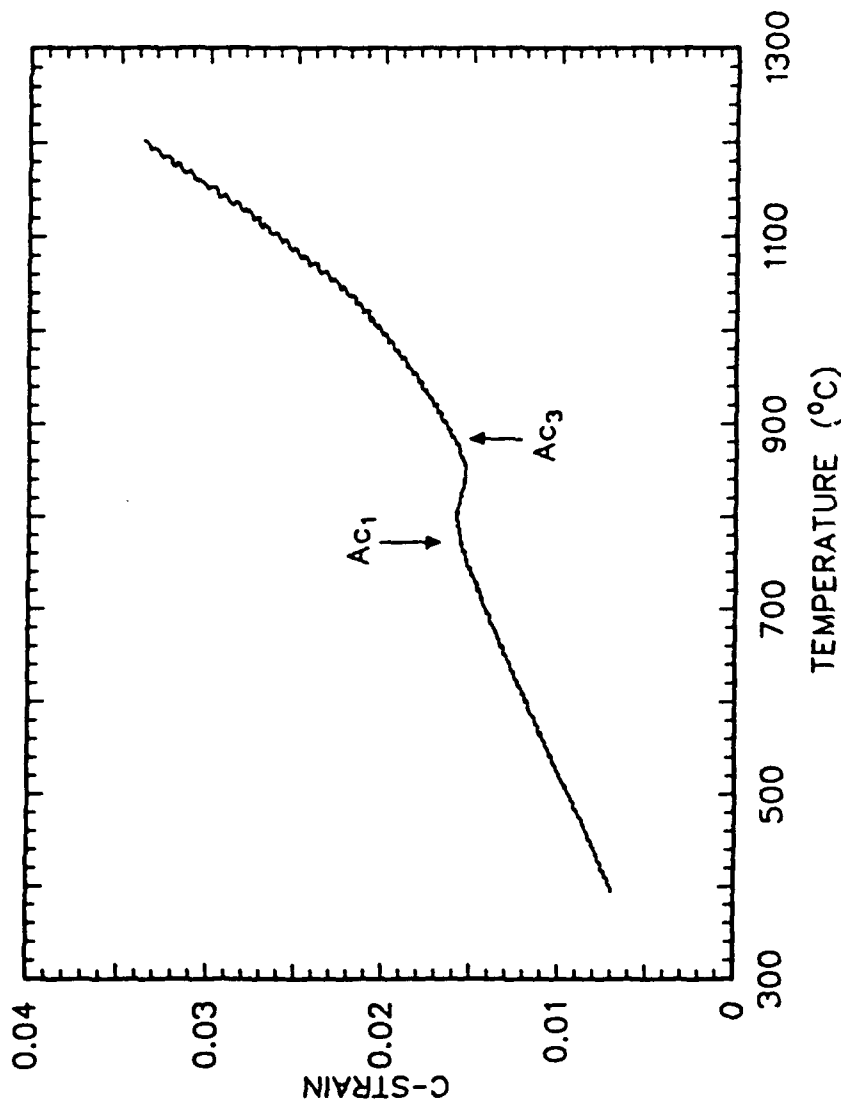
Figure 3.4 Dilatation curve for steel B. The specimen was heated up to 1200°C at a rate of 3°C/s.

The arrowed inflection points clearly define the start of austenite formation at low temperatures and the completion of austenite formation at high temperatures.

A comparison between calculated and measured critical transformation temperatures for all of the three steels shows inconsistency, especially for the lower critical temperatures. These are due to the lack of molybdenum term in the formula used to calculate the Ac_1 temperature, and the slight difference in the range of compositions for carbon and molybdenum. For comparison, Colvin (20) reported Ac_1 and Ac_3 temperatures of 690°C and 860°C, respectively, for a modified A710 steel with 1.45% manganese.

3.3 Prior Austenite Grain Size

A grain size study was initiated to determine what range of austenite grain sizes could be developed in the present set of alloys. The aim was to produce about 10 to 15 μm grain size, similar to Colvin's work. An austenitizing temperature of 905°C was chosen (except for steel A which was 920°C). The first component of the grain size study showed that grain size did not change much with time, up to a one-hour austenitizing time. Hence five minutes holding time was chosen for the rest of study. The

results of these studies are presented in Table 3.4. The
first stage of the study showed that grain sizes are mostly
about 30 μm, except for steel A after a 60 minutes holding
period. This specimen was accompanied by an abnormal grain
coarsening phenomenon. This stage also showed that these
grain sizes are about two to three times larger than
desired.

A great number of heat treatments were examined in an
attempt to create a 10 to 15 μm grain size. Despite many
processing variations, two extremes were typically observed.
Specimens which were reaustenitized once and quenched,
usually had a grain size close to about 30 μm. Specimens
which were reaustenitized twice and quenched after each
treatment had grain sizes of about 7 μm and less. Figure
3.5 demonstrates some representative micrographs of these
studies. Because of the above results, it was decided to
examine both fine-grained and coarse-grained material
throughout the rest of study.

3.4 Transformation Kinetics

Although most of this study was based on steel B with
1.5% manganese, it was decided later to choose four cooling
rates to examine the relative positions of the CCT diagrams

Table 3.4   Austenite grain sizes for various austenitizing times.

Steel	Heat Treating Time (min)	Grain Diameter (μm)
A	0.5	27.3
A	2	29.7
A	5	29.2
A	15	33.7
A	30	37.8
A	60	67.5
B	0.5	33.7
B	2	33.7
B	5	34.8
B	15	33.7
B	30	33.7
B	60	38.2
C	0.5	30.3
C	2	31.4
C	5	33.7
C	15	34.8
C	30	33.7
C	60	38.2
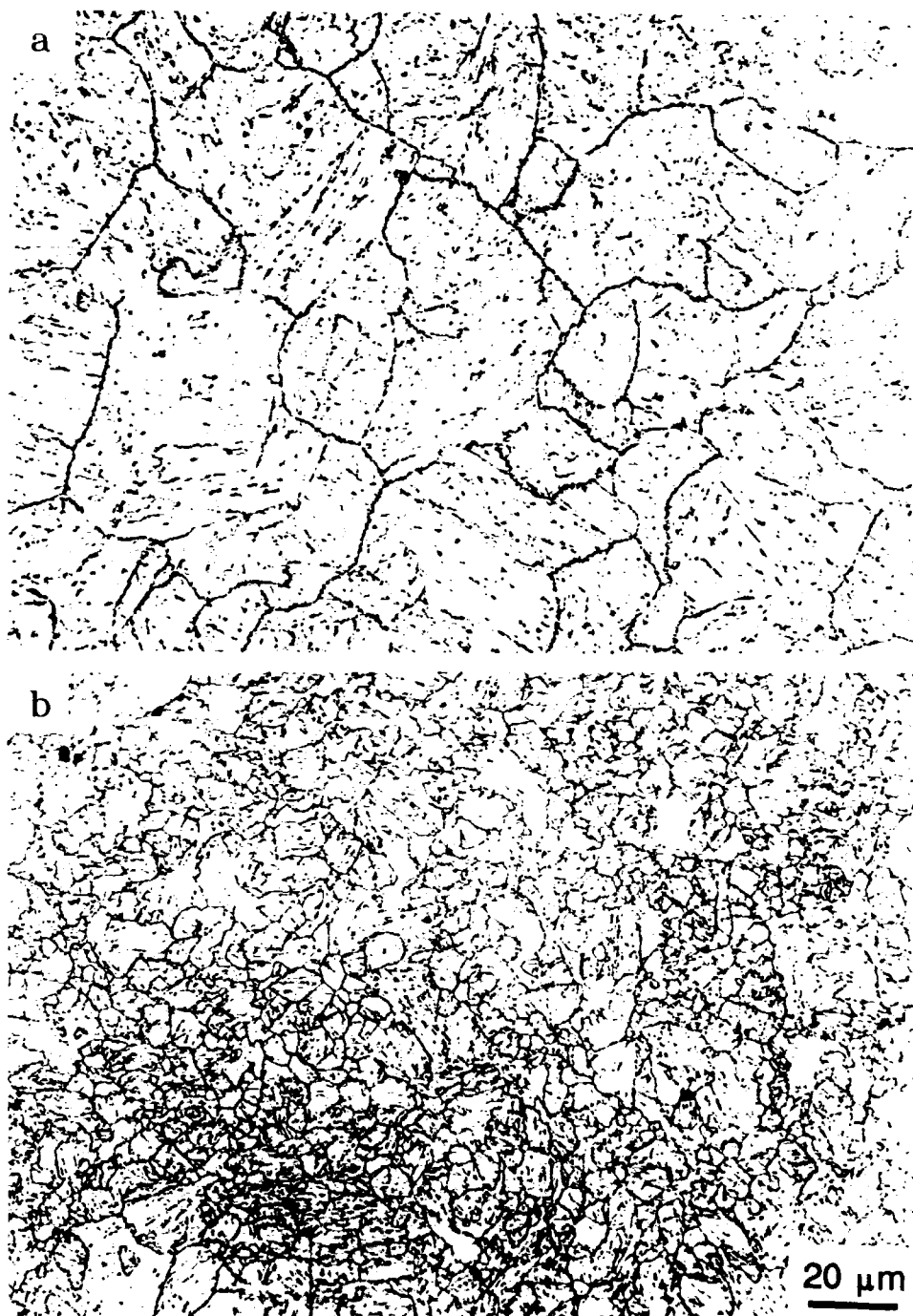
Figure 3.5   (a) Prior austenite grain size (about 30 μm)
after one reaustenitizing treatment followed by
quenching.   (b) Prior austenite grain size
(about 7 μm) after two reaustenitizing
treatments followed by quenching.

for steels A and C. This section presents the results of these studies.

3.4.1   Dilatation Curves

A typical dilatation curve for steel B is shown in Figure 3.6. C-strain is plotted versus temperature for cooling of typical samples. For the 2X condition, these data are for cooling after the second austenizing treatment. Austenite transformation start and finish temperatures were determined by inflections in the C-strain versus temperature curve. The well-defined austenite transformation start and finish temperatures observed for all of the dilatation curves is an indication of significant transformation of the parent austenite phase. The change in C-strain at the start point is abrupt, but slows down by decreasing the temperature. This indicates that most of the transformation occurs closer to the start points (also see the CCT diagrams).

There is no significant difference between the dilatation curves for the specimens examined at slow and fast cooling rates. In addition, the dilatation curves for all of the three steels are similar.
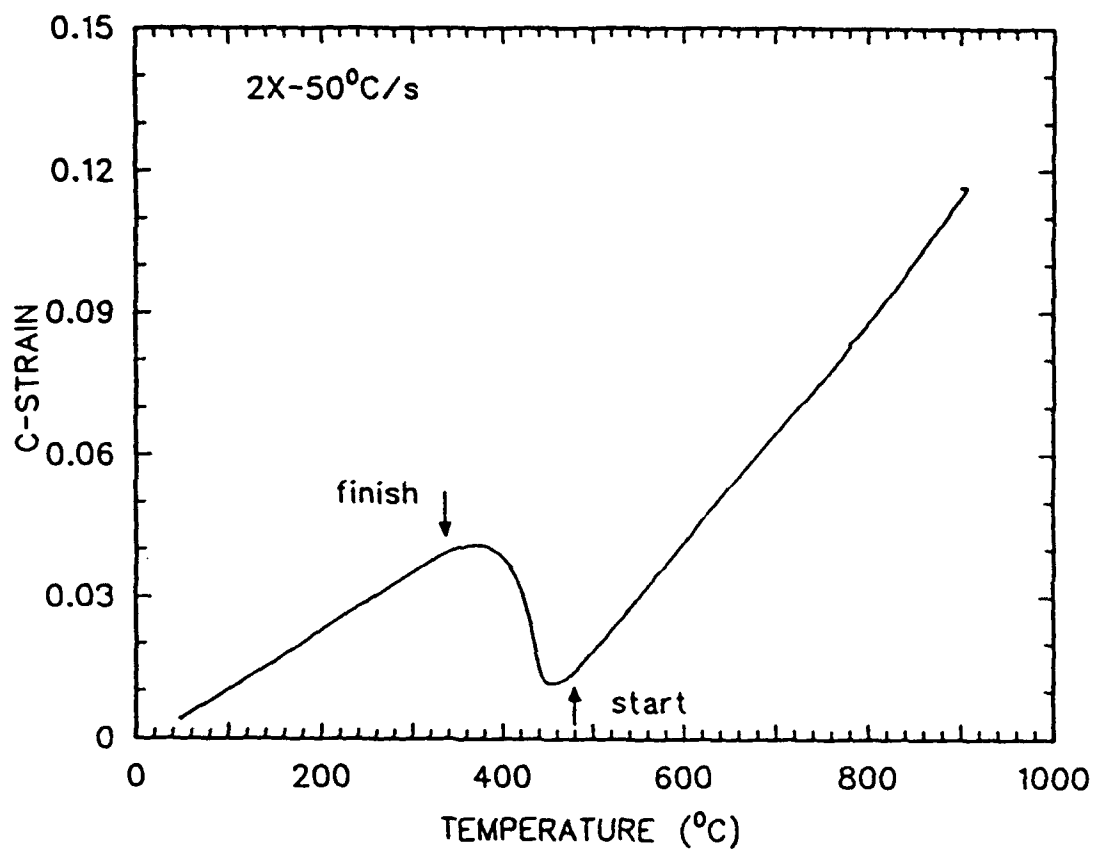
Figure 3.6   Plot of C-Strain versus temperature for a sample
reaustenitized twice followed by cooling at 50°C/s
after the second austenitizing treatment.

3.4.2   Continuous Cooling Transformation Diagrams

The results of 15 tests for each condition (1X and 2X) are plotted versus log time in order to outline the general form of the CCT diagrams. Figure 3.7 shows the CCT diagram for steel B. As was expected, the 2X condition (finer grain size) exhibits higher transformation start and finish temperatures. The CCT curves are consistent with several other studies (20,35,36,62) in that there is a broad, flat-topped transformation region typical of bainitic steels. In contrast to some of the aforementioned studies (20), there is no indication of high-temperature transformation products (polygonal ferrite). This could be due to the high molybdenum content of the present steels. The presence of molybdenum and other strong carbide formers lead to a solute drag like effect (SDLE) (90-91) which has been discussed before. All the transformation start temperatures are about the same for all cooling rates, with slight variations which could be attributed to experimental errors.

The 25, 50 and 75 percent transformation temperatures for the 1X and 2X conditions are shown in Figure 3.8a and 3.8b, respectively.
As these figures show, the lines representing the 25%, 50% and 75% transformation are much closer to the transformation
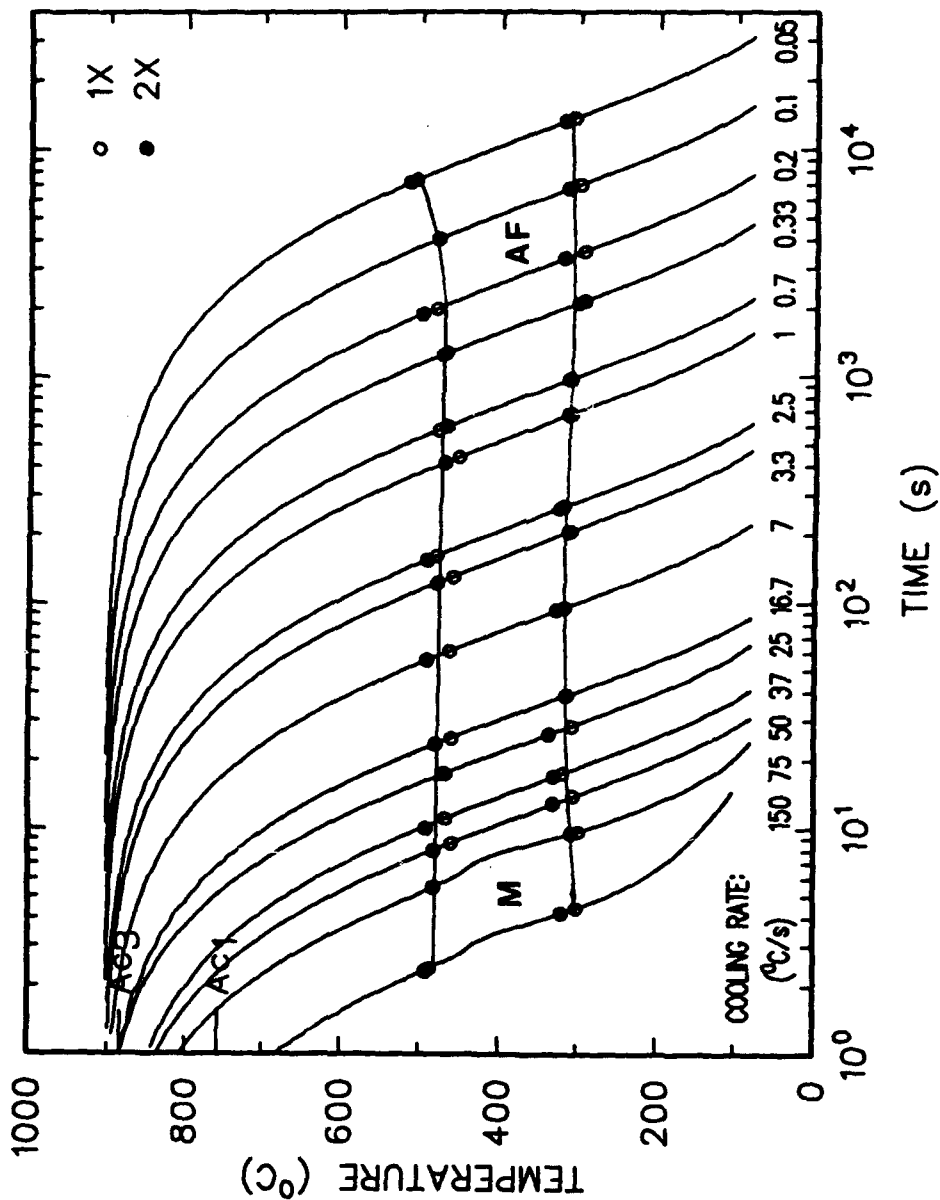
Figure 3.7 CCT diagram for steel B.
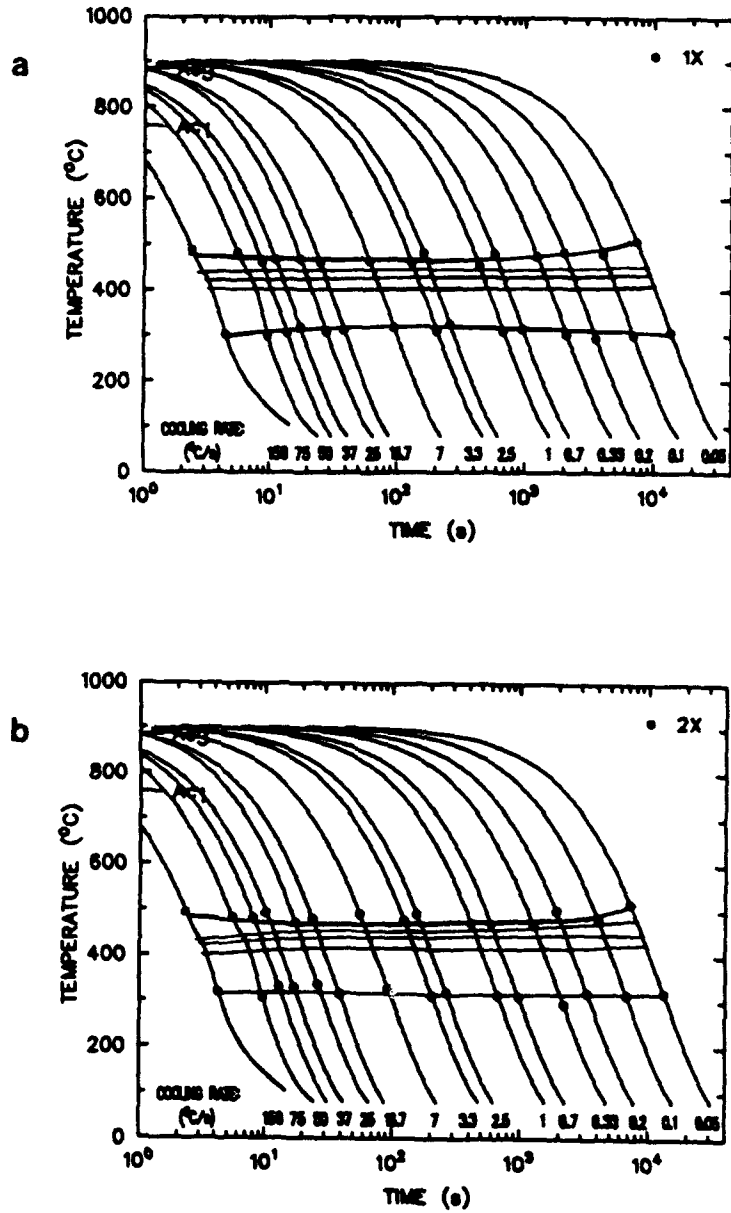
Figure 3.8   25, 50 and 75 percent transformation lines
              for (a) 1X and (b) 2X conditions.

start temperatures than the transformation finish

temperatures. This observation indicates that the reaction

occurs to a greater extent at higher temperatures.   Table

3.5 presents the calculated and measured B_s and M_s

temperatures for steels A, B and C.

Table 3.5   Calculated and measured B_s and M_s temperatures
            for steels A, B and C.

STEEL	measured B_s	Calculated B_s	Measured M_s	Calculated M_s H[*]	A[**]
A	495	280	495	375	405
B	482	245	482	361	392
C	458	225	458	355	386

*   Ref 124
** Ref 123

To identify the microstructures which form as the

result of different cooling rates, microhardness tests and

light microscopy were conducted for each cooling rate.

Hardness values for each cooling rate were plotted versus

log Δt_{8-5} to show a "hardness profile."   A change in the

slope of the hardness profile was taken to indicate a change

in the transformation products, or a change in the amounts

of two different austenite decomposition products.   Figure

3.9 shows the hardness values for both the 1X and the 2X
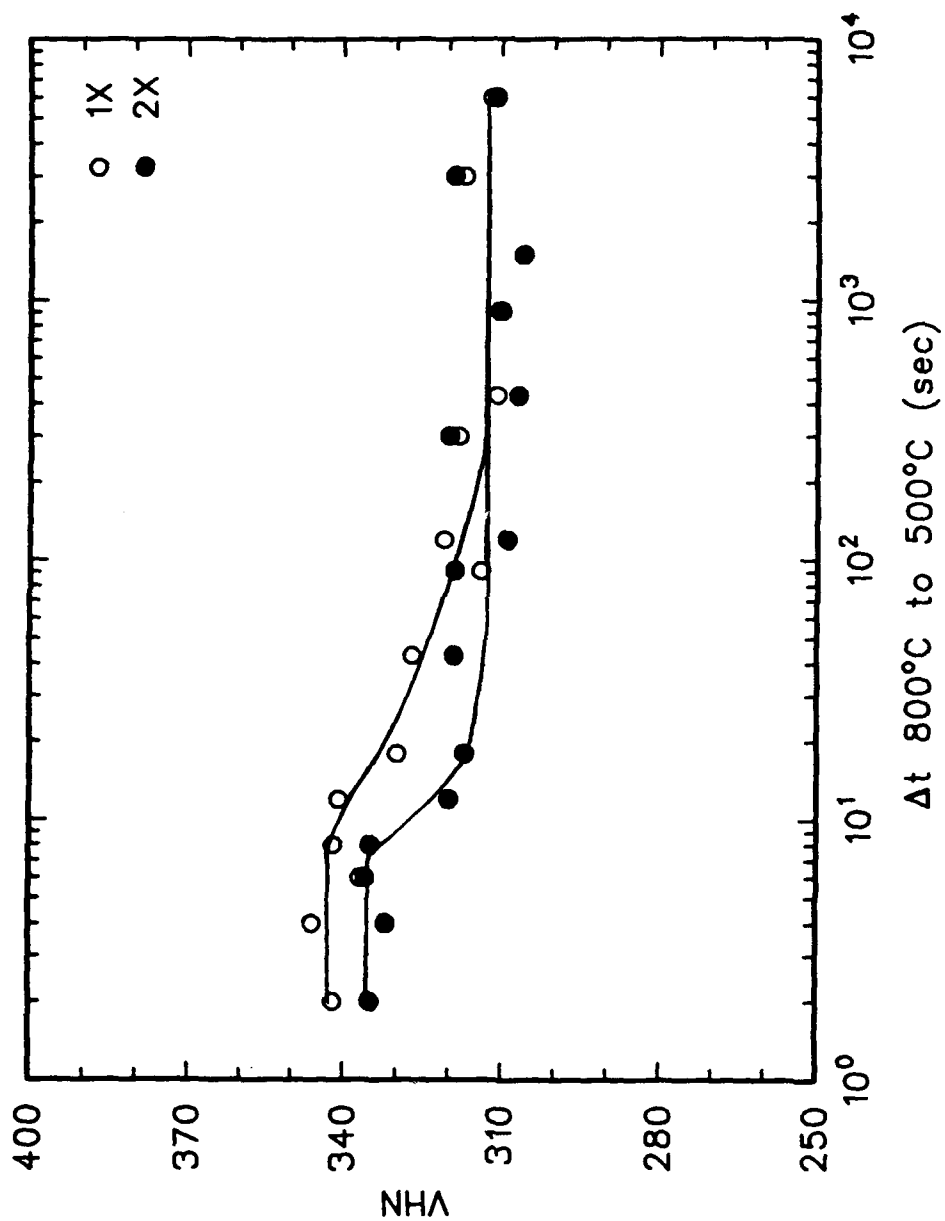
Figure 3.9 Microhardness versus cooling time between 800°C and 500°C.

conditions for steel B. Although at slower cooling rates the hardness values of both the 1X and 2X conditions seem to be similar, with increasing cooling rates these values are consistently higher for the 1X conditions than those of the 2Xs. The lower hardness of the 2X condition in the martensite region may be related to percipitate formation and coarsening.

Four cooling rates out of each condition were chosen for more detailed studies. These cooling rates are 0.1, 3.3, 25 and 150°C/s. What follows is a discussion of the microstructures produced as a result of these cooling rates, accompanied by the as-received microstructures of the steels under investigation.

3.5 Microstructural Characterization

Figure 3.10 shows a light micrograph of the structure generated as part of the Ac_1-Ac_3 study, where the specimen was heated up to 1200°C and then cooled to room temperature. The measured cooling rate was 50°C/s. This microstructure strongly resembles the martensitic microstructures observed by other investigators (98,106,107,109) in low-carbon steels. The coarse prior austenite grain size (about 50-100 μm), which corresponds to

Figure 3.10   Martensitic microstructure of steel B after
              austenitization at 1200°C followed by
              quenching.

the high austenitizing temperature, provides excellent
martensite hardenability compared with the finer grain sizes
examined in the rest of study. Therefore this
microstructure provides an excellent basis for comparison.

It was mentioned before that of etching these steels is
very difficult. The similar orientation of martensitic
laths within a prior austenite grain may be responsible for
this difficulty. It should be mentioned here that prior
austenite grain size, as well as cooling rate, had a
noticeable effect on the etching behavior of these steels.

In contrast to the microstructure shown in Figure 3.10,
recall the as-received microstructure (Figure 3.3). These
microstructures seem to be very different from the
martensitic structure in Figure 3.10. Etching of these as-
received steels was relatively easy. In Figure 3.3, the
thick, dark linear features are prior austenite grain
boundaries and packet boundaries, while the small dark
regions (arrowed) are islands of austenite and/or
martensite. The size of these small islands ranges from
about 1 to 2 μm, for larger blocky islands, to about 0.2-0.4
μm, for small islands. The bright areas are crystals and/or
packets of acicular ferrite. These features are consistent
with those observed in thin foils. Figure 3.11 shows a
representative feature of the as-received microstructure in

Figure 3.11 Acicular ferrite with islands of retained
             austenite. (a) BF and (b) CDF images of the
             as-received steel B.

steel B. The small dark regions in the bright-field image
(BF) are martensite-austenite islands (M-A constituent).
These islands of retained austenite/martensite are aligned
at both prior austenite grain boundaries and at interlath
boundaries. The direction and alignment of these
constituents indicates the acicular nature of this
structure. Acicularity is more evident in the centered-
dark-field (CDF) image of the same area in Figure 3.11. The
diffraction pattern (DP) corresponding with this pair is
shown in Figure 3.12, and the CDF image was produced with an
austenite reflection. Notice the size of these islands,
which are the same as those shown in light micrographs.

The acicular nature of the as-received steel B is more
evident in Figure 3.13. The average lath width measured is
about 0.8 μm. An interesting features in these images is
the jagged edges (arrowed) of a lath in this structure.
There are two possible explanations for this feature.
The first explanation that comes to the mind is that these
jagged edges could be "bainitic" subunits. The repeated
nucleation and growth model proposed by Oblak and Hehemann
(31) suggests that the formation of bainite involves
repeated nucleation of substructural units. A schematic
presentation of this mechanism is shown in Figure 3.13c.
The dark regions between light areas appear to be regions of
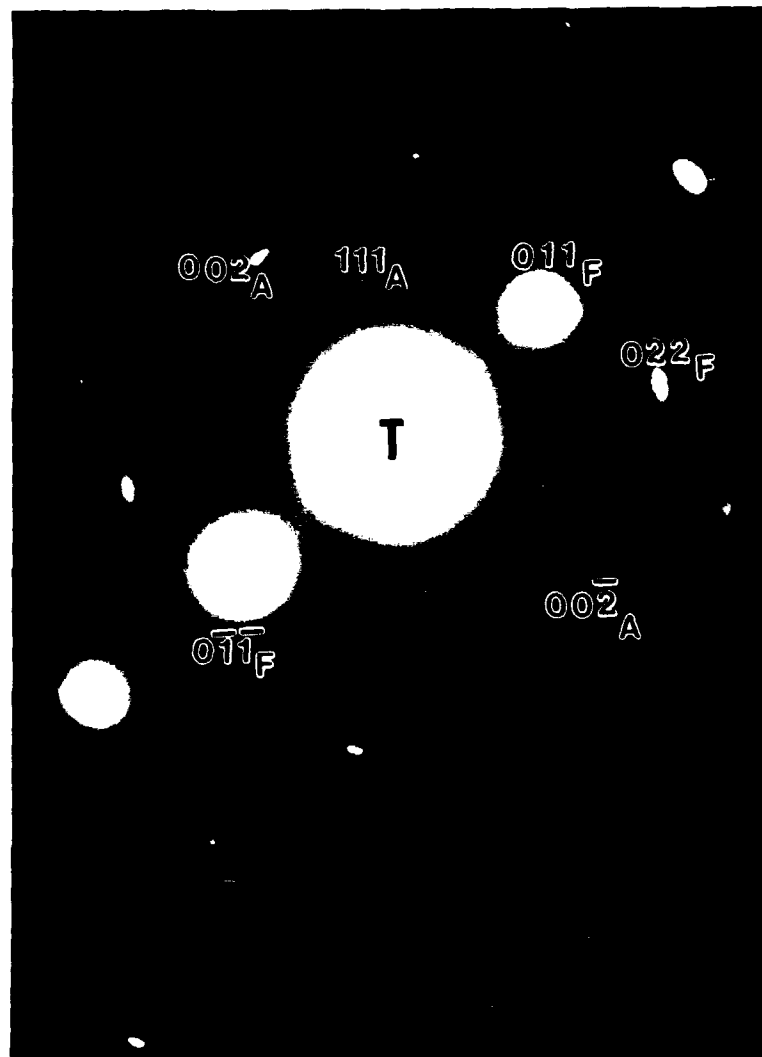
Figure 3.12   SADP corresponding to the region shown in
Figure 3.11.
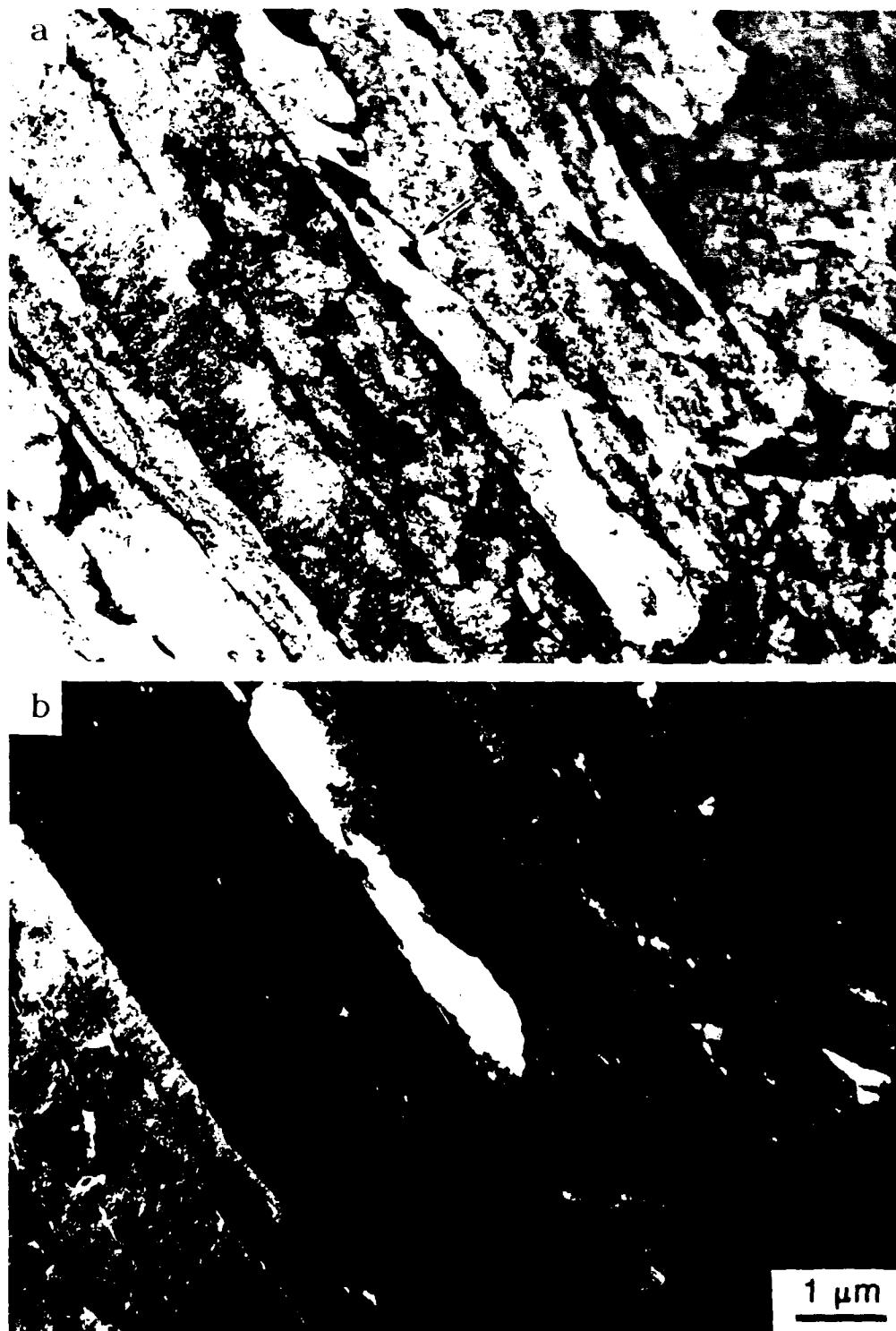
Figure 3.13   The as-received steel B showing acicular
              ferrite structure and the jagged edges of a
              lath.   (a) BF and (b) CDF images.
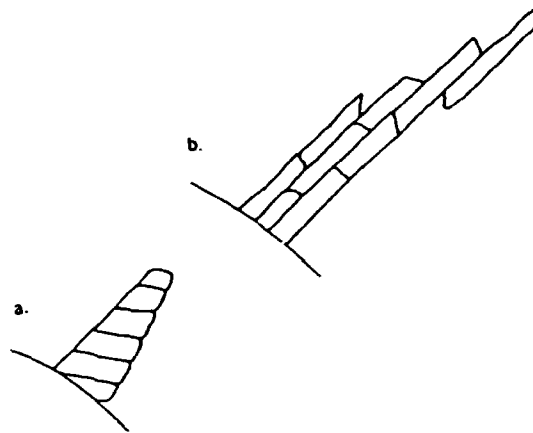
Figure 3.13c   Schematic illustration of structures produced
               by repeated nucleation of subunits, which
               rapidly attain a limiting size (31).

high-carbon martensite and/or austenite entrapped between

these subunits. The reason for retention of some

untransformed austenite adjacent to ferrite laths is the

enrichment of these regions with carbon as a consequence of

transformation. Therefore, the formation of ferrite becomes

progressively more difficult. It has been shown that the

existence of M-A constituents depends on the cooling rate

and the composition of steel (125). Coldren et al.

suggested that rapid cooling tends to prevent the formation

of M-A islands. At slower cooling rates, there is more time

for diffusion of carbon and consequently more M-A islands

are present (126).

     A second possibility for the unusual image of Figure

3.13 is related to sectioning effects. These jagged edges could be the intersections of different laths. It is very likely that a combination of the two explanations is responsible for this phenomenon.

More evidence of retained austenite regions in the as-received steel is shown in Figures 3.14 and 3.15. These observations strongly dispute the conclusion made by DeArdo and co-workers (125) that these very low carbon steels lack the M-A constituent. DeArdo et al. showed no direct evidence to prove this conclusion. In fact, the presence of retained austenite at room temperature, considering the high transformation temperature of these steels (about 500°C), could be because the high strength of austenite does not allow the shear transformation to martensite to happen.

Figure 3.3 and Figures 3.10 through 3.15 show that distinct microstructural types are produced in steel B. These figures provide a basis for comparison for the remainder of the Gleeble work. Figure 3.16 shows representative light micrographs of steel B in the 1X and 2X conditions followed by cooling at 150°C/s. There are almost no similarities between these microstructures and what was shown in Figure 3.3 for the as-received steels. Unlike the as-received samples, these microstructures were very resistant to etching. Although the prior austenite grain

Figure 3.14   Microstructure of the as-received steel B.
              Notice the black M-A islands.

1 μm
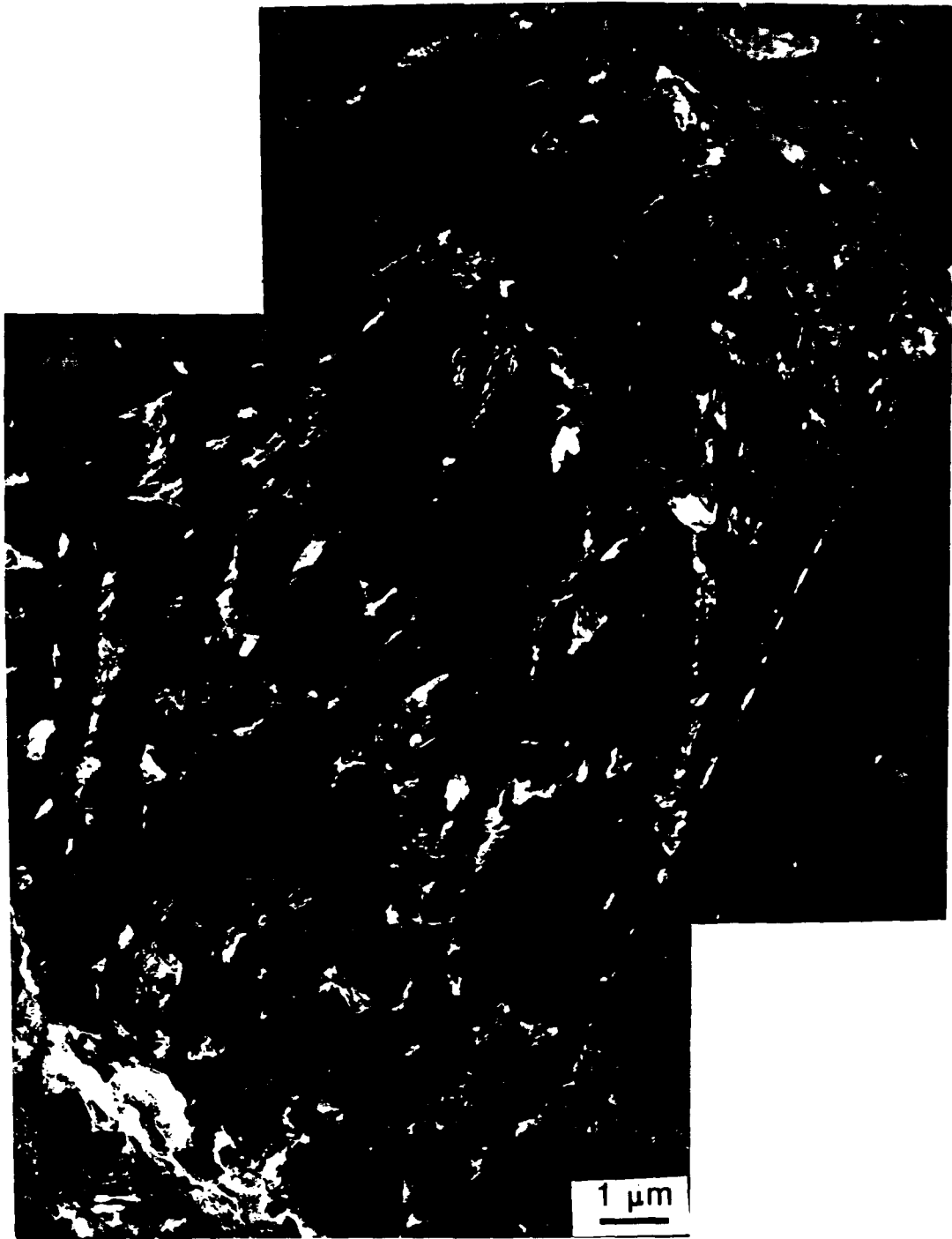
Figure 3.15   Austenite centered-dark-field Image of the same
region shown in Figure 3.14.

Figure 3.16   Martensitic microstructures in specimens cooled
               at 150°C/s.   (a) 1X condition and (b) 2X
               condition.   Light micrographs.

boundaries are not evident, the martensitic structure in Figure 3.16 is similar to what is shown in Figure 3.10. There is no strong evidence of retained austenite, especially in the 1X condition (Figure 3.16a). In other words, small, dark islands are mostly absent. The elongated ferrite packets resemble the blocky martensitic nature of the micrograph shown in Figure 3.10.

Figures 3.17 and 3.18 represent different regions of the thin foils examined for this cooling rate. These structures exhibit the fine lath structure typical of low-carbon martensite. The lath structure of martensite is much more evident in these micrographs. It is noteworthy that there was no evidence of retained austenite regions, as in the as-received structure, despite an extensive search. While this result is consistent with the light micrographs in Figure 3.16, other researchers (127) have reported thin films, and not equiaxed islands, in martensite. Still, no thin films of retained austenite were observed either. The average lath width for this cooling rate is about 0.2 μm for the 1X and the 2X conditions. A comparison between the lath width of the as-received steels and the specimens cooled at 150°C/s shows at least four times bigger lath size for the as-received condition. This is consistent with the previous observations indicating that the lath size decreases with an
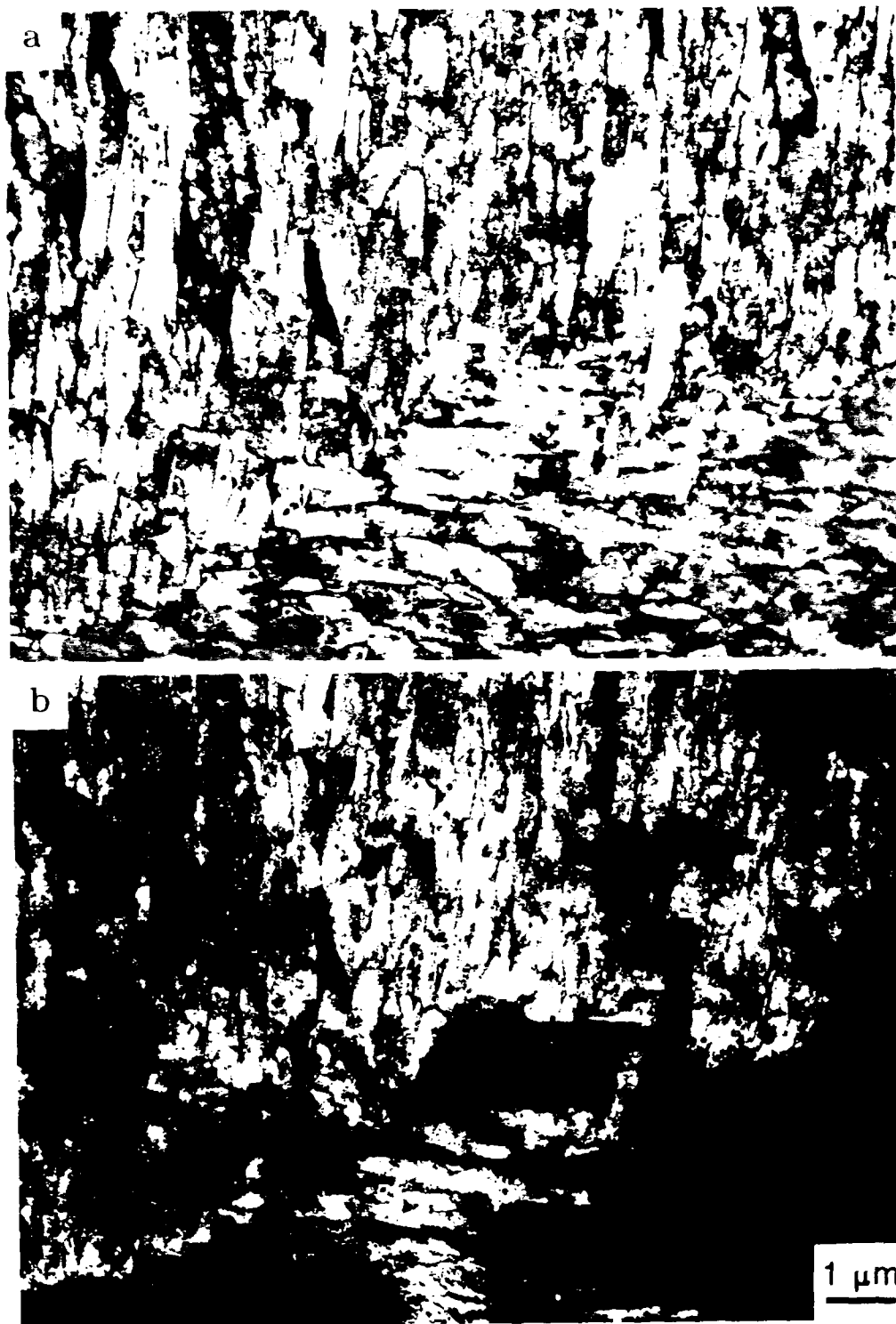
Figure 3.17   Fine martensitic lath structure produced after cooling at 150°C/s for the 1X condition.
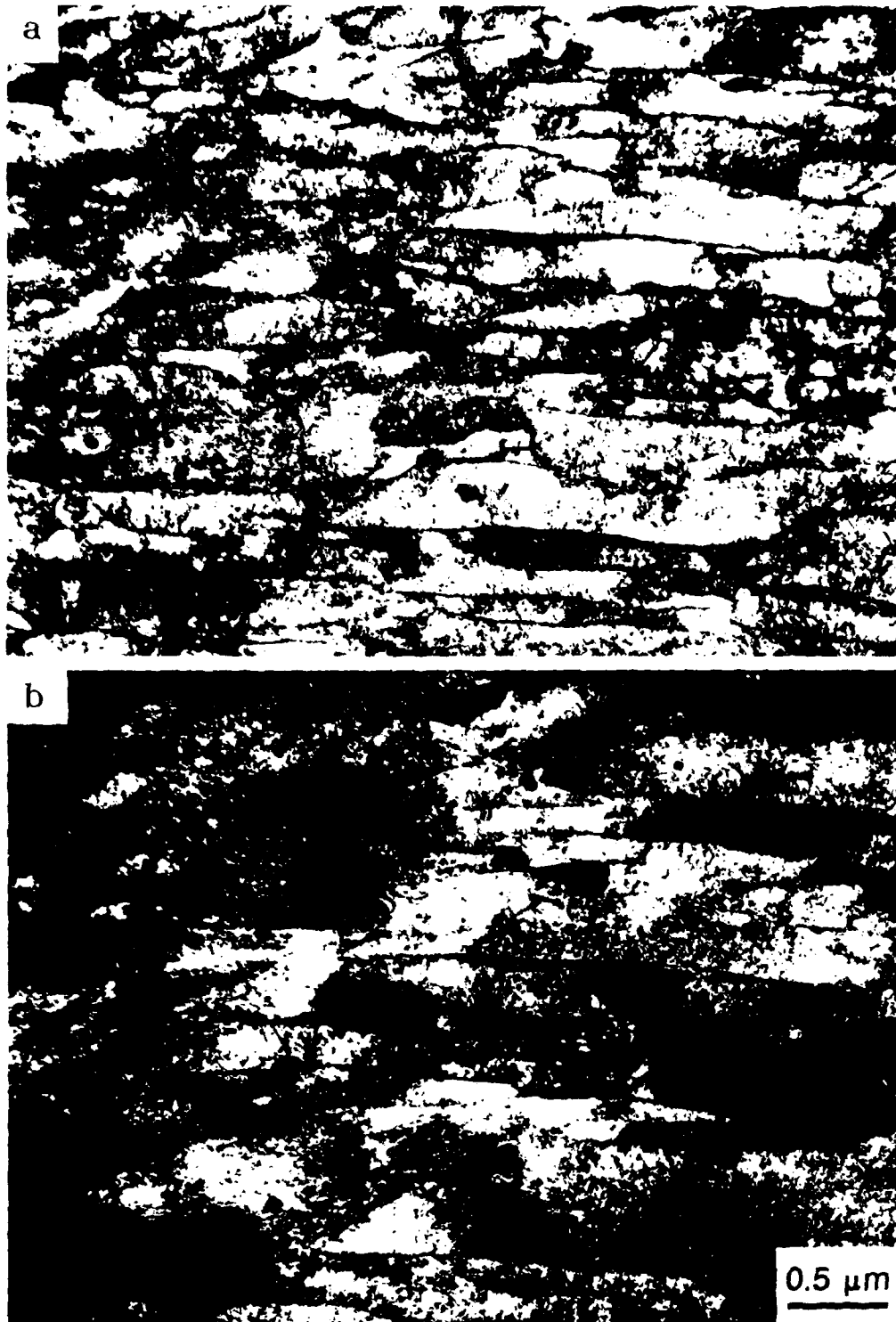
Figure 3.18 Fine martensitic lath structure produced after cooling at 150°C/s for the 1X condition.

increased cooling rate.

A comparison between the etching and electropolishing behaviors of the as-received structure and the specimens cooled at 150°C/s indicates major differences between these two structures. The as-received steels are much easier to etch than specimens cooled at 150°C/s and show better contrast in the light microscope. The strong etching effect was evident in electrochemically polished foils examined in the TEM as shown by Figure 3.14. In contrast, the martensitic specimens are not easy to etch, yet they electropolish much more uniformly. These observations, coupled with the existence of the upper plateau in the hardness profile for fast cooling rates, are indicative of differences in the mechanisms of austenite transformation for the as-received steels (cooling rate of about 1°C/s), versus the Gleeble samples cooled at 150°C/s. Figure 3.19 strongly supports the martensitic reaction at these high cooling rates. The presence of twinned martensite leaves no doubt about the martensitic nature of these microstructures.

The presence of the spherical particles arrowed in Figure 3.19 is probably a redeposition effect associated with thin foil preparation during electropolishing. These particles were not observed on surfaces of specimens from the as-received condition. This indicates that the
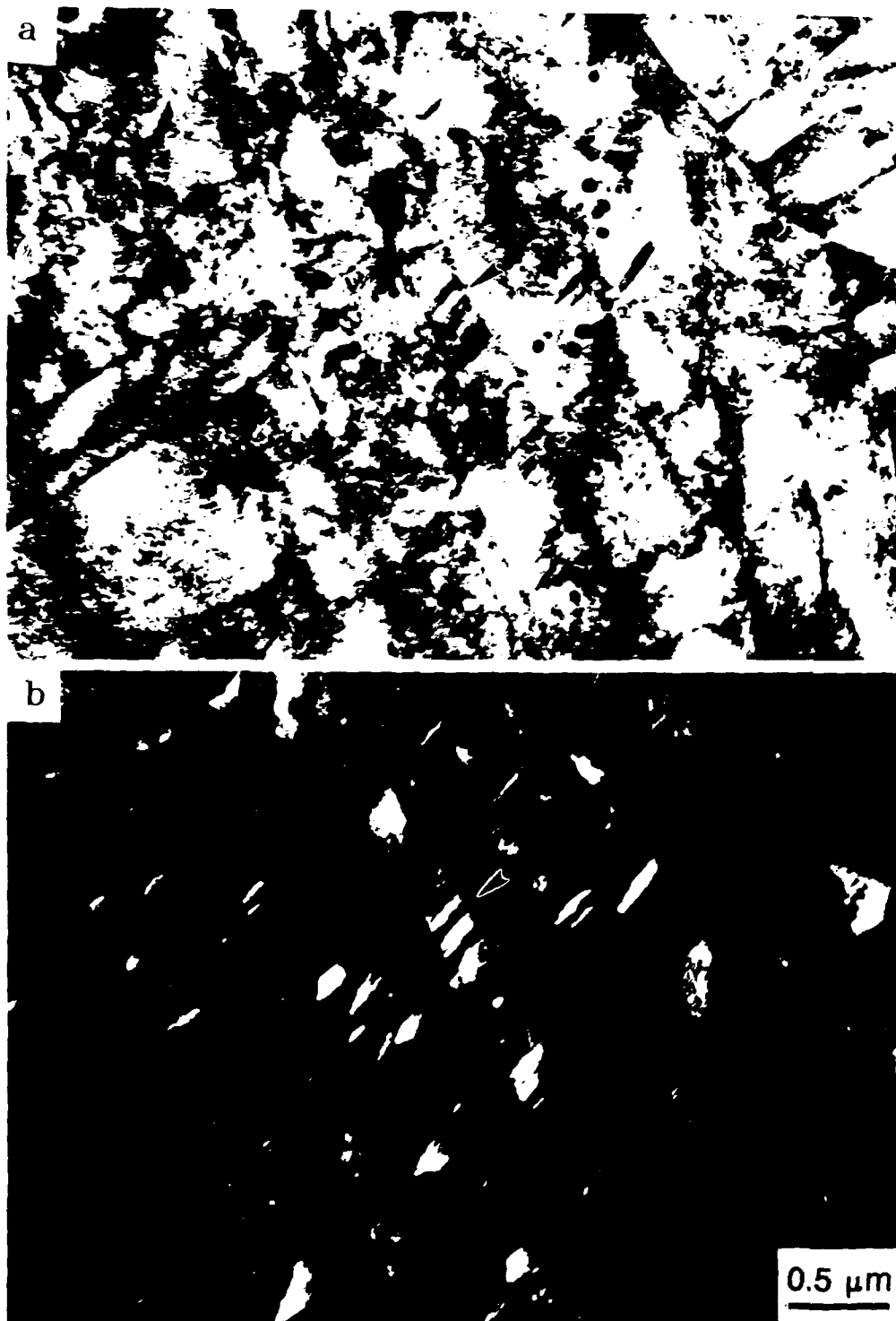
Figure 3.19   Twinned martensite in the sample cooled at
               150°C/s, for the 1X condition.

reaustenitizing treatments are somehow responsible for the formation of these particles. EDS analysis was employed in order to establish the nature of these particles. The result of one analysis is shown in Figure 3.20. Because the EDS analysis did not show any evidence of an unusual concentration of any alloying elements in these particles, the nature, reason and mechanism of formation of these particles remain unclear.

Figure 3.21 represents the light micrographs for the cooling rate of 25°C/s, for both the 1X and 2X conditions. These microstructures are still very different from those of the as-received steels. Their etching behavior is the first noticeable factor. Here again, the etching was not as easy as with the as-received specimens, but the samples cooled at 25°C/s show much better contrast than those of the 150°C/s samples. There also appears to be more M-A constituent in these microstructures than those of the 150°C/s microstructures, particularly for the 2X condition. Recall the 2X micrograph for 150°C/s cooling rate. There was some evidence of dark, etched small particles in that microstructure which did not exist in the 1X condition. A comparison of these two cooling rates shows indications of some variations in the 1X and 2X transformation products. The first major difference between the 1X and the 2X
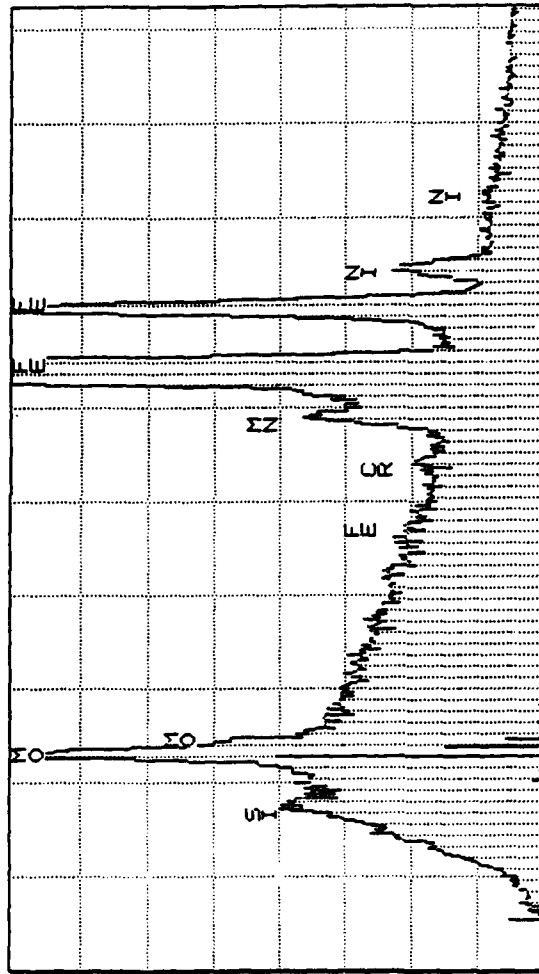
Figure 3.20   EDS analysis of the dark particles found on all of the TEM foils, except for the as-received condition.
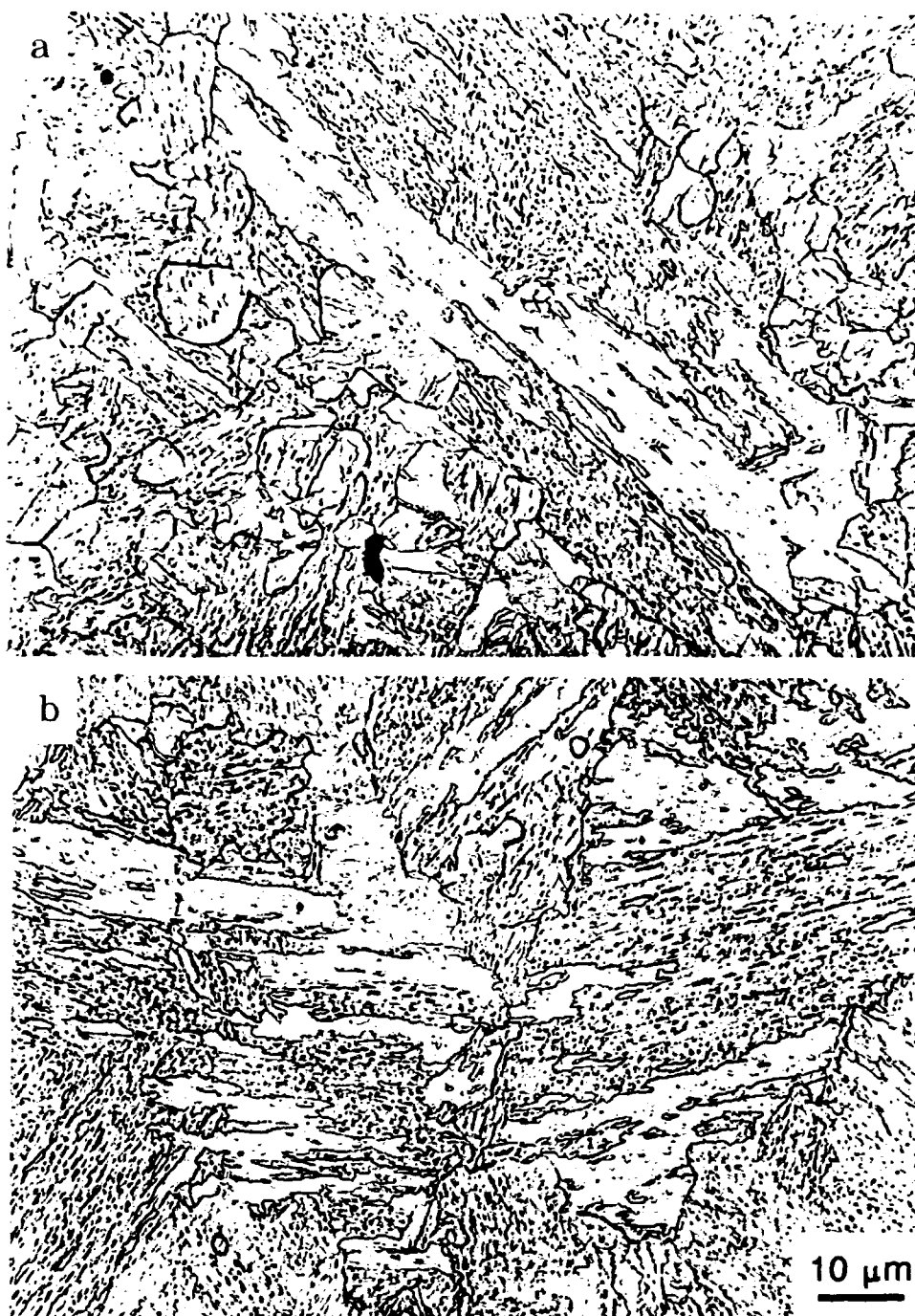
Figure 3.21   Light micrographs of the specimens cooled at
              25°C/s.   (a) 1X condition and (b) 2X condition.

conditions is in prior austenite grain sizes. Coupled with this difference, the 1X condition has a lower transformation temperature and a higher hardness value. This is consistent for all of the cooling rates. The double reaustenitizing treatment (2X) could give rise to a more complex transformation behavior which leads to these differences. It is very likely that the 2X samples contain more acicular ferrite and retained austenite than the 1X samples.

To get a better understanding of the transformation behavior of these steels at cooling rate of 25°C/s, examination of TEM micrographs is essential. Figures 3.22 and 3.23 represent the lath structure of the 1X and 2X conditions, respectively. A close look at these micrographs shows that the M-A islands are present, but the relative number density of these islands seems to be far less than that of the as-received steels. This structure is concluded to be acicular ferrite with M-A islands. In addition to this feature, the average lath width is about 0.35 μm, which shows about 0.15 μm increase compared to that of the 150°C/s cooling rate.

Figure 3.24 shows a pair of BF and CDF images for the 1X condition. These micrographs compare favorably with Figures 3.17 and 3.18, suggesting similar austenite transformation behavior. The only apparent difference is in

Figure 3.22   Microstructure of specimen cooled at 25°C/s
               for the 1X condition.
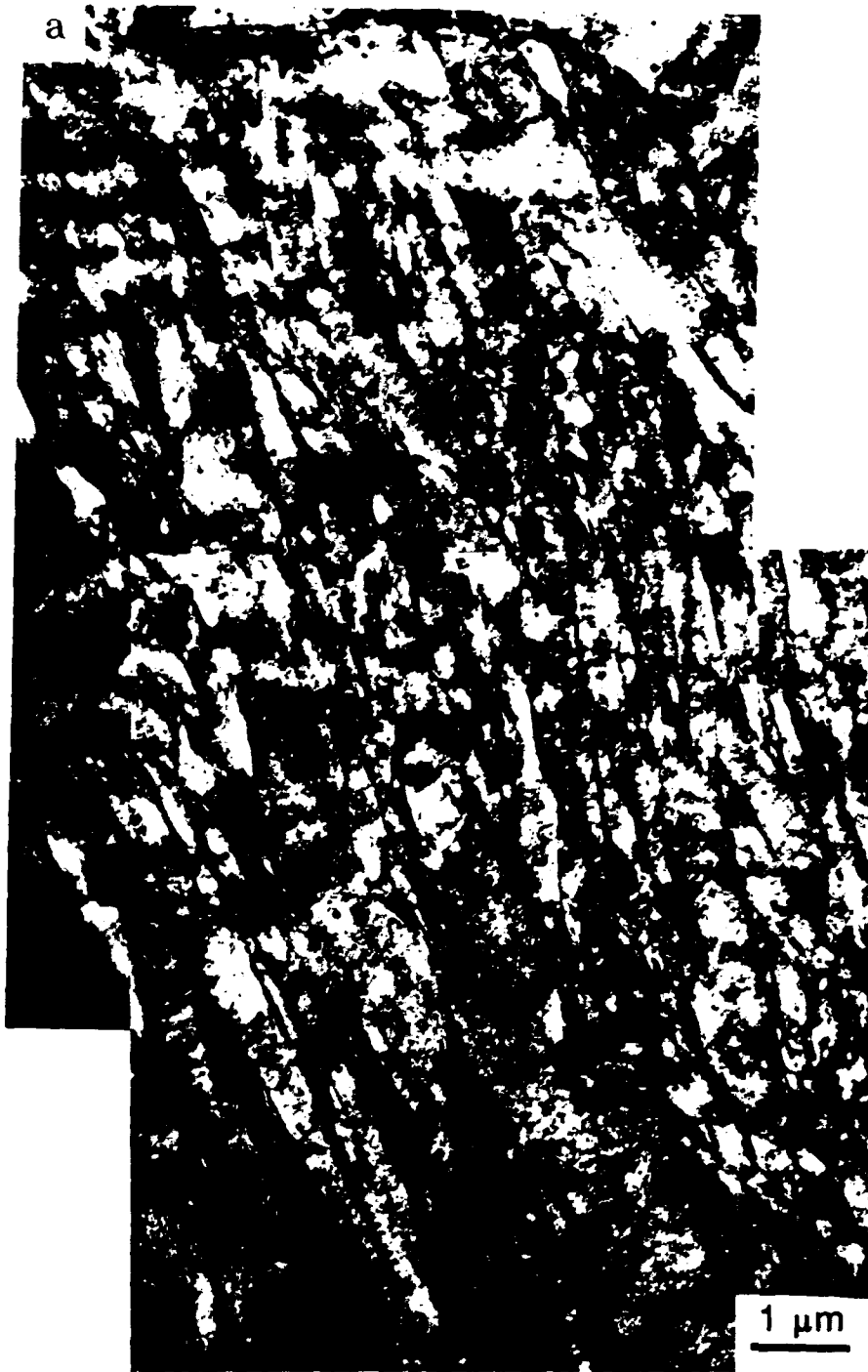
Figure 3.23a   Acicular ferrite microstructure in specimen
               cooled at 25°C/s for the 2X condition, BF
               image.

Figure 3.23b Austenite centered-dark-field image of the
same region shown in Figure 3.23a.

Figure 3.24a   Martensitic microstructure in specimen cooled
at 25°C/s for the 1X condition, BF image.
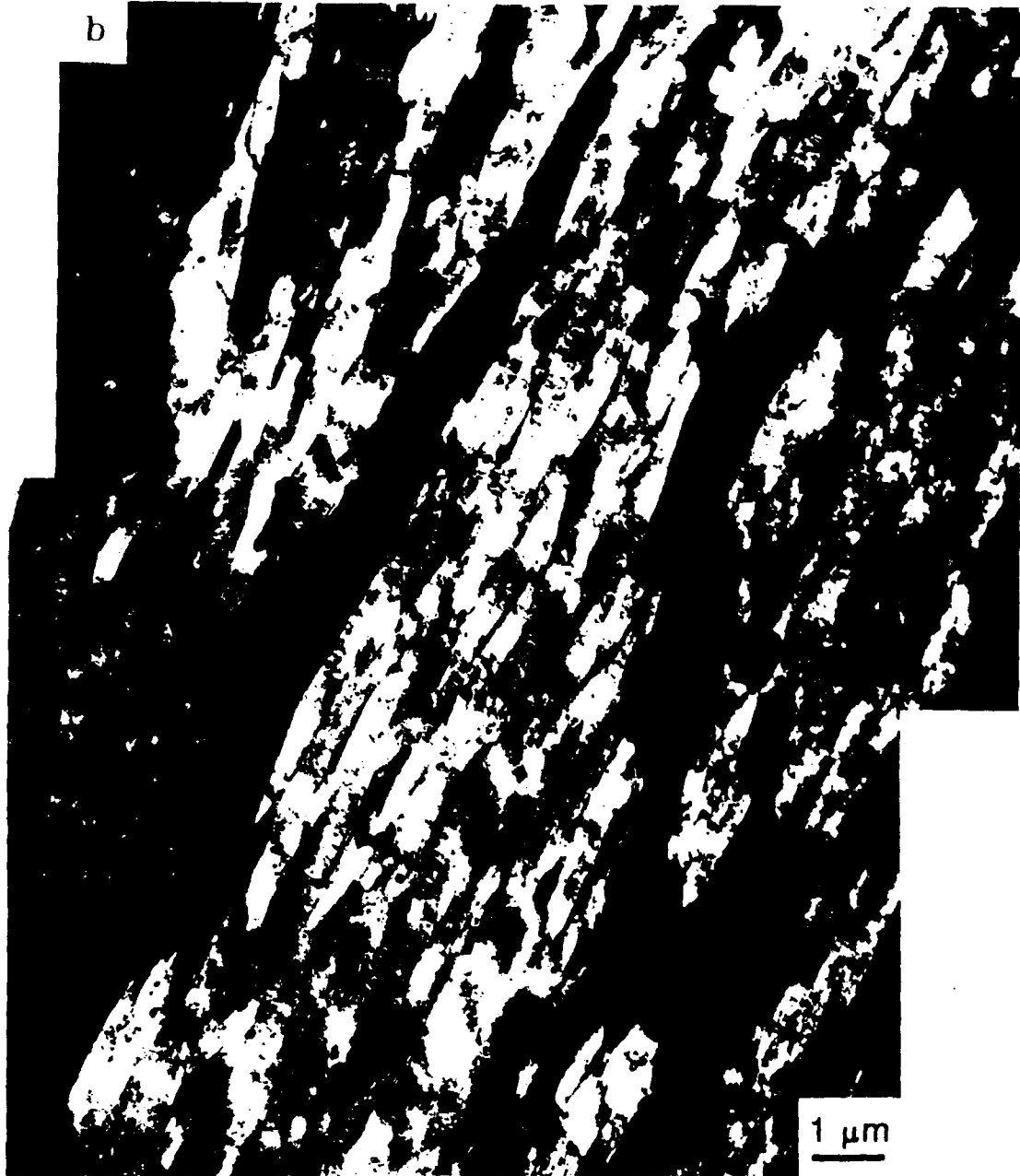
Figure 3.24b   Martensite centered-dark-field image of the
               same region shown in Figure 3.24a.

the lath width, which is related to the cooling rate. The diffraction pattern related to these packets of martensite shows two dominant orientations, Figure 3.25. The angle between these two packets of martensite is 31.5°, which is a high angle boundary.

Figure 3.26 shows a dark-field image of the precipitates present within foils of the 2X condition. The origin and identity of these particles are uncertain.

A closer examination of TEM micrographs for the 2X condition shows that, opposed to the 1X condition, there are further differences between this treatment and the ones at 150°C/s. Figure 3.27 shows a pair of BF-CDF images for the 2X condition at 25°C/s cooling rate. The presence of M-A islands at a density similar to what was observed in the as-received steels is another indication that there is a transition in transformation mode in the vicinity of this cooling rate, at least for the 2X condition. The presence of the fine twinned martensite and interlath M-A islands in Figure 3.28 supports this hypothesis. A comparison between the hardness values shows that the hardness value for the 1X condition is on the upper plateau, but that of the 2X condition is in the lower plateau region. This evidence suggests that at 25°C/s there is a mixture of acicular ferrite and primarily martensite for the 1X condition, while
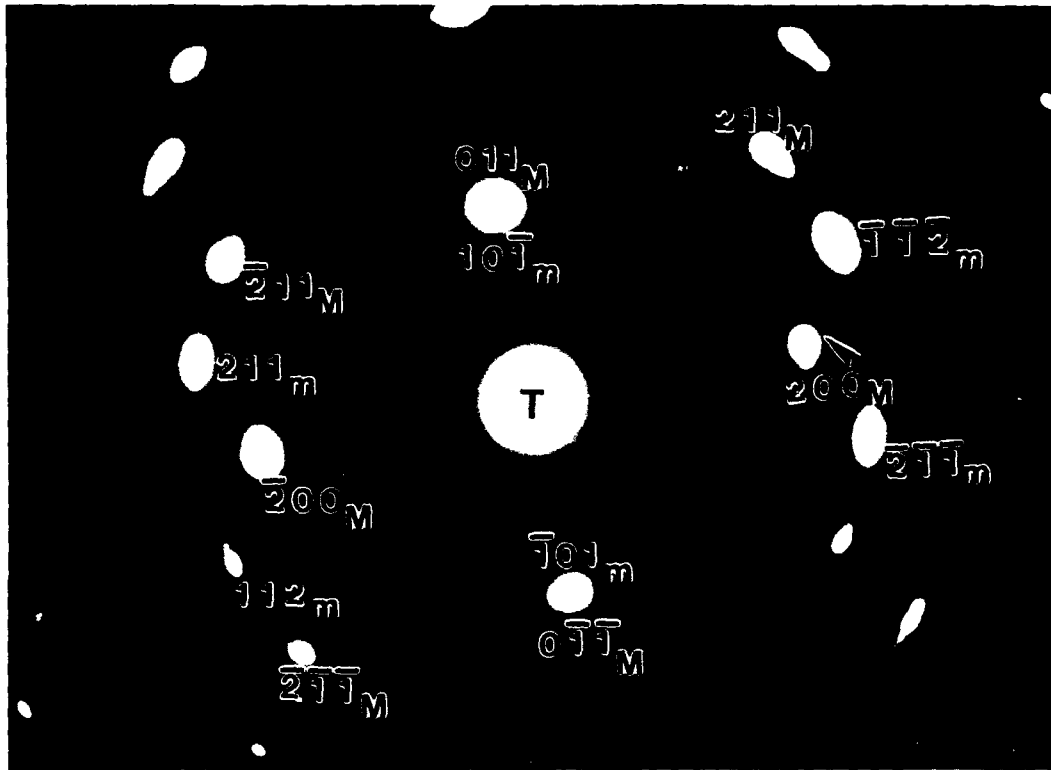
Figure 3.25   SADP from the region shown in figure 3.24.
              "M" and "m" are from two different martensite
              packets.   "T" is the transmitted beam.
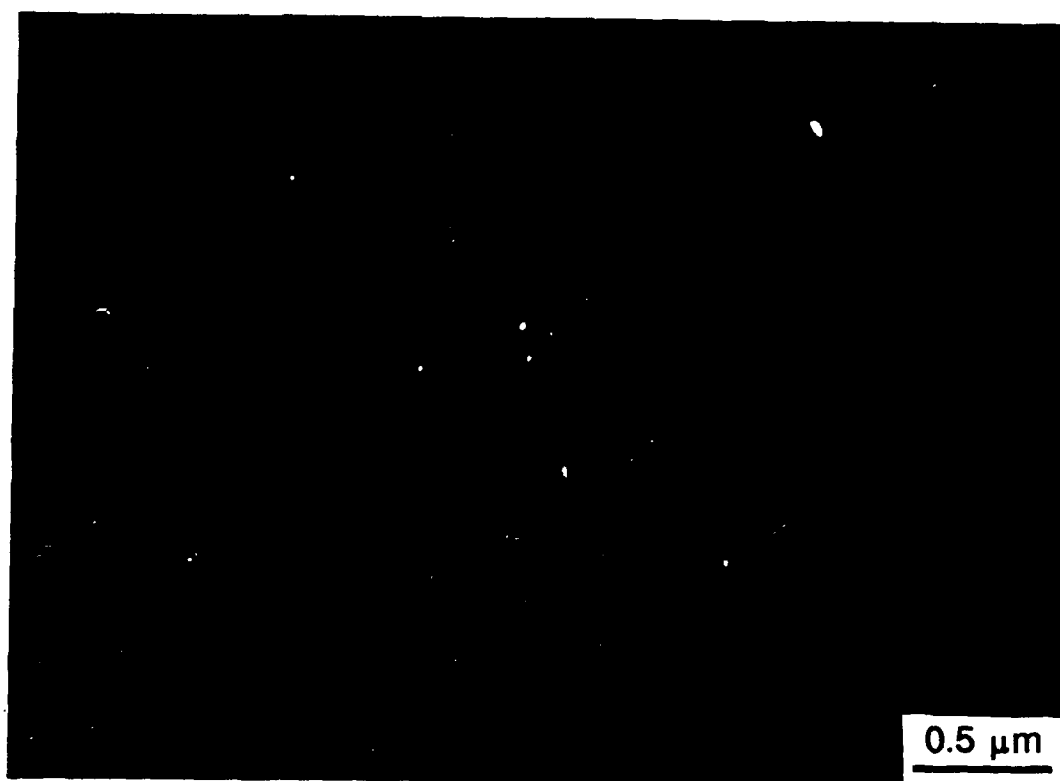
Figure 3.26   DF image showing precipitates observed within a
             TEM foil.   Cooled at 25°C/s, 2X condition.
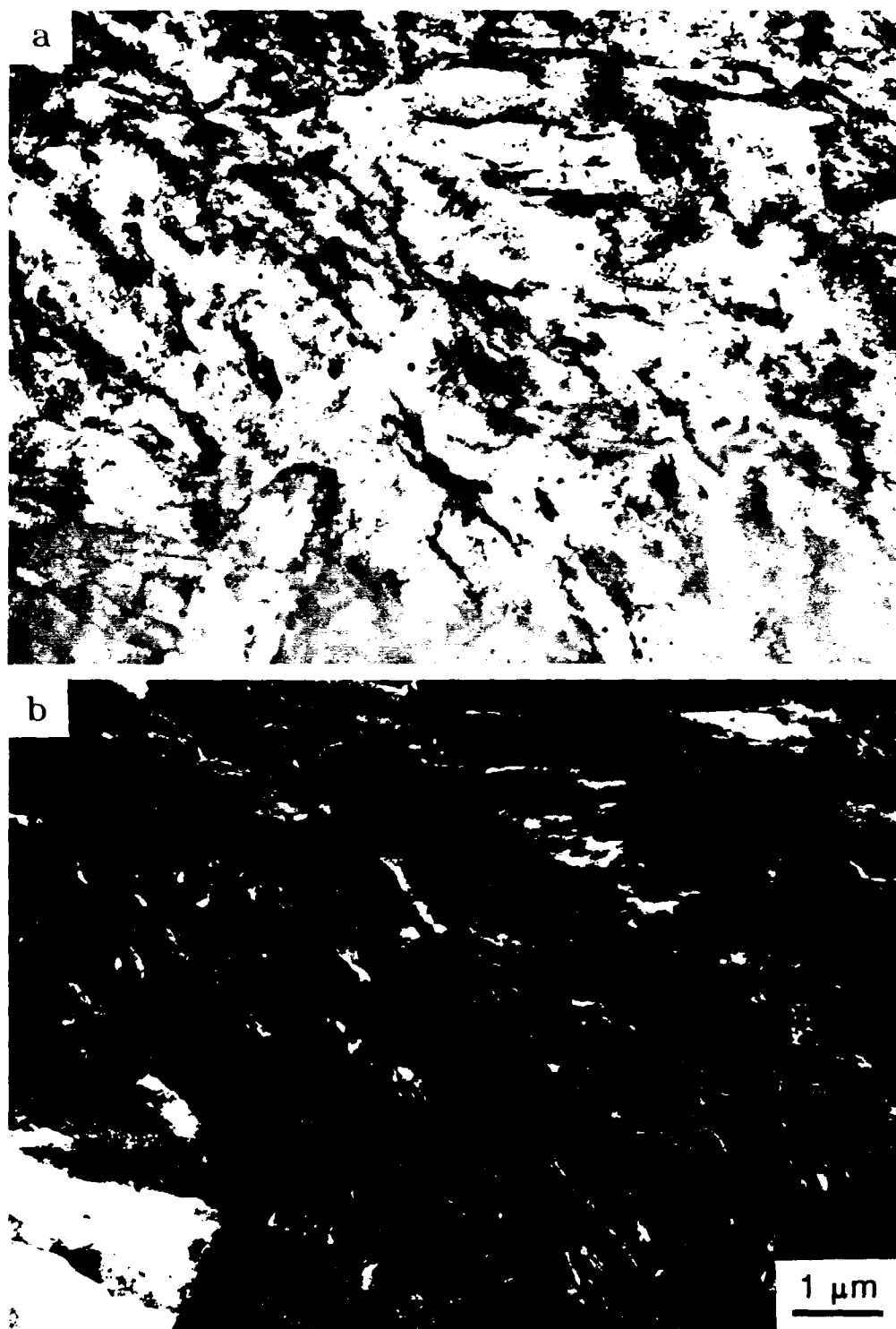
Figure 3.27   Acicular ferrite and retained austenite in
              specimen cooled at 25°C/s - 2X condition.
              (a) BF and (b) austenite CDF images.
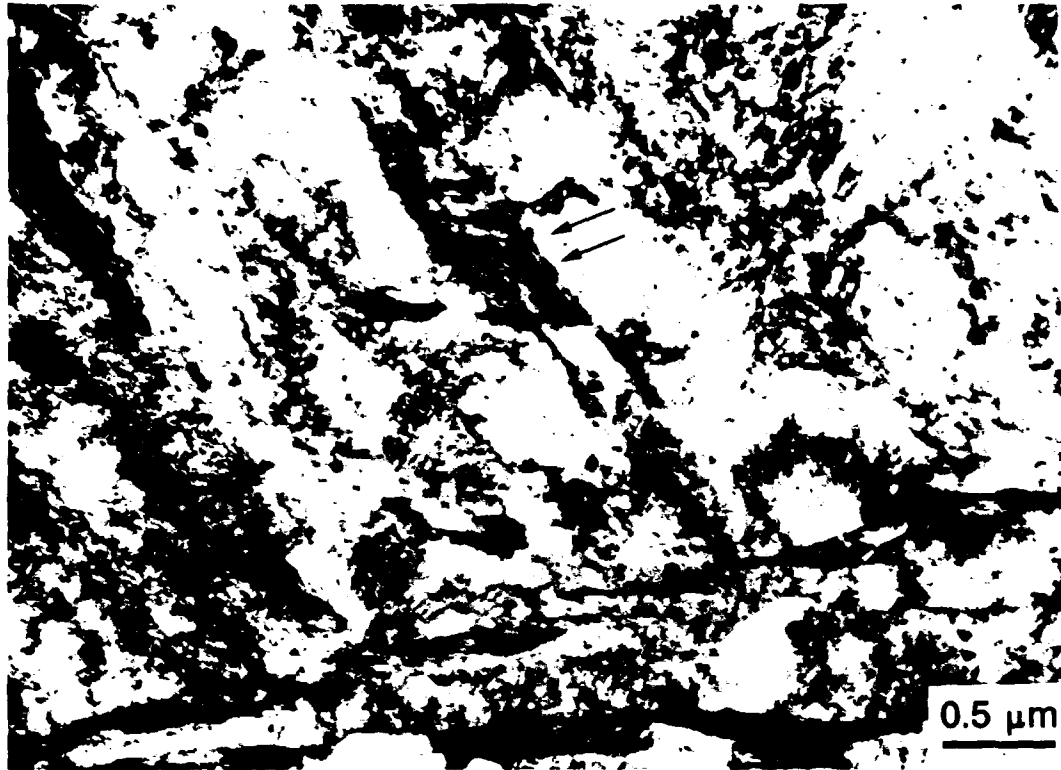
Figure 3.28   A pool of twinned martensite between laths of
              acicular ferrite in specimen cooled at 25°C/s,
              2X condition.

the microstructure of the 2X condition consists mostly of acicular ferrite.

An example of a mixed microstructure is shown in the SEM micrograph of Figure 3.29. This microstructure represents the cooling rate of 7°C/s for a 1X condition. Although it is difficult to judge about the presence of martensite packets in this micrograph, the following reasons can explain why this microstructure contains both acicular ferrite and martensite. The acicular nature of the microstructure, the lath width and the M-A pool sizes are consistent with the previous observations. The hardness value for this cooling rate on the 1X hardness profile is not on the lower or upper plateau, thereby providing more evidence that this microstructure may be a mixture of acicular ferrite and martensite. The amount of acicular ferrite in the 2X condition compared to that of the 25°C/s-1X condition has increased, and that explains the improved etching behavior and the decrease in the hardness. At slower cooling rates (3.3°C/s), the microstructures shown in Figure 3.30 resemble those of the as-received specimens. Etching behavior in these samples was relatively good, as shown by the many clear features in the light micrographs. The number of retained austenite/martensite islands has increased, and the acicularity of the microstructure is
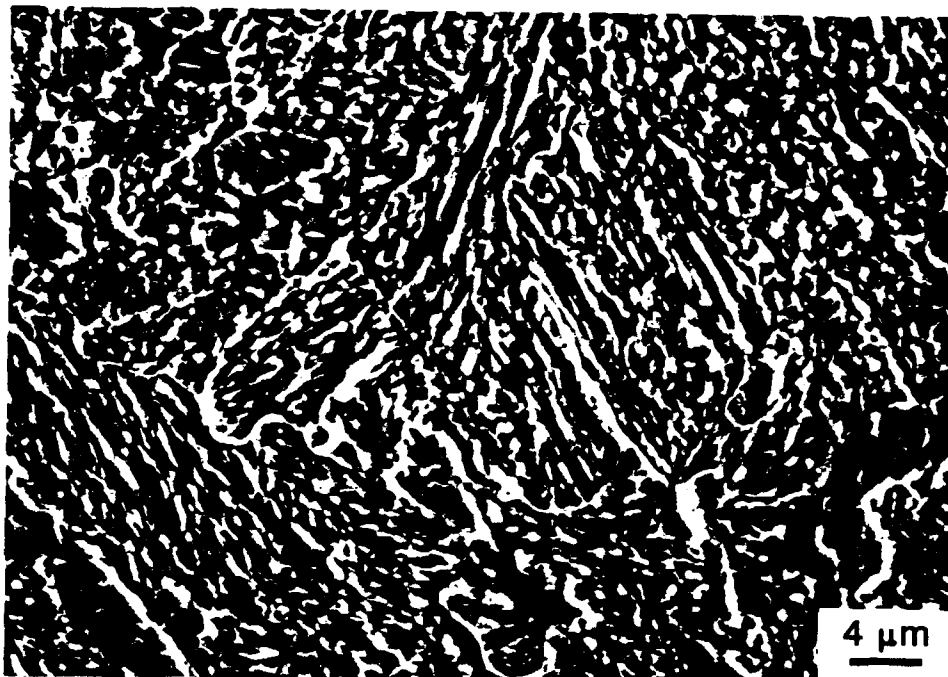
Figure 3.29   Acicular microstructure in a specimen cooled at
               7°C/s, 1X condition.   SEM micrograph.
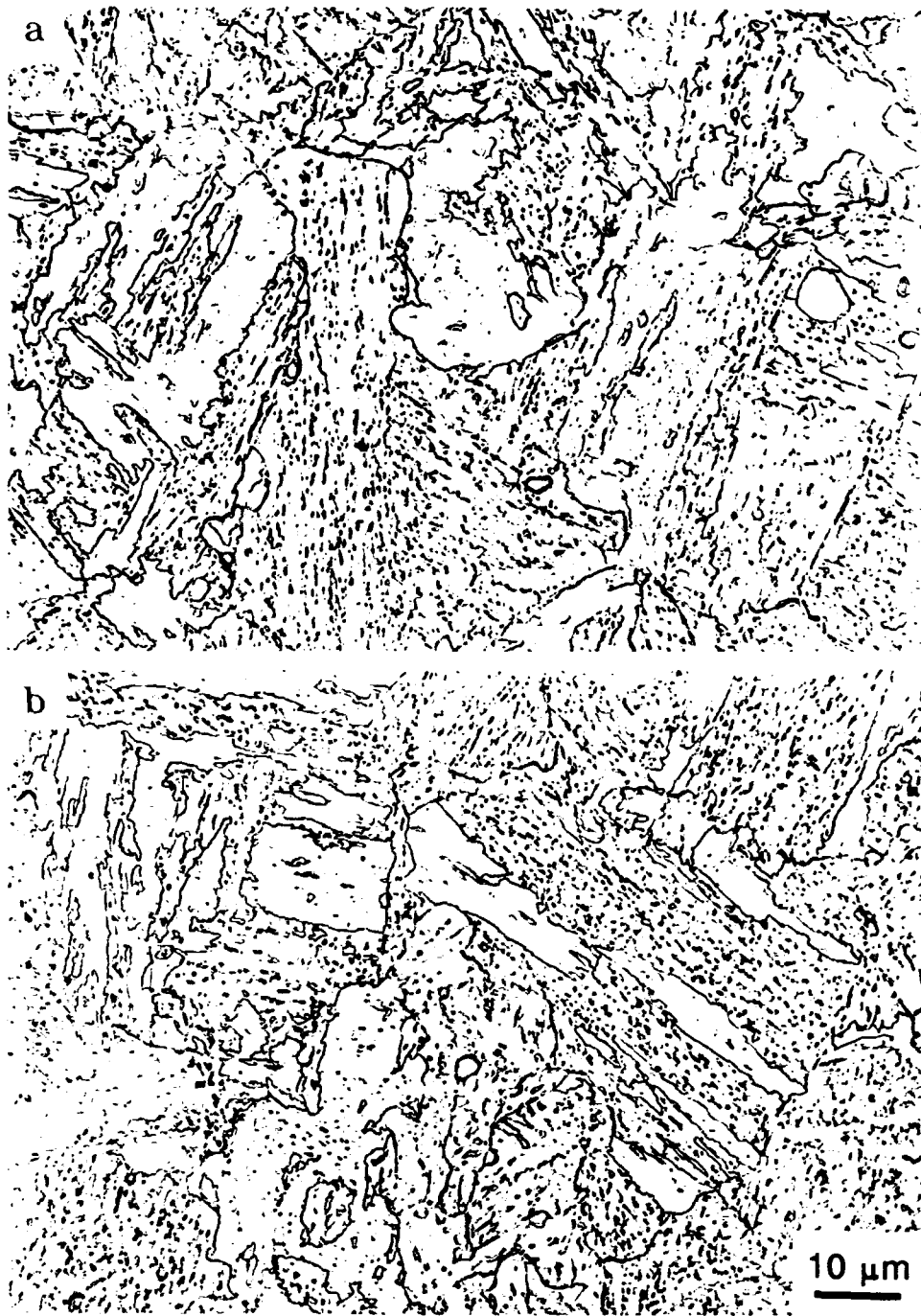
Figure 3.30   Light micrographs of the specimens cooled at 3.3°C/s.   (a) 1X condition and (b) 2X condition.

still evident. There is no evidence of a granular structure, and this observation is consistent with the as-received structure. The hardness profiles for both the 1X and 2X conditions show that the hardness values of these specimens are in the lower plateau, which represents the acicular ferrite region.

Observations with the transmission electron microscope support the above conclusions. Figure 3.31 shows a representative micrograph of the specimen for the 1X condition. The ferrite laths are elongated and the dislocation density is high. Although the dislocation density was not measured, it seems to be consistent with the previous observations for the acicular ferrite microstructure. Some pools of retained austenite/martensite are present in this microstructure. In addition, as with the as-received microstructure, the jagged edges of some ferrite laths are evident (arrowed). This phenomenon was observed in the as-received samples and the possible reasons for that were explained in association with Figure 3.13c. The montage in Figure 3.32 represents a bigger picture of this microstructure. The acicular nature of ferrite laths is very obvious, and the islands of the M-A constituent are elongated between the ferrite laths. Considering this montage and the light micrograph for this cooling rate, it

Figure 3.31   The edges of "bainitic" ferrite subunits.
              Specimen cooled at 3.3°C/s, 1X condition.

Figure 3.32   Acicular ferrite and M-A islands in specimen
                cooled at 3.3°C/s, 1X condition.

is clear that the rows of small dark islands in the light
micrograph represent both acicularity of the microstructure
and the retention of some austenite between ferrite laths.
The measured average lath width for these microstructures is
about 0.45 μm and the size of M-A islands are about 1 to 1.5
μm, consistent with the other cooling rates.

It is interesting to notice the same directions of the
ferrite laths within different packets. The low-angle
features of the ferrite boundaries make them insensitive to
etching, therefore only packet boundaries and interfaces
between ferrite crystals and M-A islands can be revealed in
the light microscope.

Figures 3.33 and 3.34 represent two different regions
of a specimen cooled at 3.3°C/s for the 2X condition. There
is not much difference between the 1X and the 2X conditions.
The presence of small round particles indicates the same
redeposition effect observed at the higher cooling rates.
As mentioned before, reaustenitizing treatments may be
responsible for this phenomenon. In particular,
precipitation and coarsening may occur at 905°C.

The light micrographs in Figure 3.35 represent the
microstructure of both 1X and 2X conditions for specimens
cooled at 0.1°C/s. The relatively good etching behavior of
these specimens is similar to that of the as-received and

Figure 3.33   Acicular ferrite in specimen cooled at
3.3°C/s, 2X condition.

Figure 3.34   Acicular ferrite in specimen cooled at
               3.3°C/s, 2X condition.
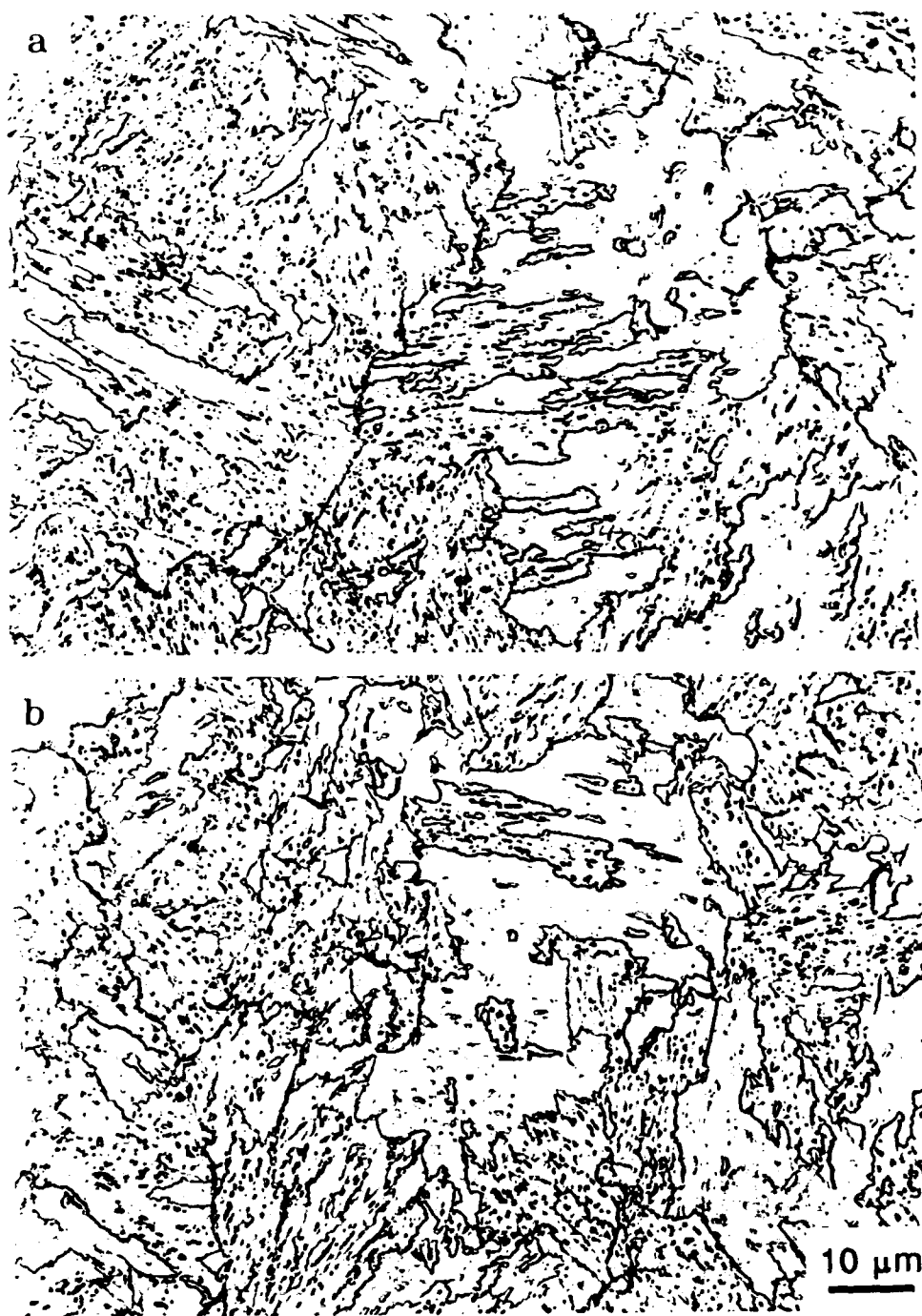
Figure 3.35   Light micrographs of the specimens cooled at
              0.1°C/s.   (a) 1X condition and (b) 2X
              condition.

the 3.3°C/s cooling rate specimens. All the features in these microstructures are similar to what was observed for the 3.3°C/s cooling rate. Although the cooling rate is very slow, the rows of retained austenite pools are indicative of the acicular nature of these microstructures. The hardness values of both the 1X and 2X conditions are in the lower plateau, an implication of non-martensitic structure. There is no indication of a granular structure.

TEM micrographs show the acicularity of these microstructures in more detail. Figure 3.36 is a montage (with a very slight gap) from the 2X condition. Notice the acicular ferrite laths and their interwoven nature. A large packet of ferrite "C" has separated the two sections of packets "A" and "B". A BF montage for the 1X condition is shown in Figure 3.37, and the CDF corresponding to the same area is represented in Figure 3.38. Notice the similarity of this microstructure with that of the as-received specimens. The different directions of ferrite packets are clearly shown in Figure 3.38.

Polishing behavior is the reason that some areas in these micrographs do not show the elongated laths. As mentioned before, the etching and polishing behaviors of these specimens act inversely. The electropolishing and thinning behavior is very good for the martensitic

Figure 3.36   Acicular ferrite in specimen cooled at
0.1°C/s, 2X condition.

Figure 3.37 Acicular ferrite in specimen cooled at
            0.1°C/s, 2X condition. BF image.

Figure 3.38   CDF image of the same region shown in Figure
               3.37.

specimens, but they do not etch well. In opposition to this behavior, the acicular ferrite structure responds better to the etching, but does not polish well. This behavior makes the thin areas on the TEM foil very small. Such behavior also explains why the etching behavior of the specimens cooled at different cooling rates can be a basis for comparison of the microstructures corresponding to each cooling rate.

In addition, an obscure but interesting feature was occasionally observed in these microstructures. Figure 3.39 shows an example of this observation. A block of martensite about 5.5 μm long and 0.6 μm thick seems to be perpendicular to the direction of ferrite laths. An interlath island of retained austenite/martensite which is almost perpendicular to the direction of this block indicates the direction of ferrite laths. The exact reason for this phenomenon is not clear. The lighter marks on this block suggest a martensitic structure. The accumulation of carbon in this region could be responsible for this phenomenon.

Figure 3.39   Angular martensite island in specimen cooled at
0.1°C/s, 2X condition.

3.6 Mechanical Properties

3.6.1   Tensile Properties

Tensile data for as-cooled (1°C/s, 1X and 2X) and as-cooled-plus tempered steels A, B and C are given in the appendix. These data include a 0.2% offset yield strength, tensile strength and total elongation.

Figure 3.40 represents these data in graphical form as a function of manganese content. As it is seen in this figure, the tensile strength and the yield strength increase with mangenese content. The total elongation decreases slightly with an increase in manganese content, which is expected to demonstrate an inverse relationship with the ultimate tensile strength behavior. The increase in tensile strength is a reflection of the increase in the hardness values as a function of manganese content, as described before.

There are two features about the tensile behavior of these steels to discuss. First is the behavior of the steels as a function of reaustenitizing cycles. The second feature is the effect of tempering on the tensile behavior of these steels.

The data show that both the yield strength and the
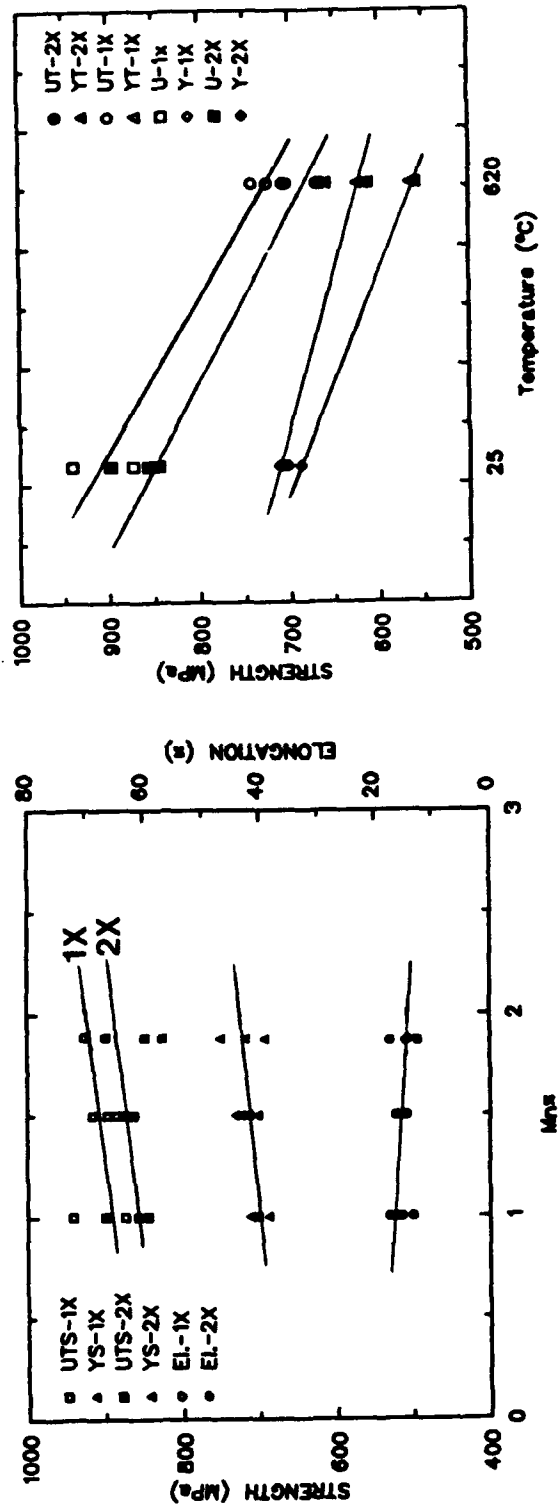
Figure 3.40 (a) Tensile data for steels A, B and C (1X and 2X conditions).
(b) Tensile properties of steel A before and after tempering.

ultimate tensile strength are higher for the 1X condition.
This is consistent with the hardness values as a function of
cooling rate, Figure 3.9. Since tensile tests were
conducted on specimens cooled at about 1°C/s, the specimens
are expected to have a microstructure of acicular ferrite
and M-A islands. The effect of grain size on the strength
of steel has been discussed before. In acicular ferrite,
several microstructural features play important roles in
addition to the prior austenite grain size. The lath and
packet size (also the degree of misorientation between the
packets), the average dislocation density and the M-A island
size and number density are the major factors that influence
the strength of steels with this microstructure (10,12,60).
These features are influenced by the austenite
transformation temperature and steel composition. The lower
the transformation temperature, the more dislocated the
structure, and the finer the lath size. This discussion
provides the basis for explaining the difference in the
tensile strengths of 1X and 2X conditions. Since the 1X
condition has a lower transformation temperature, finer
packet size and higher dislocation density should be
expected.

Coldren et al. showed that the presence of M-A
constituents increases the tensile strength of steel (126).

This phenomenon could be explained by the role of austenite-martensite islands as nucleation sources for mobile dislocations during deformation. It is possible that there is some difference in the average volume fraction of M-A islands which could lead to the difference in tensile strength between the 1X versus 2X conditions. Since the volume fraction of M-A islands has not been measured, this hypothesis is subject to verification.

The effects of tempering on the tensile properties of steel A for both the 1X and 2X conditions are shown in Figure 3.40b. Tempering at 620°C for 35 minutes caused a noticeable drop in the yield strength, but the effect on the tensile strength was dramatic. It has been shown (128) that tempering of low-carbon bainitic steels decreases their tensile strength and improves the fracture toughness. The increase in total elongation values for both 1X and 2X conditions is in agreement with previous observations.

3.6.2 Charpy Impact Properties

Charpy impact data for the as-cooled and the as-cooled-plus-tempered steels A, B and C are given in the appendix. These data include both the test temperature and the absorbed energy.

Figure 3.41 shows a graphical representation of these data. The data reveal that the 2X condition shows a better impact toughness and a lower transition temperature than the 1X condition. This is not true for steel C which contains 1.76% manganese. Generally, the effect of manganese on impact toughness is opposite of its effect on the strength of these steels. Steel A, with the lowest manganese level, shows the best impact toughness, while steel C has the lowest toughness among all of the three steels. This observation is true for both the 1X and 2X conditions.

The superiority of the 2X condition in impact properties over the 1X condition is due to the smaller prior austenite grain size and lower strength of the 2X condition. It is well known that grain refinement improves the impact properties of steel (3,128). The high-angle prior austenite grain boundaries are effective obstacles to propagation of cracks. When a crack reaches a high-angle grain boundary, a change in the direction of the crack is unavoidable. The propagation of the crack at this stage requires more energy. In discussion of the difference in tensile strengths between the 1X and 2X conditions, it was pointed out that this difference could be partly due to the presence of more M-A constituents in the 1X microstructure. Here, the higher transition temperature of the 1X condition could be related
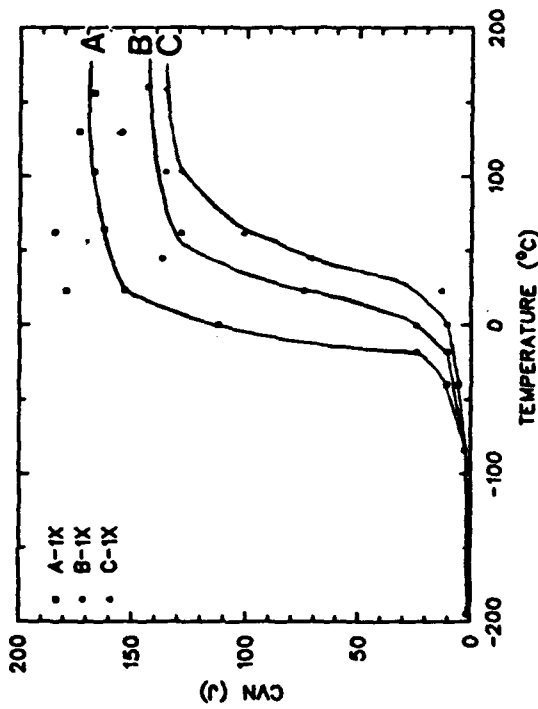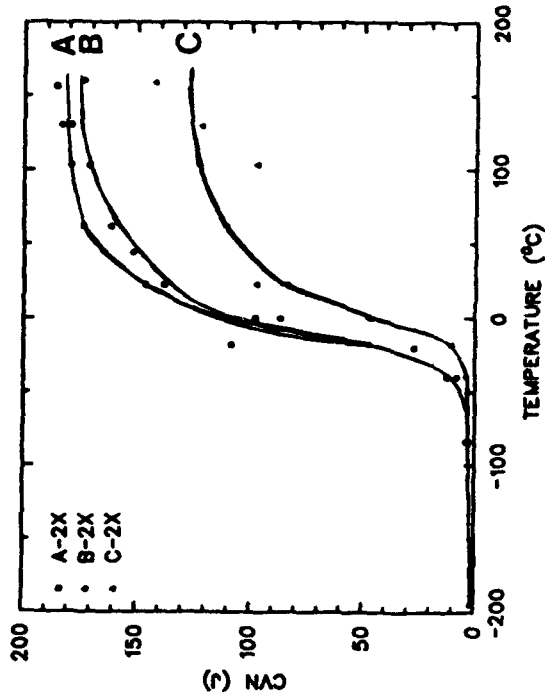
Figure 3.41 (a) Energy Absorbed versus temperature for steels
                  A, B and C, 1X condition.
             (b) Energy Absorbed versus temperature for steels
                  A, B and C, 2X condition.

to the deleterious effect of the higher volume fraction of M-A islands (126). Figure 3.41c shows the impact properties of steel A for the 1X and 2X conditions which were tempered at 620°C for 35 minutes.

According to Coldren et al. (126), the deleterious influence of M-A islands can be eliminated by tempering at 540-650°C. DeArdo et al. (22) also showed that tempering of steels very similar to those in the present study improved the fracture toughness of those steels. In another investigation, DeArdo and coworkers (129) stated that ductile fracture characteristics in the transverse direction are related to the amount, size and shape of the nonmetallic inclusions present in the steel. The resistance to brittle fracture has been related to the metallurgical condition of the parent austenite (the grain size of the austenite is the most important factor), the cleanliness of the steel and the strength level. They also concluded that the presence of hard particles, either inclusions, carbides and/or high-carbon martensite islands, could have an adverse effect on brittle fracture resistance.

Upon tempering, some of the high-carbon metastable austenite could have transformed isothermally to ferrite-carbide aggregates. The embrittlement effect of the carbides and the variation in the carbide dispersion can
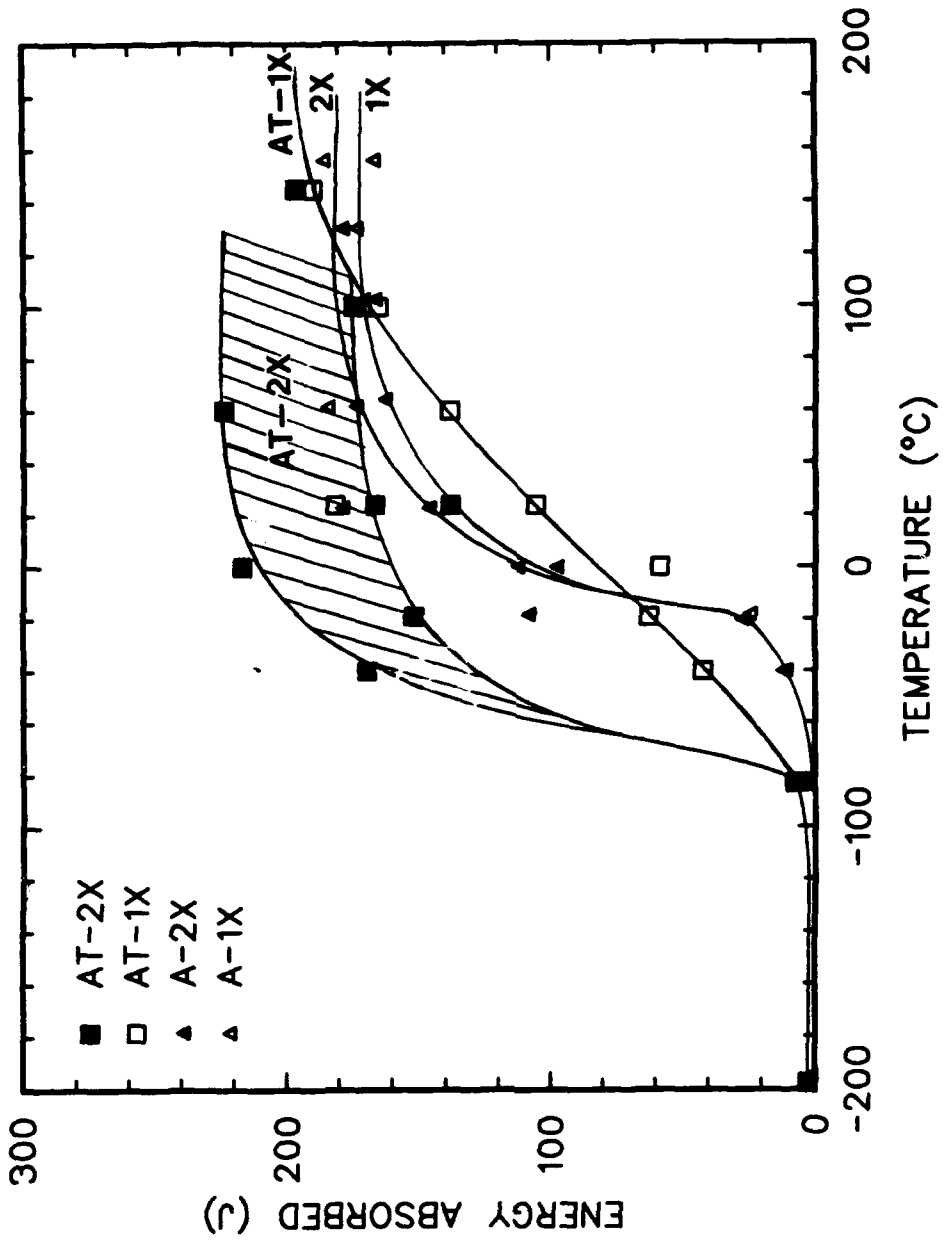
Figure 3.41   (c) Energy Absorbed versus temperature for steel A in the as-cooled and 620°C-tempered treatments. Includes data for the 1X and 2X conditions.

lead to lower toughness. This has been confirmed by Smith et al. (16).

With this in mind, tempering of the steels with the presence of M-A constituents may have mixed results. Although the transition temperature of the 2X condition has shifted to lower temperatures, the effect of tempering on the upper shelf energy is not very clear. The appearance of a "dual upper shelf" could be the result of the mixed effect of tempering when M-A constituents are present. There is another possibility for this behavior. A delamination effect, which will be shown in the fractography of the non-tempered specimen, could be responsible. One can also argue that the so-called delamination did not have such an effect on the as-cooled specimens, which may make the above argument invalid.

The effects of tempering showed an absolute inverse effect on the transition temperature of the 1X condition. Here again, the possibility of more M-A islands for the 1X condition arises. As indicated above and according to the previous observations, the presence of M-A islands could have negative effect on the toughness of steel after tempering.

3.6.3 Fractography

An investigation of the fracture surfaces of steel B for the 1X and 2X conditions was conducted using SEM. Three samples, from the lower shelf (-195°C), the transition region (23°C) and the upper shelf (100°C), were examined for each condition. Figure 3.42 shows the fracture surfaces of specimens tested at all three temperatures for the 1X condition. At 15X magnification, the transition from the brittle fracture to the ductile fracture is clear. Notice the "delamination" in Figure 3.42c.

Figure 3.43 represents the fracture surfaces for the 1X and 2X conditions at -195°C. It is clear from these pictures that a cleavage fracture developed in both conditions. The energy absorbed was about 3 J for both samples. A comparison between the facet sizes in Figures 3.43a and b clearly shows the larger facet size associated with the 1X condition.

Figure 3.44 shows the fracture surfaces for both the 1X and 2X conditions at room temperature. Both of the samples showed a mixed mode of fracture, although there was more ductile rupture in the 2X condition compared to the 1X. The energy absorbed for the 1X condition was 74 J while that of the 2X condition was 84 J. The higher strength and larger
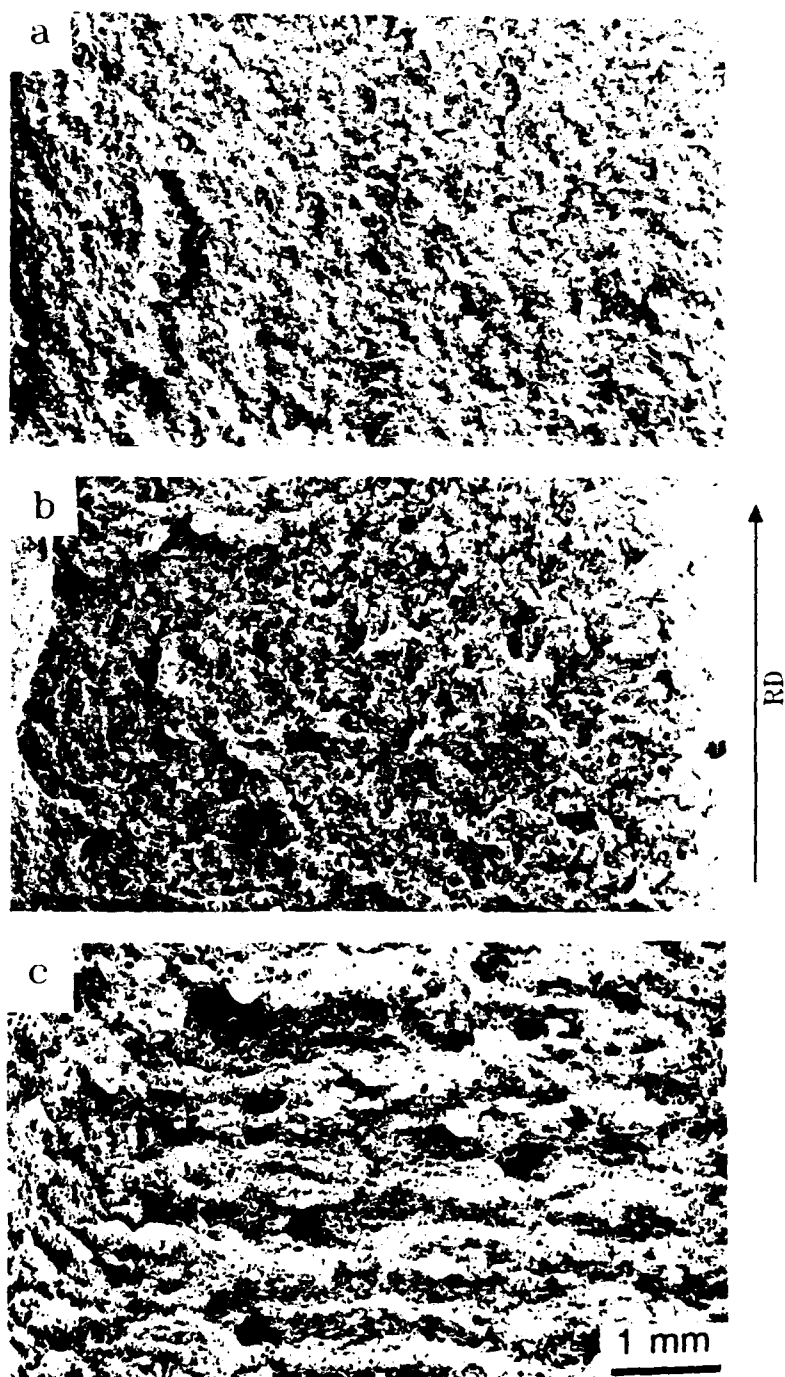
Figure 3.42   SEM micrographs of the fracture surfaces after testing at (a) -195°C, (b) 23°C and (c) 100°C. Steel B, 1X condition.

Figure 3.43   Fracture surfaces for steel B tested at -195°C.
              (a) 1X and (b) 2X conditions.
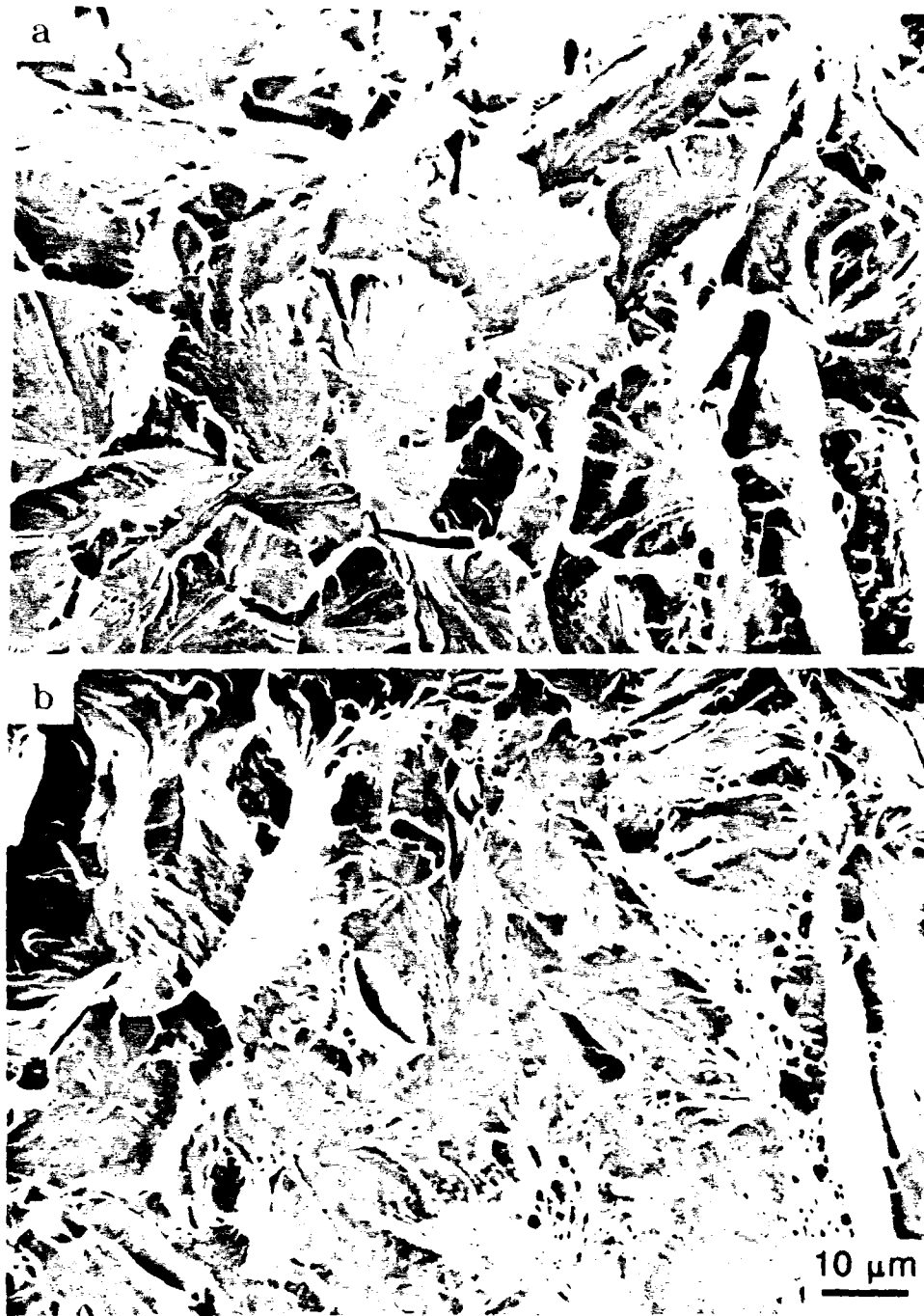
Figure 3.44   Fracture surfaces for steel B tested at 23°C.
(a) 1X and (b) 2X conditions.

grain size of the 1X condition explain this difference. The
presence of small particles are apparent where ductile
rupture has occurred.

The fracture surfaces of the specimens tested at about
100°C are shown in Figure 3.45. The energy absorbed by each
sample was 167 and 179 J, for the 1X and 2X conditions,
respectively. Ductile microvoid nucleation, coalescence and
growth produce this type of fracture surface. The presence
of inclusions within each dimple is in agreement with the
role of the hard particles, including inclusions, in the
initiation of fracture (128). Elongated inclusion particles
in the rolling direction caused the elongated shape of the
dimples, while round inclusions do not show the same effect.
These observations reinforce the idea that cleanliness is an
important factor in determining the fracture toughness of
the steel (128,129). Irvine and Pickering (128) suggested
that the presence of particles in every dimple is not
necessary for the formation of dimples. Most of the dimples
in these micrographs contain inclusions. This indicates the
high inclusion content of these steels, which is probably
responsible for their having a lower toughness than what was
expected.
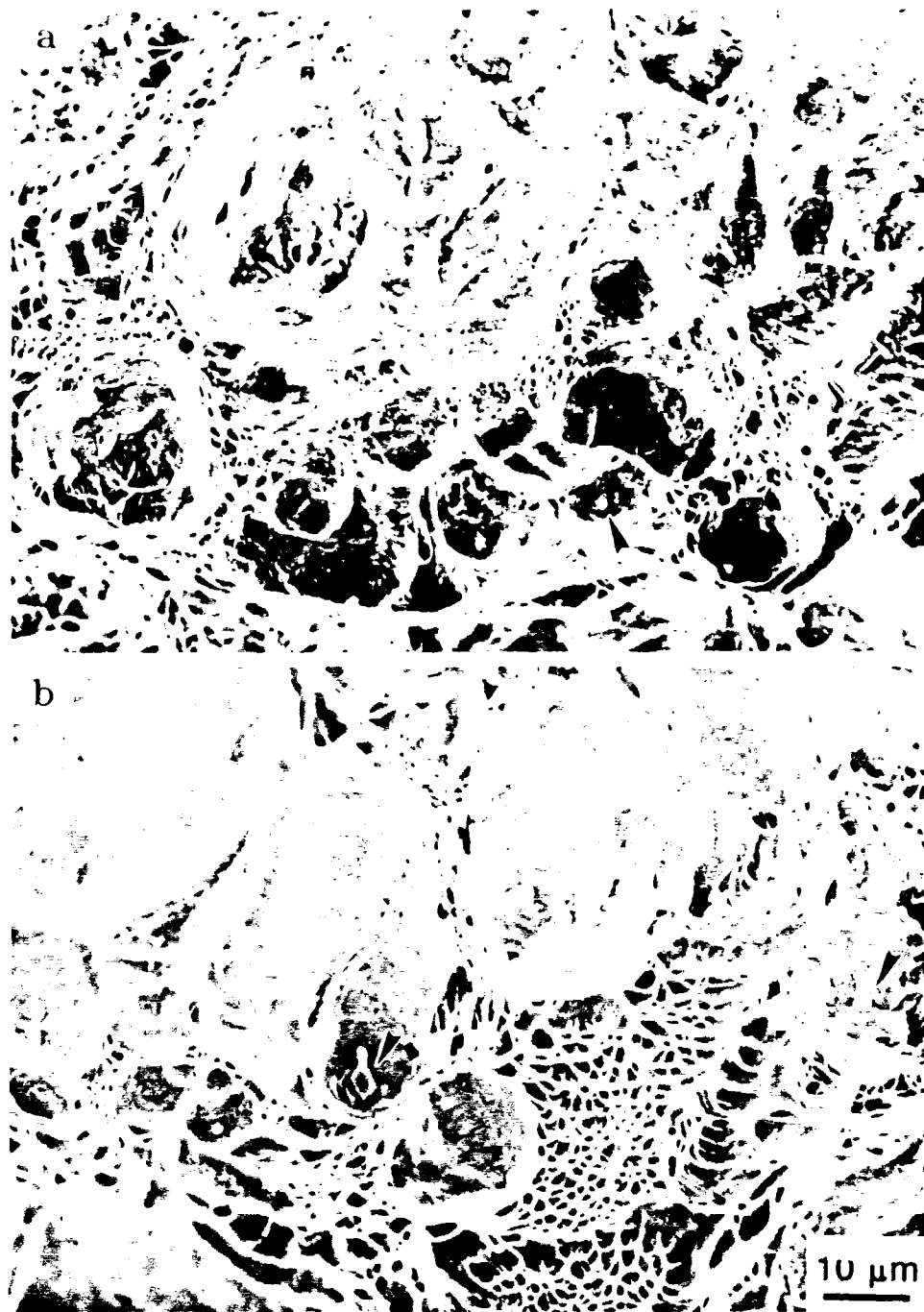
Figure 3.45   Fracture surfaces for steel B tested at 100°C.
               (a) 1X and (b) 2X conditions.

3.7 Summary and Conclusions

The continuous cooling transformation of these very low-carbon steels revealed interesting features of their transformation behavior. Although the broad, flat-topped CCT diagrams do not present any noticeable indication of changes in the transformation products upon cooling at different cooling rates, the hardness profiles are clearly indicative of important changes. These changes are coupled with differences in the etching and electropolishing behavior of the specimens cooled at different cooling rates to prove the existence of changes in austenite transformation behavior.

The light microscopy and transmission electron microscopy of the specimens examined for generation of the CCT diagrams, as well as the as-received specimens, showed the following features:

1. A martensitic microstructure is the product of fast cooling rates. At cooling rates faster than about $25^{\circ}C/s$, the 1X condition (i.e. prior austenite grain size of about 30 μm) exhibits predominantly martensitic microstructure. For the 2X condition (i.e., prior austenite grain size of about 7 μm), martensite is formed at cooling rates faster than about $37^{\circ}C/s$. These structures do not respond well to the chemical etching, but their response to electropolishing

(thinning for TEM) is quite good. The upper plateau on
the hardness profiles corresponds to the martensitic
structure. Very fine, elongated and sometimes interwoven
lath structures, in addition to some twinned martensite, are
characteristics of this structure.

2. Acicular ferrite is the dominant austenite decomposition
product for the cooling rates below about 7°C/s for the 1X
condition. For the 2X condition this range is below about
25°C/s. Elongated ferrite laths, interlath retained
austenite and/or martensite and high dislocation density are
characteristics of this microstructure. The lowest cooling
rate examined was 0.05°C/s. The etching response of these
structures is much better than the martensitic structures,
but their response to electropolishing is very poor. The
lower plateau on the hardness profiles corresponds to the
acicular ferrite structure.

3. At cooling rates intermediate to those at which the
martensitic structure and the acicular ferritic structure
form, mixed microstructures consisting of acicular ferrite
and martensite form during cooling. The higher the cooling
rate, the more martensite is in the microstructure. This is
consistent with the higher hardness values for higher
cooling rates.

4. The ferritic lath width increases with decreasing

cooling rate. This value is about 0.2 μm for the
martensitic structure produced at a 150°C/s cooling rate,
and increases to about 0.55 μm for the acicular ferrite
formed upon cooling at 0.1°C/s. An anomaly was found in the
as-received steel (0.8 μm), but this was probably due to an
insufficient number of measurements.

5. Both the yield strength and the ultimate tensile strength
increased with manganese content. However, the 1X condition
shows higher strength than the 2X condition regardless of
the manganese content. This is consistent with the hardness
data. Tempering at 620°C for 35 minutes decreased both the
tensile and the yield strengths of steel A.

6. The Charpy impact behavior of all three steels is
consistent with other data. The 2X condition showed higher
impact toughness and a lower transition temperature than the
1X condition. Generally, the effect of manganese on impact
toughness is opposite its effect on the strength of these
steels.

   Tempering lowered the transition temperature and
increased the toughness of steel A for the 2X condition.
For the 1X condition, the transition temperature increased
after tempering. This is attributed to the possible higher
number density of M-A islands in the 1X condition than the
2X condition.

REFERENCES

1. E.E. Fletcher, <u>High-Strength, Low-Alloy Steels: Status, Selection and Physical Metallurgy</u>, Battelle Press, Columbus, Ohio, 1979.

2. F.B. Pickering, "High-Strength, Low-Alloy Steels - A Decade of Progress", <u>Proceedings of an International Symposium on High-Strength, Low-Alloy Steels</u>, Microalloying 75, Union Carbide Corp., New York, N.Y., 1977, pp. 9-31.

3. F.B. Pickering, <u>Physical Metallurgy and the Design of Steels</u>, Applied Science Publishers, London, England, 1978.

4. W.C. Leslie, <u>The Physical Metallurgy of Steels</u>, McGraw-Hill, Tokyo, Japan, 1982.

5. J.M. Rigsbee and P.J. VanderArend, "Laboratory Studies of Microstructures and Structure-Property Relationships in 'Dual-Phase' HSLA Steels", in <u>Conference Proceedings: Formable HSLA and Dual-Phase Steels</u>, ed. A.T. Davenport, AIME, New York, N.Y., 1977, pp. 56-86.

6. R.L. Brockenbrough, "Design Trends for High-Strength, Low-Alloy Steels", <u>Processing and Properties of Low Carbon Steel</u>, ed. J.M. Gray, AIME, New York, N.Y., 1973, pp. 389-397.

7. I. Takahashi, T. Kato, T. Tanaka and T. Mori, "Development of a High Strength, Hot Rolled Steel With 100 ksi Yield Strength", in <u>Conference Proceedings: Toughness Characterization and Specifications for HSLA and Structural Steels</u>, ed. P.L. Mangonon Jr., AIME, New York, N.Y., 1979, pp. 308-337.

8. J.D. Evensen, J. Lereim and J.D. Embury, "Microstructural Aspects of the Fracture Parameters of Controlled Rolled HSLA Steels", in <u>Conference Proceedings: Toughness Characterization and Specifications for HSLA and Structural Steels</u>, ed. P.L. Mangonon Jr., AIME, New York, N.Y., 1979, pp. 187-215.

9.   High-Strength, Low-Alloy and High-Strength Intermediate
      Manganese Steel, AISI Steel Products Manual 17, 1967.
      From ref. 4.

10.   F.B. Pickering, "The Structure and Properties of
      Bainite in Steels", in Symposium: Transformation and
      Hardenability in Steels, Climax Molybdenum Co.,
      Ann Arbor, Michigan, 1967, pp. 109-132.

11.   R.W.K. Honeycombe and F.B. Pickering, "Ferrite and
      Bainite in Alloy Steels", Metallurgical Transactions,
      Vol. 3, 1972, pp. 1099-1112.

12.   A.J. McEvily, R.G. Davies, C.L. Magee and T.L.
      Johnston, "Structure, Hardenability and Toughness of
      Low-Carbon High-Strength Steels", Symposium:
      Transformation and Hardenability in Steels, Climax
      Molybdenum Co., Ann Arbor, Michigan, 1967, pp. 179-194.

13.   A.J. McEvily and C.L. Magee, "Transformation-Structure-
      Property Characteristics of Low-Carbon Alloy Steels",
      in Low-Alloy Steels, ISI Publication 114, London,
      England, 1968, pp. 111-117.

14.   K.J. Irvine and F.B. Pickering, "Low-Carbon Bainitic
      Steels", JISI, London, England, 1957.

15.   A.P. Coldren, Y.E. Smith and R.L. Cryderman,
      "Microstructure and Properties of Low-Carbon Mn-Mo-Cb
      Steels", Processing and Properties of Low Carbon Steel,
      ed. J.M. Gray, AIME, New York, N.Y., 1973, pp. 163-189.

16.   Y.E. Smith, A.P. Coldren and R.L. Cryderman,
      "Manganese-Molybdenum-Niobium Acicular Ferrite Steels
      With High Strength and Toughness", Symposium:
      Toward Improved Ductility and Toughness, Climax
      Molybdenum Co., Ann Arbor, Michigan, 1971, pp. 119-142.

17.   R.R. Irving, "A Cost Effective Replacement for HY-80",
      Iron Age, May 16, 1986, pp. 53-55.

18.   A.P. Coldren and T.B. Cox, "Development of 100 ksi
      Yield Strength HSLA Steel", AMAX Report No. CPR-20,
      1986.

19.   L.G. Kvidahl, "An Improved High Yield Strength Steel
      for Shipbuilding", Welding Journal, Vol. 64, 1985,
      pp. 42-48.

20. D.J. Colvin, "The Physical Metallurgy of Some Low-Carbon, Cu-Bearing HSLA Plate Steels", M.Sc. Thesis, T 3600, Colorado School of Mines, Golden, CO, 1988.

21. Sherri A. Richardson, "The Effects of Thermal Processing on the Microstructure and Mechanical Properties of a HSLA-100 Plate Steel", M.Sc. Thesis, T 3949, Colorado School of Mines, Golden, CO,1990.

22. M.R. Blicharski, C.I. Garcia, S. Pytel and A.J. DeArdo, "Structure and Properties of ULCB Plate Steels for Heavy Section Applications", in Processing, Microstructure and Properties of HSLA Steels, ed. A.J. DeArdo, AIME, New York, N.Y., 1988, pp. 317-329.

23. H.K.D.H. Bhadeshia and D.V. Edmonds, "The Bainite Transformation in a Silicon Steel", Metallurgical Transactions A, Vol. 10A, 1979, pp. 895-907.

24. H.K.D.H. Bhadeshia and D.V. Edmonds, "Bainite in Silicon Steels: New Composition-Property Approach Part 1", Metal Science, Vol. 17, 1983, pp. 411-419.

25. H.K.D.H. Bhadeshia and D.V. Edmonds, "Bainite in Silicon Steels: New Composition-Property Approach Part 2", Metal Science, Vol. 17, 1983, pp. 420-425.

26. V.T.T. Miihkinen and D.V. Edmonds, "Microstructural Examination of Two Experimental High-Strength Bainitic Low-Alloy Steels Containing Silicon", Materials Science and Technology, Vol. 3, 1987, pp. 422-431.

27. H.I. Aaronson and H.J. Lee, "Another Visit to the Three Definitions of Bainite", Scripta Metallurgica, Vol. 21, 1987, pp. 1011-1016.

28. First Progress Report of Subcommittee XI: "Electron Microstructure of Steel", ASTM Committee E-4, Proceedings ASTM, Vol. 50, 1950, pp. 444-492.

29. Second Progress Report by Subcommittee XI of Committee E-4, "Electron Microstructure of Bainite in Steel", Proceedings ASTM, Vol. 52, 1952, pp. 543-572.

30. D.N. Shackleton and P.M. Kelly, "Morphology of Bainite", Physical Properties of Martensite and Bainite, ISI, Special Report 93, London, England, 1965, pp. 126-134.

31. J.M. Oblak and R.F. Hehemann, "Structure and Growth of Widmanstätten Ferrite and Bainite", Symposium: Transformation and Hardenability in Steels, Climax Molybdenum Co., Ann Arbor, Michigan, 1967, pp. 15-38.

32. H.K.D.H. Bhadeshia and A.R. Waugh, Proc. Int. Conf. on Solid-Solid Phase Transformations, ed. by Aaronson, Laughlin, Sekerka and Wayman, AIME, New York, N.Y., 1982, p. 1581.

33. G.R. Purdy and M. Hillert, "On the Nature of the Bainite Transformation in Steels", Acta Metallurgica, Vol. 32, No. 6, 1984, pp. 823-828.

34. R.H. Goodenow, R.H. Barkalow and R.F. Hehemann, "Bainite Transformations in Hypoeutectoid Steels", Physical Properties of Martensite and Bainite, ISI, Special Report 93, London, England, 1965, pp. 135-152.

35. L.J. Habraken and M. Economopoulos, "Bainitic Microstructures in Low-Carbon Alloy Steels and Their Mechanical Properties", Symposium: Transformation and Hardenability in Steels, Climax Molybdenum Co., Ann Arbor, Michigan, 1967, pp. 69-108.

36. S.W. Thompson and G. Krauss, "Structure and Properties of Continuously Cooled Bainitic Ferrite-Austenite-Martensite Microstructures", in Mechanical Working and Steel Processing Proceedings, 1989, pp. 467-481.

37. S.W. Thompson, D.J. Colvin, and G. Krauss, "Continuous Cooling Transformations and Microstructures in a Low-Carbon, High-Strength Low-Alloy Plate Steel", Metallurgical Transactions A, Vol. 21A, 1990, pp. 1493-1507.

38. B.S. Kloberdanz, ongoing M.S. thesis work, Colorado School of Mines, 1992.

39. J.H. Woodhead and J.A. Whiteman, "Structure and Properties of Apolygonal Ferrites", Processing and Properties of Low Carbon Steel, ed. J.M. Gray, AIME, New York, N.Y., 1973, pp. 145-162.

40. S.H. Avner, Introduction to Physical Metallurgy, Second Edition, McGraw-Hill, Singapore, 1985.

41. E.C. Bain and H.W. Paxton, Alloying Elements in Steels, Second Edition, Third Revised Printing, ASM, Metals Park, Ohio, 1966.

42. S.W. Poole and J.E. Franklin, "High-Strength Structural and High-Strength Low-Alloy Steels", Metals Handbook, 9th Edition, ASM, Metals Park, Ohio, pp. 403-420.

43. R.J. Jessman and G.J. Murphy, "Precipitation Hardening Alloy Steels Provides Strength and Low Temperature Toughness Under Sever Service Conditions", Industrial Heating, Sept. 1979, pp. 27-32.

44. George Krauss, Steels: Heat Treatment and Processing Principals, ASM, Metals Park, Ohio, 1989.

45. Y.J. Park and F.B. Fletcher, "Effects of Manganese, Chromium, and Molybdenum on the Isothermal Transformation of Austenite in Eutectoid Steels", J. Heat Treating, Vol. 4, No. 3, 1986, ASM, pp. 247-252.

46. P. Henry, The Importance of Molybdenum in Heavy Steel Sections, Climax Molybdenum Co., London, England, 1972.

47. J.C. Greenbank, "Carbon Solute Interactions in Fe-Cr-C, Fe-Mo-C and Fe-W-C Alloys", Journal of the Iron and Steel Institute, 1971, pp. 986-990.

48. H. Wada, "Thermodynamics of the Fe-Mo-C System at 985K", Metallurgical Transactions A, Vol. 17A, 1986, pp. 391-398.

49. J.A. Straatmann, D.V. Doane and Y.J. Park, "Using CCT Diagrams in the Development of Low-Carbon, High Strength Steels" in Processing, Microstructure and Properties of HSLA Steels, ed. A.J. DeArdo, AIME, New York, N.Y., 1988, pp. 287-303.

50. F.G. Berry and R.W.K. Honeycombe, "The Isothermal Decomposition of Austenite in Fe-Mo-C Alloys", Met. Trans., Vol. 1, 1970, pp. 3279-3286.

51. R.A. DePaul and A.L. Kitchin, "The Role of Nickel, Copper, and Columbium (Niobium) in Strengthening a Low-Carbon Ferritic Steel", Metallurgical Transactions, Vol. 1, Feb. 1970, pp. 389-393.

52. A.P. Coldren and G.T. Eldis, "Using CCT Diagrams to Optimize the Composition of an As-Rolled Dual-Phase Steel", Journal of Metals, March 1980, pp. 41-48.

53. M.R. Krishnadev and A. Galibois, "Development of a High-Strength Low-Alloy Steel Strengthened by Transformation Substructure and Precipitation of Copper and Niobium", Metals Technology, Vol. 1, 1974, pp. 300-302.

54. K.J. Irvine, JISI, 1962, p. 820.

55. R.L. Smith, G. Spangler and R.M. Brick, Trans Am. Soc. Metals, Vol. 46, 1954, p. 973.

56. E.O. Hall, Proc. Phys. Soc., London, Vol. B64, 1951, p. 747.

57. N.J. Petch, JISI, Vol. 174, 1953, p. 25.

58. R.W.K. Honeycombe, Structure and Strength of Alloy Steels, Climax Molybdenum Co., London, England.

59. R.W. Armstrong, "The Influence of Polycrystal Grain Size on Several Mechanical Properties of Materials", Met. Trans., Vol. 1, 1970, pp. 1169-1176.

60. K.J. Irvine, "A Comparison of the Bainite Transformation With Other Strengthening Mechanisms in High-Strength Structural Steels", Symposium: Steel-Strengthening Mechanisms, Climax Molybdenum Co., Greenwich, Connecticut, 1969, pp. 55-65.

61. J. Malcolm Gray, "Columbium (Niobium) as a Grain Refiner in Hot-Rolled Steels", Processing and Properties of Low Carbon Steel, ed. J.M. Gray, AIME, New York, N.Y., 1973, pp. 225-247.

62. M. Durbin and P.R. Krahe, "Controlled Rolling and the Properties of Very Low Carbon, High Manganese Steels Containing Strong Carbide Formers", in Processing and Properties of Low Carbon Steel, ed. by J.M. Gray, AIME, New York, N.Y., 1973, pp. 109-131.

63. I. Kozasu and T. Osuka, "Processing Conditions and Properties of Control-Rolled Steel Plates", in Processing and Properties of Low Carbon Steel, ed. by J.M. Gray, AIME, New York, N.Y., 1973, pp. 47-67.

64. Tomo Tanaka, N. Tabata, T. Hatomura and C. Shiga, "Three Stages of the Controlled-Rolling Process", Proceedings of an International Symposium on High-Strength, Low-Alloy Steels, Microalloying 75, Union Carbide Corp., New York, N.Y., 1977, pp. 107-119.

65. B. Karlsson, "Grain Refinement in Fe-C Alloys by Thermal Cycling", Materials Science and Engineering, Vol. 11, 1973, pp. 185-193.

66. J.Y. Koo and G. Thomas, "Thermal Cycling Treatments and Microstructures for Improved Properties of Fe-0.12% C-0.5% Mn Steels", Materials Science and Engineering, Vol. 24, 1976, pp. 187-198.

67. R.A. Grange, Trans. Am. Soc. Metals, Vol. 59, 1966, p. 26.

68. R.B. Nicholson, "Strong Microstructures From the Solid State" in Strengthening Mechanisms in Crystals ed. A. Kelly and R.B. Nicholson, John-Wiley and Sons, New York, N.Y., 1971, p. 542.

69. J.H. Bucher, "The Toughness of Ferritic Steel Strengthened by Precipitation of CbC", Trans. AIME, Vol. 239, 1967, pp. 478-485.

70. E.C. Hamre and A.M. Gilroy-Scott, "Properties of Acicular-Ferrite Steel for Large-Diameter Line Pipe", in Proceedings of an International Symposium on High-Strength, Low-Alloy Steels, Microalloying 75, Union Carbide Corp., New York, N.Y., 1977.

71. Paul E. Repas, "Control of Strength and Toughness in Hot-Rolled Low-Carbon Manganese-Molybdenum-Columbium-Vanadium Steels", Proceedings of an International Symposium on High-Strength, Low-Alloy Steels, Microalloying 75, Union Carbide Corp., New York, N.Y., 1977, pp. 387-398.

72. T. Gladman, D. Dulieu and Ian D. McIvor, "Structure-Property Relationships in High-Strength Microalloyed Steels", in Proceedings of an International Symposium on High-Strength, Low-Alloy Steels, Microalloying 75, Union Carbide Corp., New York, N.Y., 1977, pp. 32-58.

73. P.R. Kirkwood, "Welding of Niobium Containing Microalloyed Steels", in Niobium: Proceedings of the International Symposium, edited by Harry Stuart, AIME, New York, N.Y., 1981, pp. 761-802.

74. A.L. Mincher, R.A. Bosch and P.R. Morgan, "Commercial Production of High-Strength, Titanium-Bearing Hot-Rolled Steel", Proceedings of an International Symposium on High-Strength, Low-Alloy Steels, Microalloying 75, Union Carbide Corp., New York, N.Y., 1977, pp. 251-260.

75. B. Aronsson, "The Microstructure and Mechanical Properties of Some Martensitic Steels With Special Reference to the Influence of Niobium and Molybdenum", Symposium Steel-Strengthening Mechanisms, Climax Molybdenum Co., Greenwich, Connecticut, 1969, pp. 77-87.

76. S.W. Thompson and G. Krauss, "Precipitation and Fine Structure in Medium-Carbon Vanadium and Vanadium/Niobium Microalloyed Steels", Metallurgical Transactions A, Vol. 20A, 1989, pp. 2279-2288.

77. T. Tanaka, "Controlled Rolling of Steel Plate and Strip", International Metals Review, 1981, pp. 185-212.

78. N.P. Allen, "Effect of Solute Element on the Mechanical Properties of Iron" ,in Proceedings of a Conference on Iron and Its Dilute Solid Solutions, ed. C.W. Spencer and F.E. Werner, Interscience Publishers, New York, N.Y., 1963, pp. 271-314.

79. R.E. Reed-Hill, Physical Metallurgy Principles, Van Nostrand Co., New York, N.Y., 1964.

80. George E. Dieter, Mechanical Metallurgy, Second Edition, McGraw-Hill, New York, N.Y., 1984.

81. P.M. Kelly and J. Nutting, "Strengthening Mechanisms in Martensite", Physical Properties of Martensite and Bainite, ISI, Special Report 93, London, England, 1965, pp. 166-170.

82. G.R. Speich and P.R. Swann, "Yield Strength and Transformation Substructure of Quenched Iron-Nickel Alloys", JISI, 1965, pp. 480-485.

83. G.E. Hicho, S. Singhal, L.C. Smith and R.J. Fields, "Effect of Thermal Processing Variations on the Mechanical Properties and Microstructure of a Precipitation Hardening HSLA Steel", Journal of Heat Treating, Vol. 3, No. 3, 1984, pp. 205-212.

84. W.E. Creswick, "Commercial Development of a Rimmed Low-Alloy Precipitation-Hardening High-Strength Steel", Strong Tough Structural Steels, ISI No. 104, London, England, 1967, pp. 86-92.

85. P. Morcinek, V. Smid, T. Heczko and T. Prenka, "Structural Steels With Acicular Ferrite", in Proceedings of an International Symposium on High-Strength, Low-Alloy Steels, Microalloying 75, Union Carbide Corp., New York, N.Y., 1977, pp. 272-278.

86. M. Cohen and W. S. Owen, "Thermo-mechanical Processing of Microalloyed Steels" Proceedings of an International Symposium on High-Strength, Low-Alloy Steels, Microalloying 75, Union Carbide Corp., New York, N.Y., 1977, pp. 2-8.

87. M.G. Gemmill, "The Merits and Demerits of Strengthening Mechanisms is Low-Alloy Steels", Symposium: Steel-Strengthening Mechanisms, Climax Molybdenum Co., Greenwich, Connecticut, 1969, pp. 67-75.

88. J.W. Christian, "Military Transformations: An Introductory Survey", Physical Properties of Martensite and Bainite, ISI, Special Report 93, London, England, 1965, pp. 1-25.

89. R.F. Hehemann, K.R. Kinsman and H.I. Aaronson, "A Debate on the Bainite Reaction", Metallurgical Transactions, Vol. 3, 1972, pp. 1077-1094.

90. K.R. Kinsman and H.I. Aaronson, "Influence of Molybdenum and Manganese on the Kinetics of the Proeutectoid Ferrite Reaction", Symposium: Transformation and Hardenability in Steels, Climax Molybdenum Co., Ann Arbor, Michigan, 1967, pp. 39-55.

91. H.I. Aaronson, "On the Problem of the Definitions and the Mechanisms of the Bainite Reaction", The Mechanism of Phase Transformations in Crystalline Solids, pp. 270-312.

92.   J.W. Christian, "The Origin of Surface Relief Effects
      in Phase Transformations", in <u>Decomposition of
      Austenite by Diffusional Processes</u>, ed. by V.F. Zackay
      and H.I. Ironstone, InterScience Publishers, Easton,
      Pennsylavania 1962, pp. 371-386.

93.   S.K. Liu and G.Y. Zhang, "The Effect of Mn and Si on
      the Morphology and Kinetics of the Bainite
      Transformation in Fe-C-Ti Alloys", Metallurgical
      Transactions A, Vol. 21A, June 1990, pp. 1509-1515.

94.   H.K.D.H. Bhadeshia and J.W. Christian, "Bainite in
      Steels", Metallurgical Transactions A, Vol. 21A, April
      1990, pp. 767-797.

95.   S.W. Thompson, Private communication based on
      unpublished research.

96.   H.K.D.H. Bhadeshia, Proc. Int. Conf. <u>Solid-Solid Phase
      Transformations</u>, ed. by G.W. Lorimer, Institute of

97.   Bainite Committee of Iron & Steel Institute of Japan,
      <u>Atlas for Bainitic Microstructures</u>, Vol. 1, 1992.
      Metals, London, England, 1988, pp. 321-386.

98.   G.R. Speich and H. Warlimont, "Yield Strength and
      Transformation Substructure of Low-Carbon Martensite",
      JISI, 1968, pp. 385-392.

99.   W.D. Swanson and J. Gordon Parr, "Transformations in
      Iron-Nickel Alloys", JISI, Feb. 1964, pp. 104-106.

100. D.W. Gomersall and J. Gordon Parr, "Transformations in
      Iron-Manganese Alloys," JISI, March 1965, pp. 275-279.

101. J.M. Wallbridge and J. Gordon Parr, "Transformations in
      Fe-Cr Alloys," JISI, Feb. 1966, pp. 119-121.

102. J. Gordon Parr, "Transformations in Fe-Co Alloys,"
      JISI, April 1967, pp. 426-427.

103. E.A. Wilson, "The $\gamma \rightarrow \alpha$ Transformation in Iron,"
      Scripta Metallurgica, Vol. 12, 1978, pp. 961-968.

104. E.A. Wilson, "The $\gamma \rightarrow \alpha$ Transformation in Iron and its
      Dilute Alloys," Scripta Metallurgica, Vol. 4, 1970, pp.
      309-312.

105. A. Gilbert and W.S. Owen, "Diffusionless Transformation in Iron-Nickel, Iron-Chromium and Iron-Silicon Alloys," Acta Metallurgica, Vol. 10, 1962, pp. 45-54.

106. A.R. Marder and G. Krauss, "The Morphology of Martensite in Iron-Carbon Alloys," Trans. ASM, Vol. 60, 1967, pp. 651-660.

107. R.H. Goodenow and R.F. Hehemann, "Transformations in Iron and Fe-9 Pct Ni Alloys," Trans. AIME, Vol. 233, 1965, pp. 1777-1786.

108. J.M. Marder and A.R. Marder, "The Morphology of Iron-Nickel Massive Martensite," Trans. ASM, Vol. 62, 1969, pp. 1-10.

109. G. Krauss and A.R. Marder, "The Morphology of Martensite in Iron Alloys," Met. Trans., Vol. 2, 1971, pp. 2343-2357.

110. Lee Dillinger, "Hardness Testing", Met-Tips, Ideas for Metallographic Procedures, Leco Corp., Michigan, 1980.

111. George T. Eldis, "A Critical Review of Data Sources for Isothermal Transformation and Continuous Cooling Transformation Diagrams", in Proceedings of an International Conference on Solid-Solid Phase Transformations, TMS-AIME, Warrendale, PA, 1982, pp. 126-157.

112. "Standard Test Methods for Determining Average Grain Size", ASTM Designation: E112-88, Annual Book of ASTM Standards, Vol. 03.01, ASTM, Philadelphia, PA, 1989, pp. 284-306.

113. Halle Abrams, "Grain Size Measurement by Intercept Method", Metallography, Vol. 4, 1971, pp. 59-78.

114. "Standard Test Methods for Characterizing Duplex Grain Sizes", ASTM Designation: E1181-87, Annual Book of ASTM Standards, Vol. 03.01, ASTM, Philadelphia, PA, 1989, pp. 828-841.

115. E.E. Underwood, "Applications of Quantitative Metallography", Metals Handbook, ASM, Metals Park, Ohio, 1988, pp. 37-47.

116. <u>Dynamic Thermal/Mechanical Metallurgy Using the Gleeble 1500</u>, Second Edition, Duffers Scientific Inc., Troy, N.Y., 1986.

117. G.R. Speich and T.M. Scoonover, "Continuous-Cooling-Transformation Behavior and Strength of HSLA-80 (A710) Steel Plates", in <u>Processing, Microstructure and Properties of HSLA Steels</u>, ed. A.J. DeArdo, AIME, New York, N.Y., 1988, pp. 263-286.

118. W.W. Cias, <u>Phase Transformation Kinetics and Hardenability of Medium-Carbon Alloy Steels</u>, Climax Molybdenum Co., Greenwich, Connecticut.

119. "Standard Test Method for Vickers Hardness of Metallic Materials", ASTM Designation: E92-82, <u>Annual Book of ASTM Standards</u>, Vol. 03.01, ASTM, Philadelphia, PA, 1989, pp. 264-272.

120. "Standard Test Methods of Tension Testing of Metallic Materials", ASTM Designation: E8-89, <u>Annual Book of ASTM Standards</u>, Vol. 03.01, ASTM, Philadelphia, PA, 1989.

121. R.F. Johnson, "The Measurement of Yield Stress", <u>Strong Tough Structural Steels</u>, ISI Publication 104, London, England, 1967, pp. 51-60.

122. "Standard Test Methods for Notched Bar Impact Testing of Metallic Materials", ASTM Designation: E23-88, <u>Annual Book of ASTM Standards</u>, Vol. 03.01, ASTM, Philadelphia, PA, 1989.

123. K.W. Andrews, "Empirical Formulae for the Calculation of Some Transformation Temperatures", JISI, London, England, 1965, pp. 721-727.

124. W. Steven and A.G. Haynes, "The Temperature of Formation of Martensite and Bainite in Low-Alloy Steels: Some Effects of Chemical Composition", JISI, London, England, 1956, pp. 349-359.

125. V. Biss and R.L. Cryderman, "Martensite and Retained Austenite in Hot-Rolled, Low-Carbon Bainitic Steels", Metallurgical Transactions, Vol. 2, 1971, pp. 2267-2276.

126. A.P. Coldren and R.L. Cryderman, "Strength and Impact
     Properties of Low-Carbon Structural Steels Containing
     Molybdenum", in Symposium: Steel-Strengthening
     Mechanisms, Climax Molybdenum Co., Greenwich,
     Connecticut, May 1969, pp. 17-44.

127. Written discussion by B.V. Narashima Rao, following G.
     Krauss, "Martensitic Transformation, Structure and
     Properties in Hardenable Steels," Proceedings
     Hardenability Concepts With Applications to Steel,
     editors D.V. Doane and J.S. Kirkaldy, AIME,

128. K.J. Irvine and F.B. Pickering, "The Impact
     Properties of Low Carbon Bainitic Steels", JISI,
     London, England, 1963, pp. 518-531.

129. C.I. Garcia, A.K. Lis, S.M. Pytel and A.J. DeArdo
     "Ultra -Low Carbon Bainitic Plate Steels: Processing,
     Microstructure and Properties" I&SM, October 1991, pp.
     97-106.

Table 1.   Charpy Impact Data

STEEL	TEMPERATURE (°C)	ENERGY ABSORBED (J) 1X	TEMPERATURE (°C)	ENERGY ABSORBED (J) 2X
A	-195	1.35	-195	1.35
A	-84	2.71	-84	2.71
A	-40	10.84	-40	12.20
A	-18	24.40	-20	27.11
A	0	112.53	-18	108.46
A	23	178.97	0	97.62
A	61.7	184.39	23	146.43
A	64.5	162.70	23	138.30
A	103	166.76	61.7	173.54
A	130	173.54	103	170.83
A	156	166.76	130	178.97
			156	185.75
B	-195	1.35	-195	1.35
B	-84	2.70	-84	4.07
B	-40	6.78	-40	8.13
B	-18	10.85	-18	47.45
B	0	24.45	0	86.77
B	23	74.57	23	84.06
B	44.5	136.94	44.5	151.85
B	62	128.80	62	161.34
B	103	135.58	103	178.96
B	130	154.56	130	183.03
B	160	143.71	160	173.54
C	-195	1.35	-195	1.35
C	-84	2.70	-84	4.07
C	-40	5.42	-40	4.07
C	-18	10.85	-18	10.85
C	0	10.85	0	47.45
C	23	13.56	23	97.62
C	44.5	71.86	61.7	111.17
C	61.7	101.69	103	97.62
C	103	128.80	103.5	123.38
C	129	155.92	129	122.03
C	159	135.61	159	142.36
AT*	-197	2.70	-197	2.70
AT	-83	7.46	-83	6.10
AT	-40	42.03	-40	169.47
AT	-19	62.37	-19	151.85
AT	0	58.30	0	216.93
AT	24	181.60	24	138.29
AT	60	138.29	60	223.71
AT	100	165.41	100	174.90
AT	145	189.81	145	196.59

Table 2.   Tensile Data

STEEL	Mn%	YS(MPa)	UTS(MPa) 1X	EL(%)	YS(MPa)	UTS(MPa) 2X	EL(%)
A-1	1.00	712	899	13.35	703	857	13.25
A-2	1.00	707	874	15.21	711	898	17.40
A-3	1.00	688	941	15.35	703	845	16.24
B-1	1.45	723	916	14.72	702	872	14.62
B-2	1.45	731	885	14.37	731	862	15.94
B-3	1.45	716	896	16.40	714	876	16.23
C-1	1.76	751	927	13.10	752	899	12.47
C-2	-	-	-	-	719	848	14.61
C-3	-	-	-	-	694	826	17.40
AT-1	1.00	612	704	19.71	559	664	25.14
AT-2	1.00	625	725	19.80	618	708	23.60
AT-3	1.00	660	742	20.74	565	670	24.20

* TEMPERED